

**Energy Research and Development Division  
FINAL PROJECT REPORT**

**THE USE OF WIND BARRIERS TO  
MITIGATE THE EFFECT OF WIND ON  
AIR-COOLED CONDENSERS**

Prepared for: California Energy Commission  
Prepared by: Maulbetsch Consulting



JULY 2016  
CEC-500-2016-047

**PREPARED BY:**

***Primary Author(s):***

John Maulbetsch  
Michael DiFilippo

Maulbetsch Consulting  
770 Menlo Ave, Suite 211  
Menlo Park, CA 94025-4764

***Contract Number: PIR-11-024***

***Prepared for:***

**California Energy Commission**

Joe O'Hagan  
***Contract Manager***

Aleecia Gutierrez  
***Office Manager***  
***Energy Generation Research Office***

Laurie ten Hope  
***Deputy Director***  
***ENERGY RESEARCH AND DEVELOPMENT DIVISION***

Robert P. Oglesby  
***Executive Director***

**DISCLAIMER**

This report was prepared as the result of work sponsored by the California Energy Commission. It does not necessarily represent the views of the Energy Commission, its employees or the State of California. The Energy Commission, the State of California, its employees, contractors and subcontractors make no warranty, express or implied, and assume no legal liability for the information in this report; nor does any party represent that the uses of this information will not infringe upon privately owned rights. This report has not been approved or disapproved by the California Energy Commission nor has the California Energy Commission passed upon the accuracy or adequacy of the information in this report.

## PREFACE

The California Energy Commission Energy Research and Development Division supports public interest energy research and development that will help improve the quality of life in California by bringing environmentally safe, affordable, and reliable energy services and products to the marketplace.

The Energy Research and Development Division conducts public interest research, development, and demonstration (RD&D) projects to benefit California.

The Energy Research and Development Division strives to conduct the most promising public interest energy research by partnering with RD&D entities, including individuals, businesses, utilities, and public or private research institutions.

Energy Research and Development Division funding efforts are focused on the following RD&D program areas:

- Buildings End-Use Energy Efficiency
- Energy Innovations Small Grants
- Energy-Related Environmental Research
- Energy Systems Integration
- Environmentally Preferred Advanced Generation
- Industrial/Agricultural/Water End-Use Energy Efficiency
- Renewable Energy Technologies
- Transportation

*The Use of Wind Barriers to Mitigate the Effect of Wind On Air-Cooled Condensers* is the final report for the Wind Barriers to Mitigate Wind Effects on Air-Cooled Condensers project (contract number PIR-11-024) conducted by Maulbetsch Consulting. The information from this project contributes to Energy Research and Development Division's Energy-Related Environmental Research Program.

When the source of a table, figure, or photo is not otherwise credited, it is the work of the author of the report.

For more information about the Energy Research and Development Division, please visit the Energy Commission's website at [www.energy.ca.gov/research/](http://www.energy.ca.gov/research/) or contact the Energy Commission at 916-327-1551.

## ABSTRACT

As competition for California's limited freshwater supplies increases, more power plants are using air-cooled condensers; use of this technology is commonly referred to as dry cooling. An important challenge in the use of this cooling technology is the effect of ambient wind conditions on both the thermal performance of power plants and the level of wind-induced stress on air-cooled condenser fans. This report documents the methodology and results from a study evaluating the effects of wind protection screens and barriers used to minimize damage from ambient wind. The study had three elements: field testing, physical modeling, and computational modeling.

Field testing was conducted on an air-cooled condenser, equipped with retractable windscreens at an operating power plant. Tests were run for a full year to capture the greatest range of wind speed and direction. Measurements were made with the windscreens fully deployed, fully retracted, and at intermediate positions.

Physical modeling of a scale model of the field-tested, air-cooled condenser and surrounding site was conducted in an atmospheric boundary layer wind tunnel. The full range of wind speed, direction, and screen position was simulated in the modeling. Numerical modeling with computational fluid dynamics was conducted for the same unit over a similar range of conditions.

Field test measurements demonstrated a significant reduction in wind-induced stress on the fan blades when the windscreens were deployed. Throughout most of the ambient wind conditions, there was little effect, except at the highest wind speeds from screen position on thermal performance. Results from the physical and analytical modeling efforts showed reasonable agreement with the field test. These results suggest that modeling studies can provide valuable predictive value in selecting the most suitable design and positioning of wind barriers for air-cooled condensers.

**Keywords:** Air-cooled condensers, wind effects, windscreens, wind tunnel modeling, computational fluid dynamics, power plants

Please use the following citation for this report:

Maulbetsch, John, Michael DiFilippo. 2016. *The Use of Wind Barriers to Mitigate the Effect of Wind on Air-Cooled Condensers*. California Energy Commission. Publication number: CEC-500-2016-047.

# TABLE OF CONTENTS

<b>PREFACE .....</b>	<b>i</b>
<b>ABSTRACT .....</b>	<b>ii</b>
<b>TABLE OF CONTENTS.....</b>	<b>iii</b>
<b>LIST OF FIGURES .....</b>	<b>vi</b>
<b>LIST OF TABLES .....</b>	<b>xi</b>
<b>EXECUTIVE SUMMARY .....</b>	<b>13</b>
Introduction .....	13
Project Purpose.....	13
Project Process .....	14
Results.....	15
<b>CHAPTER 1: Introduction.....</b>	<b>17</b>
1.1 Background .....	17
1.2 Wind Effects.....	17
1.3 Prior Experience and Knowledge .....	22
1.4 Organization of Report.....	23
<b>CHAPTER 2: Existing Installations .....</b>	<b>25</b>
2.1 WyGen 1 .....	25
2.2 Desert Star Energy Center (formerly El Dorado Energy Center) .....	28
2.3 Walter M. Higgins Generating Station (formerly Bighorn) .....	30
2.4 Gateway.....	32
2.5 Caithness .....	33
2.6 Power Plants in England.....	35
2.7 Power Plants in Mexico.....	38
2.8 Power Plants in Canada .....	41
2.9 SPX Louver Concept.....	43
<b>Chapter 3: Prior Work.....</b>	<b>46</b>
3.1 General.....	46

3.2	Recirculation Patterns.....	46
3.2	Computational Analysis .....	49
<b>CHAPTER 4: Approach.....</b>		<b>54</b>
4.1	Introduction .....	54
4.2	Field Testing.....	54
4.2.1	Plant Data.....	55
4.2.2	Airport Weather Data.....	57
4.3	Physical (Wind Tunnel) Modeling.....	57
4.4	CFD Modeling .....	60
<b>CHAPTER 5: Field Test Results .....</b>		<b>65</b>
5.1	Field Test Introduction.....	65
5.2	Establishment of Far-Field Ambient Conditions.....	65
5.1.1	Ambient Temperature .....	65
5.1.2	Wind Speed and Direction.....	68
5.1.3	Comparisons among On-Site Measurements.....	69
5.1.4	Comparisons with Fans on and Off.....	72
5.1.5	Comparison with Nearby Airports .....	74
5.1.6	Wind Tunnel Simulation.....	78
5.2	ACC Airflow .....	79
5.2.1	Effect of Screen Position on Inlet Air Velocity to Fans .....	81
5.3	Static Pressure Variations .....	96
5.4	Motor Current Variations .....	99
5.5	Recirculation .....	101
5.6	ACC Performance--Q/ITD .....	102
5.7	Wind-induced Dynamic Blade Loading.....	107
5.7.1	Blade Excitation Frequency .....	110
5.7.2	Source of Excitation .....	111
5.7.3	Effect of Screen Deployment .....	114

<b>CHAPTER 6: Modeling Results .....</b>	<b>117</b>
6.1 Physical Modeling.....	117
6.1.1 Governing Flow Mechanisms.....	117
6.1.2 Effect of ACC and Tank on Field Measurements of Wind Speed .....	125
6.1.3 Selection of Base Case Model Runs .....	128
6.1.4 Modeling of Field Test Conditions .....	131
6.2 Numerical Modeling.....	142
6.2.1 Fan/Bundle Characteristics .....	142
6.2.2 Incoming wind profile.....	143
6.2.3 Detailed Representation of Flow.....	146
6.2.4 Deflection of Diverted Flow .....	149
<b>CHAPTER 7: Summary and Conclusions.....</b>	<b>155</b>
7.1 Field tests.....	155
7.1.1 Effect on Air Flow .....	155
7.1.2 Effect on Recirculation.....	156
7.1.3 Effect on ACC Thermal Performance.....	156
7.1.4 Blade loading .....	156
7.2 Physical Modeling.....	157
7.3 Numerical Modeling.....	158
7.4 Additional observations.....	158
7.4.1 Agreement with Observations Elsewhere .....	158
7.4.2 Fully Retracted Screens Vs. No Screens Installed.....	159
7.4.3 Cleanliness of Screens.....	159
<b>GLOSSARY .....</b>	<b>160</b>
<b>REFERENCES .....</b>	<b>161</b>
<b>APPENDIX A: Instrumentation and Data Acquisition System —Howden Report No. ECD 1307 .....</b>	<b>163</b>

## LIST OF FIGURES

Figure 1: Effect of Wind on Turbine Exhaust Pressure.....	18
Figure 2: Surface Cracking on ACC Fan Blade .....	19
Figure 3: ACC Fan Blade Failure .....	20
Figure 4: Hot Air Recirculation on an ACC .....	20
Figure 5: Degradation of Fan Performance and Inlet Air Flow Reduction.....	21
Figure 6: Relative Effects of Recirculation and Reduced Air Flow .....	21
Figure 7: Aerial View of Neil Simpson Complex .....	25
Figure 8: ACC Original Streets With Added Cells.....	26
Figure 9: Wind Barrier at End of ACC (Between ACC and Turbine Hall) .....	27
Figure 10: Cruciform Wind Wall under ACC .....	27
Figure 11: Effect of Modifications on ACC/Turbine Performance .....	28
Figure 12: Desert Star (Formerly El Dorado) Aerial View of Site .....	28
Figure 13: Desert Star ACC With Cruciform Windscreen.....	29
Figure 14: Effect of Screens on Desert Star ACC and Turbine Performance .....	30
Figure 15: Higgins (Formerly Big Horn) Aerial View of Site.....	31
Figure 16: Higgins ACC with Screen under ACC .....	31
Figure 17: Higgins ACC With “Wings” .....	32
Figure 18: Gateway – Aerial View of Site .....	32
Figure 19: Gateway ACC With “Fan Deck” Windscreen—“One Bay In” .....	33
Figure 20: Caithness Energy Center Site Aerial View.....	34
Figure 21: Caithness ACC with “Fan Deck” Windscreen at Perimeter.....	35
Figure 22: Coryton Aerial View .....	36
Figure 23: Effect of Screens at Coryton .....	37
Figure 24: Kings Lynn Aerial View .....	37
Figure 25: Effect of Screens at Kings Lynn .....	38
Figure 26: Aerial View of San Luis de la Paz Dry Cooled Power Plant .....	39
Figure 27: Wide Field View of Various Wind Mitigation Devices.....	40

Figure 28: Close-Up of Perimeter Screens and Louvers .....	40
Figure 29: Close-up of Perimeter Screen and Cruciform Barrier Wall .....	41
Figure 30: Close-up of Barrier Walls: Up From Ground and Down From Fan Deck.....	41
Figure 31: ACC With Screens at North Battleford.....	42
Figure 32: North Battleford Site Plan .....	42
Figure 33: Velocity Reduction With Wind Screens .....	43
Figure 34: Vibration Reduction With Screens .....	43
Figure 35: ACC With Louvers at WyGen III .....	44
Figure 36: ACC Thermal Performance Comparison.....	44
Figure 37: Reduction in Turbine Exhaust Pressure .....	45
Figure 38: Recirculation Patterns Measured in ABL Wind Tunnel.....	47
Figure 39: Field Measurements Compared to “Moderate/Southwest” .....	48
Figure 40: Recirculation and Wind Direction Measurements at El Dorado .....	48
Figure 41: Re-Entrainment vs. Wind Speed in Wind Tunnel .....	49
Figure 42: Re-Entrainment vs. Wind Speed in El Dorado Field Measurements.....	50
Figure 43: Validation of CFD Results Against Plant Data.....	51
Figure 44: CFD Predicted Cell Inlet Temperatures .....	52
Figure 45: Inlet Air Temperature Measurements From Field Tests at El Dorado.....	52
Figure 46: Comparison of Field Measurements and CFD Predictions of Recirculation .....	53
Figure 47: Aerial View of Caithness Site and Surroundings.....	54
Figure 48: Close in Aerial View of Caithness Site, ACC, and Other Structures.....	56
Figure 49: Schematic of Instrumentation and Measurement Points .....	57
Figure 50: Locations of Neighboring Airports.....	58
Figure 51: Schematic Diagram of the UC Davis Atmospheric Boundary Layer Wind Tunnel ....	58
Figure 52: CAD Model of Caithness Site .....	59
Figure 53: 1:130 Scale Model Installed in UC Davis ABL Tunnel .....	59
Figure 54: Wind Tunnel Measurement Locations .....	60
Figure 55: Zoomed in Top View of the Overset Surface Grid Components of the Full Site Configuration .....	62

Figure 56: Surface Geometry of CFD Model of the Plant Site (Full Site Configuration).....	63
Figure 57: Surface Geometry of CFD Model of the Reduced Site Configuration .....	63
Figure 58: Overset Surface Grid Components of the Full Site Configuration.....	64
Figure 59: Plant Temperature Probes Under ACC.....	66
Figure 60: Temperature Measurement on Top of Water Tank.....	66
Figure 61: Temperature Probe on Fan Bridge Inside Cell (Typical) .....	67
Figure 62: Comparison of On-Site Temperature Measurements .....	68
Figure 63: Plant Wind Vane on Top of Turbine Building.....	69
Figure 64: Anemometer on the Side of Cell 3.4.....	69
Figure 65: On-Site Wind Speed Measurements on August 10, 2014.....	70
Figure 66: Effect of Screen Position on Wind Speed Measurements .....	71
Figure 67: On-Site Wind Direction Measurements on August 10, 2014.....	71
Figure 68: Effect of ACC-Induced Wind.....	73
Figure 69: Comparison of Wind Direction Readings From Nearby Airports .....	75
Figure 70: Comparison of Wind Speed Readings from Nearby Airports.....	76
Figure 71: Wind Direction Comparison-On-Site Tank vs. Brookhaven Airport.....	77
Figure 72: Wind Speed Comparison---On-Site Tank vs. Brookhaven Airport .....	78
Figure 73: Tank Measurements vs. Far Field Wind Speed---Wind Tunnel Measurements .....	79
Figure 74: Howden Fan Curve for Caithness Fans .....	81
Figure 75: Cell 3.4 Average Inlet Velocity for Varying Screen Position .....	83
Figure 76: Cell 2.4 Average Inlet Velocity for Varying Screen Position .....	84
Figure 77: Cells 3.4 and 2.4 Average Inlet Velocity for Varying Screen Position.....	85
Figure 78: Cell 3.4 Inlet Velocity With NW Winds and 100 Percent vs. 0 Percent Screens .....	87
Figure 79: Cell 2.4 Inlet Velocity With NW Winds and 100 Percent vs. 0 Percent Screens .....	88
Figure 80: Cells 3.4 and 2.4 Inlet Velocity With NW Winds and 100 Percent Vs. 0 Percent Screens .....	89
Figure 81: Effect of Screen Position on Cell 3.4 Inlet Velocity (NW Wind Direction).....	90
Figure 82: Effect of Screen Position on Cell 2.4 Inlet Velocity (NW Wind Direction).....	91
Figure 83: Effect of Screen Position on Cells 3.4 and 2.4 Inlet Velocity (NW Wind Direction).....	92

Figure 84: Cell 3.4 Inlet Velocity With W Winds and 100 Percent vs. 0 Percent Screens.....	93
Figure 85: Cell 3.4 Inlet Velocity With SW Winds and 100 Percent vs. 0 Percent Screens.....	94
Figure 86: Static Pressure Measurement Comparison .....	96
Figure 87: Effect of Screen Position on Cell 3.4 Static Pressure (NW Wind Direction).....	97
Figure 88: Static Pressure Variation With Wind Speed (Screens Fully Retracted) .....	98
Figure 89: Effect of Screen Position on Cells 3.4, 2.4 and 1.4 (NW Wind Direction) .....	99
Figure 90: Motor Current vs. Wind Speed for Fully Retracted/Deployed Screens.....	100
Figure 91: Motor Current vs. Wind Speed for 5 Screen Positions.....	100
Figure 92: Motor Current vs. Fan Inlet Velocity .....	101
Figure 93: Motor Current vs. Static Pressure .....	101
Figure 94: Effect of Screen Position on Average and Maximum Recirculation—NW Wind Direction.....	103
Figure 95: Effect of Screen Position on Average Recirculation—NW Wind Direction .....	104
Figure 96: Effect of Screen Position on Maximum Recirculation—NW Wind Direction.....	105
Figure 97: Effect of Screen Position on ACC Thermal Performance—NW Wind Direction .....	106
Figure 98: Effect of Wind Direction on ACC Thermal Performance—Fully Deployed Screens.	107
Figure 99: Effect of Wind Direction on ACC Thermal Performance—Fully Retracted Screens .	108
Figure 100: Long-Term Average Blade Loading vs. Wind Speed for 5 Screen Positions .....	109
Figure 101: Filtered Sample Load Cell Outputs and Tachometer Pulse .....	110
Figure 102: Aligned Pulses and Tachometer Pulse .....	111
Figure 103: Smoke Trace Under Fan.....	112
Figure 104: Inlet Air Velocity Variations .....	112
Figure 105: Wind Speed, Inlet Velocity, and Blade Loading At Cell 3.4.....	113
Figure 106: Effect of Wind Speed Increase .....	114
Figure 107: Effect of Screen Deployment on Inlet Velocity Variability .....	115
Figure 108: Fan 3.4 and 2.4 Inlet Velocity Variability, Screen Retracted .....	115
Figure 109: Fan 3.4 and 2.4 Inlet Velocity Variability, Screen Deployed.....	116
Figure 110: Set-Up for Measurement of Wind Screen Characteristics .....	118
Figure 111: WBE for 40 Percent Solidity Fabric .....	119

Figure 112: WBE for 60 Percent Solidity Fabric .....	120
Figure 113: WBE for 75 Percent Solidity Fabric .....	120
Figure 114: WBE for 88 Percent Solidity Fabric .....	121
Figure 115: WBE From Galebreaker Tests .....	122
Figure 116: Wind Tunnel Measurements of Air Velocity Up/Downstream of Fabric.....	123
Figure 117: CFD Computational Variations vs. Tunnel Measurements .....	124
Figure 118: CFD Extension Into Pressure Recovery Zone.....	125
Figure 119: Effect of ACC-Induced Winds and Tank Blockage on Wind Speed Measurements	126
Figure 120: “Fans on/Fans off” Velocity Ratio vs. Wind Direction.....	127
Figure 121: Measured Wind Speed at Tank vs. Estimated Far-Field Wind Speed .....	128
Figure 122: Inlet Air Velocities in Cell 3.4 During Selected “Steady” Periods.....	129
Figure 123: Inlet Air Velocities in Cell 2.4 During Selected “Steady” Periods .....	130
Figure 124: Static Pressure in Cells 3.4, 2.4, and 1.4 During Selected “Steady” Periods.....	130
Figure 125: Schematic of Tested Cells .....	132
Figure 126: Definition of Coordinates in Plots of Results.....	133
Figure 127: Normalized “Z-Locations” of Measurements .....	134
Figure 128: Example Measurements.....	135
Figure 129: Velocity Measurement Under Row 4 Cells at 2.4 m/s; $z = .67$ (Retracted vs. Deployed).....	136
Figure 130: Velocity Measurement Under Row 4 Cells at 2.4 m/s; $z = .89$ (Retracted vs. Deployed).....	136
Figure 131: Velocity Measurement Under Row 4 Cells at 2.4 m/s; $z = 1.1$ (Retracted vs. Deployed).....	136
Figure 132: Velocity Measurement Under Row 4 Cells at 4. m/s; $z = .67$ (Retracted vs. Deployed) .....	137
Figure 133: Velocity Measurement Under Row 4 Cells at 4. m/s; $z = .89$ (Retracted vs. Deployed) .....	138
Figure 134: Velocity Measurement Under Row 4 Cells at 4. m/s; $z = 1.1$ (Retracted vs. Deployed) .....	138
Figure 135: Streamline Patterns.....	139

Figure 136: Horizontal Mass Flow Underneath Fans 2 & 4 m/s; $z = 0.67$ ; Retracted and Deployed .....	140
Figure 137: Horizontal Mass Flow Underneath Fans 2 & 4 m/s; $z = 0.89$ ; Retracted and Deployed .....	140
Figure 138: Horizontal Mass Flow Underneath Fans 2 & 4 m/s; $z = 1.1$ ; Retracted and Deployed .....	141
Figure 139: Comparative Images From Video Recording.....	141
Figure 140: Incoming Airflow Boundary Layer.....	144
Figure 141: Upwind Buildings and Trees .....	144
Figure 142: Total Velocity Vectors For “Near-Zero” Wind Speed Conditions; No Screen Present .....	147
Figure 143: Vertical Velocity Vectors For “Near-Zero” Wind Speed Conditions; No Screen Present .....	147
Figure 144: Total Velocity Vectors for 4 M/S Wind; Uniform Profile; No Screen Present.....	148
Figure 145: Streamline Patterns for 3 M/S Wind; No Upstream Blockage; No Screen Present ..	149
Figure 146: Streamline Patterns for 3 M/S Wind; Upstream Blockage; No Screen Present.....	149
Figure 147: Simulation of Horizontal “Lip” Concept .....	150
Figure 148: Comparative Effect of Hypothetical “Lip” On Incoming Flow Dynamics .....	151
Figure 149: Total Velocity Vectors for 3 M/S Wind; Upwind Blockage and “Lip” In Place; No Screen Present.....	152
Figure 150: Total Velocity Vectors for 3 M/S Wind; No Upwind Blockage; “Lip” In Place; No Screen Present.....	152
Figure 151: Total Velocity Vectors for 3 M/S Wind; No Upwind Blockage; “Lip” In Place; With Screen Present.....	153
Figure 152: Total Velocity Vectors for 6 M/S Wind; No Upwind Blockage; “Lip” In Place; No Screen Present.....	153

## LIST OF TABLES

Table 1: Partial Listing of ACCs with Wind Barriers .....	23
Table 2: Results of Howden Fan Test; Cell 3.3; December 5, 2012 .....	80
Table 3: Distribution of Data Points Plotted in Figures 74 through 76.....	82

Table 4: Steady Test Periods Selected For Modeling.....	131
Table 5: Fan Inlet Velocities in Near-Zero Wind Conditions.....	143
Table 6: Effect of Modifying Incoming Flow Characteristics.....	145
Table 7: Effect of Wind Speed and Screen Position.....	145
Table 8: Summary of Inlet Velocity Comparisons for Cell 3.4.....	154
Table 9: Summary of Inlet Velocity Comparisons for Cell 2.4.....	154

# EXECUTIVE SUMMARY

## Introduction

A major challenge facing deployment of thermal power plants in California is the significant water demands these facilities may impose on local limited freshwater supplies. To significantly reduce power plant water demand, air-cooled condensers are increasingly being used. Use of this technology is commonly referred to as dry cooling.

An air cooled condenser rejects heat to the atmosphere and consists of an elevated A-frame arrangement of parallel finned tube bundles. Steam is piped from the turbine or boiler to the top of the condenser and then as the steam flows down the tubes and condenses heat is transferred to air passing outside the tubes. The condensate is then reused in the power plant. To increase air flow pass the tube bundles, air-cooled condensers are generally elevated many meters above the ground and utilize a number of large, low speed axial fans located beneath the condenser.

While air-cooled condensers conserve significant amounts of water, they require higher capital and operating costs, and impose some penalties on the efficiency and output of the generating unit. A further challenge to the use of this cooling technology is that high ambient winds, often in conjunction with high ambient temperatures, can reduce power plant performance and can cause potential physical stress and damage on air-cooled condenser fans.

## Project Purpose

The adverse effect of wind on the performance of large air-cooled condensers has been recognized for many years. Wind has been shown to cause significant degradation of the thermal performance of air-cooled condensers, and impose stress on some mechanical elements, particularly the fans, the fan blades, the fan motors, and the gearboxes.

Deterioration in thermal performance due to wind is attributed to two mechanisms: recirculation and fan performance degradation. Recirculation occurs when wind patterns around the air-cooled condenser cause the hot air exiting from the top of the condenser to be blown down, and redirected into the air entering the condenser, resulting in air temperatures higher than ambient conditions and lower condenser thermal efficiency.

Degraded fan performance occurs when wind passing beneath the condenser causes a low pressure zone which reduces the amount of air being entrained by the affected fans. This reduces the amount of air passing by the condenser tubes, resulting in air temperatures higher than ambient conditions and lower condenser thermal efficiency. These winds can also cause fan fatigue and failure.

It is thought that fan degradation is the more important of the two wind effects. However, this can vary with the details of the site topography, the presence of nearby obstructions, air-cooled condenser orientation relative to the prevailing winds and wind conditions.

A number of approaches have been taken in attempt to mitigate the effects of wind on air-cooled condensers, including:

- The installation of additional cells to add compensating capacity
- Modification of original fans
- Thermal performance enhancements with inlet spray cooling

A more comprehensive approach is the use of physical wind barriers to modify the wind flow patterns around the air-cooled condenser. This approach has been used either as a retrofit or as part of the original design at several sites.

While a substantial amount of research has been conducted on the more general effects of wind on air-cooled condensers, there is a lack of detailed information on the effectiveness of this mitigation measure. The purpose of this study is to address this lack of information.

### Project Process

To understand the ways wind barriers diminish the effect of wind on air-cooled condenser performance, the study took a three-pronged approach: field testing at an operating power plant site, physical modeling in a wind tunnel, and mathematical simulation using computational fluid dynamics methods. The field tests were used to guide, calibrate, and validate the physical and computational models.

Field testing was conducted to determine the effects of windscreens on air-cooled condenser airflow and performance, and to obtain direct measurements of fan blade vibrations, stresses, and how they are mitigated by windscreens. The field tests were conducted at the only air-cooled condenser in the United States that is equipped with retractable windscreens. This allowed comparisons of the effect of wind on air-cooled condenser performance and physical stress with and without screens under very similar conditions.

Instrumentation was installed on and around the air-cooled condenser to monitor the air flow and temperature patterns in addition to the performance of selected fans and stresses on fan blades.

A physical model of the plant site and air-cooled condenser was constructed for testing in an atmospheric boundary layer wind tunnel. Wind speed and direction under and around the air-cooled condenser was measured to produce detailed airflow patterns around the condenser. Mesh material of appropriate porosity was attached to the side of the air-cooled condenser model to simulate the windscreens. Comparison with field data was used to validate the physical model results. The model was then used to explore limited variations on the windscreen arrangement in the field to determine the most effective configuration.

Using computational fluid dynamics, the researchers used analytical modeling of air flow patterns around the air cooled condenser, with and without wind barriers. Comparison with field and wind tunnel data was used to calibrate and validate the numerical simulation. Ultimately, the model was used to explore the behavior of alternative wind protection approaches, for which no physical data was available.

## Results

The dynamic loading on the fan blades was significantly reduced by the deployment of the windscreens. On the basis of field measurements averaged over all wind directions from northwest to southwest, the results suggest that a 50 percent deployment of the screens was the most favorable in that there was less reduction in airflow at the lowest wind speeds compared to full deployment. Overall, the indicators of thermal performance showed substantial variability with wind speed and direction but relatively little variation with screen position.

Wind tunnel tests were run for a range of wind speeds coming from the West (normal to the long side of the air-cooled condenser) with and without windscreens in place. Model results show that the presence of the wind screen is evidently beneficial; with the wind screen in deployed position there is less horizontal flow interfering with the vertical flow into the fans and allows for more through the ACC fan.

The computational fluid dynamic models achieved good representation of field conditions, but only at very low wind speeds, suggesting that the flow of the incoming wind is not adequately represented in the model. Although quantitative results were not obtained and the goal of producing a computational tool capable of generalizing test results from the field or the wind tunnel was not achieved, some increased understanding of the important physics was obtained to serve as a starting point for additional modeling efforts.

This study was undertaken with the goal of increasing the understanding the mechanisms by which wind screens helped, to quantify the beneficial effects and to develop guidelines for the selection and design of wind screens.

Increased understanding of the physical mechanisms which determine the effect of windscreens was obtained through a year of continuous field testing and extensive wind tunnel modeling. However, the complete development of an analytical model which was to have been used to generalize the test results was not achieved. As a result, the goal of producing guidelines for windscreen selection and design could not be met.



# CHAPTER 1:

## Introduction

This report documents the conduct of, and the results from, a study of the effectiveness of wind screens and wind barriers in mitigating the effects of wind on the thermal performance of, and the physical stress experienced by the fans, motors and gearboxes on, air-cooled condensers (ACCs) of the type and size used at electric power plants. The study consisted of three separate, but related, elements. These were field tests at the Caithness Energy Center on the southern side of Long Island, east of New York City, wind tunnel modeling of the Caithness ACC and site and computational fluid dynamics (CFD) modeling of the Caithness ACC and site. The physical and CFD models were developed to provide generalizable approaches to selecting, designing and arranging appropriate wind protection for untested sites; the field tests were used to calibrate and validate the results of the physical and CFD models.

### 1.1 Background

Dry cooling systems for power plant cooling, primarily of the direct dry cooling type utilizing ACCs, are selected increasingly often as water conservation has become a more critical concern in California, the U.S. and around the world. However, these systems, while conserving significant amounts of water, incur higher capital cost, higher operating costs and some penalty to the efficiency and output of the generating unit. In addition, even optimized systems can incur thermal performance reduction and potential physical stress and damage during periods of high winds, which can often occur in conjunction with high ambient temperatures and periods of peak power demand.

In 2011, the California Energy Commission (CEC) stated:

*“A major challenge facing natural gas-fired generation permitting and deployment in California is the significant demands such facilities may impose on the state’s limited freshwater supplies....For example, high ambient air temperatures and/or winds may degrade condenser performance and reduce electricity generation....Therefore, to reduce pressure on the state’s limited freshwater supplies, there is a need for research that can reduce the penalties associated with the use of water conserving cooling technologies.”*

### 1.2 Wind Effects

The adverse effect of wind on the performance of large ACCs has been recognized for many years. Kröger (1998), in a chapter entitled “Effect of Wind on Air-Cooled Heat Exchangers”, states the situation succinctly:

*“In general, winds have a negative effect on the performance of mechanical-draft heat exchangers. Plume air recirculation tends to increase while fan performance is usually reduced during windy periods.”*

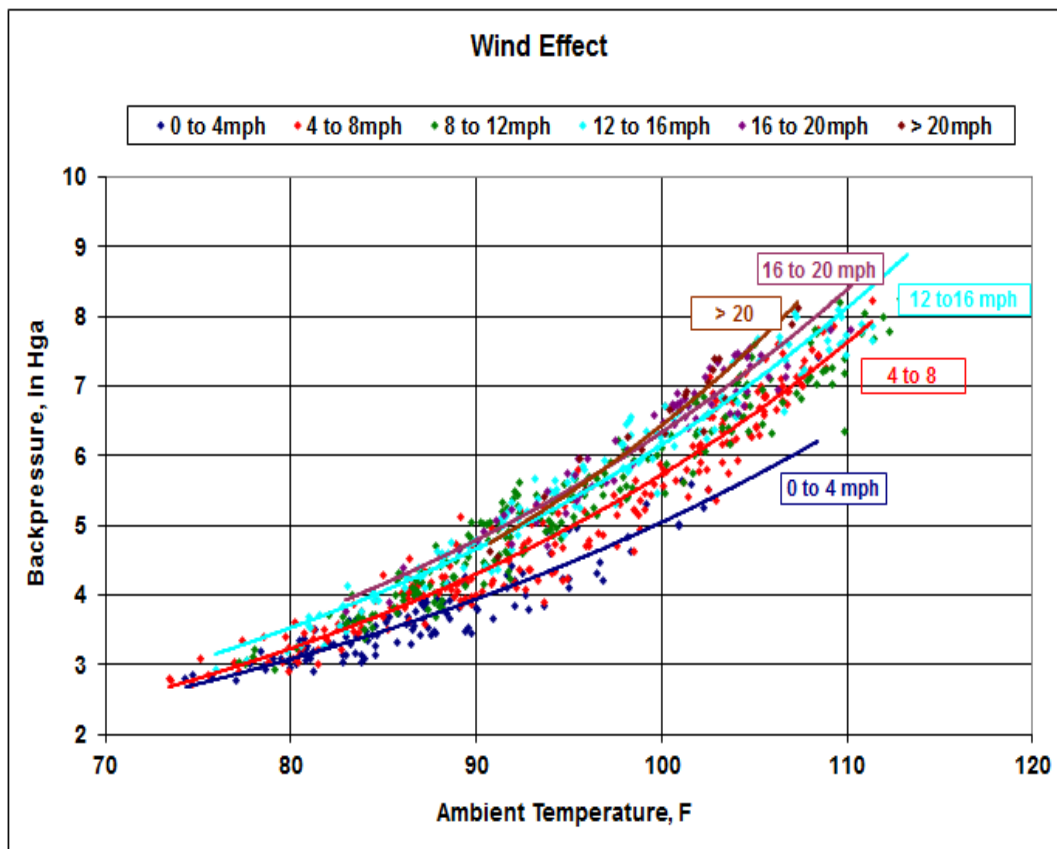
Wind has been known to create significant problems for the thermal performance of ACCs and to impose stresses on some mechanical elements, particularly the fans, the fan blades, the fan

motors and the gearboxes. Air-Cooled Condenser Design, Specification, and Operation Guidelines (Wilbur & Maulbetsch 2005) notes that:

*“The impact of ambient wind on ACC performance is not well understood by owner/operators or their representatives in the specification and bid/evaluation process,” and that “this area of wind effects in total represents the major challenge associated with ACC specification, design, and performance.”*

The effect of wind on ACC thermal performance is illustrated in Figure 1 which shows the variation in turbine exhaust pressure vs. ambient temperature for a range of wind speeds. Conditions such as these are typical of hot, arid desert locations in the southwestern part of the US.

**Figure 1: Effect of Wind on Turbine Exhaust Pressure**



At ambient temperatures above 100F, the difference between no wind or low wind and high winds (above 20 mph) can be 1.5 to 2.inches Hga with a correspondingly significant effect on turbine output.

Physical damage resulting from wind is usually evidenced by incipient surface cracking or occasional failure of the fan blades, by failures of gearboxes or by motor trips from excessive vibration or current variations. Examples of fan blade damage are illustrated in Figures 2 and 3.

**Figure 2: Surface Cracking on ACC Fan Blade**



Deterioration in thermal performance is attributed to two mechanisms: recirculation and fan performance degradation.

Recirculation occurs when wind patterns around the ACC causes the hot exhaust air from the top of the ACC to be blown down and re-entrained into the inlet air stream resulting in an inlet air temperature higher than the far-field ambient air temperature. This is illustrated in Figure 4.

Fan performance degradation, resulting in significantly reduced air flow into the ACC, is illustrated in Figure 5, where a smoke plume is shown passing directly under a fan without being entrained.

While both mechanisms contribute to degraded ACC thermal performance, the effect on fan performance is the more significant in most cases. This is illustrated in Figure 6.

**Figure 3: ACC Fan Blade Failure**



**Figure 4: Hot Air Recirculation on an ACC**

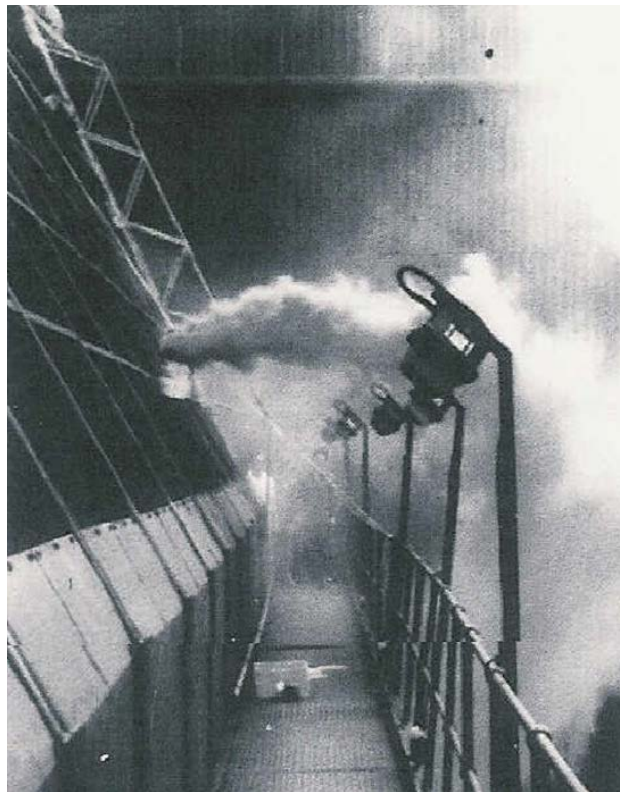
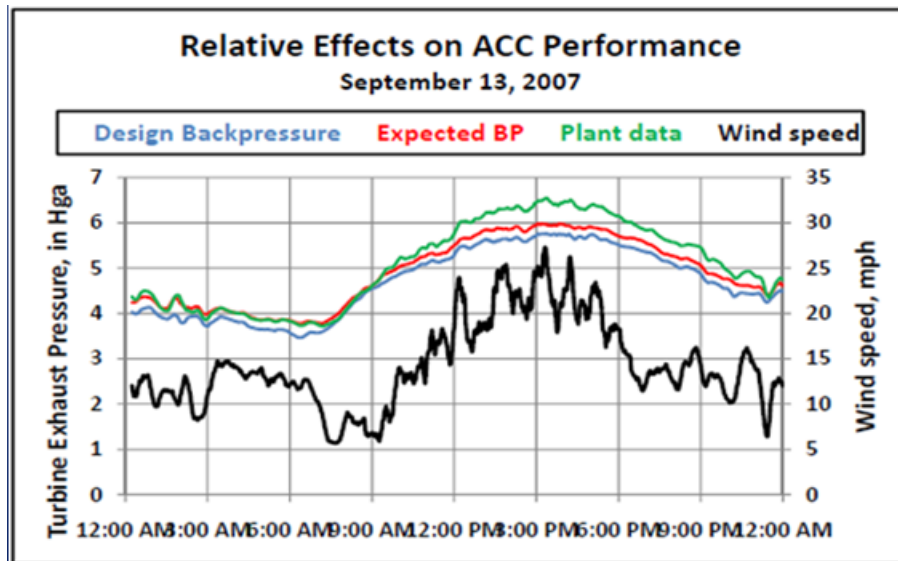


**Figure 5: Degradation of Fan Performance and Inlet Air Flow Reduction**



**Figure 6: Relative Effects of Recirculation and Reduced Air Flow**



Source: Maulbetsch and DiFilippo (2013)

In Figure 6, the measured turbine exhaust pressure (green line) is shown over the course of a day where the heat load was essentially constant, the wind speed varied as shown (black line) and the ambient temperature varied diurnally. The expected turbine exhaust pressure based on ACC design information for the operating heat load and the far-field ambient temperature is shown on the bottom (blue) line. It is clear that the difference between the measured turbine exhaust pressure and the expected, or design, turbine exhaust pressure increases with

increasing wind speed. The expected turbine exhaust pressure, based on design information for the measured inlet air temperature (average of all cells) is shown (red line) and represents the effect of hot air recirculation. The difference between that “expected” turbine exhaust pressure and the measured pressure is attributed to the reduction in air flow due to crosswinds flowing under the fans and producing the effect illustrated in Figure 5. This suggests that the deleterious effect of recirculation at the higher wind speeds is one-third to one-half that of the effect of air flow reduction.

This study was developed to address the specific issue of the effect of wind on ACC thermal performance and mechanical stress of the fan blades and the use of wind protection screens and barriers to mitigate any deleterious effects.

Air-cooled condensers transfer heat by convection and radiation instead of by evaporating water as with recirculating wet cooling towers, thus providing the opportunity to conserve millions of gallon per day of freshwater. Wind is known to adversely affect thermal performance of air-cooled condensers, through reduced airflow and increased hot air recirculation, and to increase the mechanical stresses on condenser fan blades. Benefits of this research include improved understanding of the value of wind barriers to reduce the adverse effects of ambient wind, which will ultimately improve the performance of the water conserving cooling technology.

### **1.3 Prior Experience and Knowledge**

A number of approaches have been taken in attempts to mitigate the effects of wind on ACCs. These include:

- The installation of additional cells to add compensating capacity;
- Modification of original fans from simple re-pitching of the fan blades to the replacement of original fans with others with more blades to increase the baseline flow and to reduce the stress on the individual blades; and
- Enhancing thermal performance with inlet spray cooling.

A more comprehensive approach, however, is the use of physical wind barriers, in the form of porous screens or solid walls, in various locations and of various arrangements to modify the wind flow patterns around the ACC. While not widely adopted, this approach has been used either as a retrofit for performance improvement, for reduction of motor trips and for reduction of fan maintenance or as a part of the original design in anticipation of potential wind-related problems. Table 1 lists a number of installations where wind barriers have been used.

In addition, some experimental work has been done at Saltillo (Villafuerte 2012 and North Battleford (Basham 2014) in Canada and perhaps elsewhere. Selected specific installations will be described and discussed in more detail in Chapter 2.

A substantial amount of research has been conducted on the more general problem of wind effects on ACCs (Maulbetsch and DiFilippo 2013; Maulbetsch et al. 2011, Kroger and Owen 2011; Kim et al. 2011). Some of the studies include field data, physical modeling and

computational analysis. A few contain data from installations with wind barriers (Maulbetsch and DiFilippo 2013; Maulbetsch et al. 2011; Kroger and Owen 2011 and two contain computational and physical models of the installation at the El Dorado Energy Center (Kroger and Owen 2011; Kim et al. 2011) . While many of these studies have added to the understanding of the efficacy of wind barriers, they are of limited value in developing engineering understanding and generic selection/design/operating guidelines for the most effective wind protection choices at new or existing sites. The limitation stems from the fact that almost no data are available at a single site with and without wind barriers. Although physical and computational models can be run with and without the barriers, there is no consistent field data against which to verify the models. Results of selected studies and an indication of the quality of the modeling are discussed in Chapter 3.

**Table 1: Partial Listing of ACCs with Wind Barriers**

Plant Name	Country	Utility	Location	ACC Vendor	Date	Screen type	New or Retrofit
Big Horn	US	NV Power	NV	SPX (Hamon)	2003	Perimeter	New
Maalaea, HI	US	HECO	HI	SPX	2005	One bay in	Retrofit
Gateway	US	PG & E	CA	SPX	2008	One bay in	New
Caithness	US	Caithness LLC	NJ	GEA	2012	Retractable	Retrofit
Ivanpah Solar	US	NextEra	CA	SPX	2012	One bay in	New
El Dorado	US	SDG&E	NV	GEA	2002	Cruciform	Retrofit
WyGen	US	Pacificorp	WY	GEA	2002	Cruciform	Retrofit
Deer Creek	US	Basin Electric	ND	SPX	2010	One bay in	New
Tracy	US	GWF Energy	CA	SPX	2012	One bay in	New
Comanche III	US	Xcel Energy	CO	GEA	2013	Perimeter	Retrofit
Long Beach	US	LADWP	CA	GEA	2014	Perimeter	Retrofit
Mystic #8	US	Excelon	MA	SPX	2014	Perimeter	Retrofit
Scattergood #3	US	LADWP	CA	Holtec	2015	Perimeter	New
North Bay	Canada	Atlantic Power	Ontario	GEA	2014	Perimeter	Retrofit
North Battleford	Canada	Northland Power	Saskatchewan	GEA	2014	Perimeter	Retrofit
San Luis de la Paz	Mexico	AEP	San Luis de la Paz	SPX	2014	Perimeter	New
Kings Lynn	UK	Centrica	Norfolk	SPX	1998	Cruciform	Retrofit
Kings Lynn	UK	Centrica	Norfolk	SPX	2011	Retractable	Retrofit
Peterborough	UK	Centrica	Cambridgeshire	GEA	1999	Perimeter	Retrofit
Barry	UK	Centrica	Glamorgan	GEA	2001	One bay in	Retrofit
Coryton	UK	Intergen	Essex	GEA	2004	Perimeter	Retrofit
Spalding	UK	Intergen	Lincolnshire	GEA	2007	Perimeter	Retrofit
Sutton Bridge	UK	Macquarie Group	Lincolnshire	SPX	2008	Perimeter	Retrofit
Enfield	UK	Enfield Energy Centre	London	SPX	2010	Perimeter	Retrofit
Langage	UK	Centrica	Devon	SPX	2010	One bay in	New
Stevens Croft	UK	E.ON	Cumbria	GEA	2011	Perimeter	Retrofit
Western Biomass Energy	UK	RWE	South Wales	GEA	2013	Perimeter	Retrofit
Dordrecht	Netherlands	South Holland Power	Dordrecht	SPX	2012	Perimeter	Retrofit
Wijster	Netherlands	Attero	Wijster	SPX	2006	Perimeter	Retrofit
Catalagzi	Turkey	EUAS	Catalagzi	GEA	2012	Cruciform	New
Denizli	Turkey	RWE/EUAS	Denizli	SPX	2012	One bay in	New
Hsin Tao	Taiwan	Hsin Tao Power Corp	Taiwan	SPX	2003	One bay in	Retrofit
Kuo Kuang	Taiwan	CPC	Taiwan	GEA	2009	Perimeter	Retrofit
Star Buck	Taiwan	Starbuck Power Corp	Taiwan	SPX	2012	One bay in	Retrofit
Thiva	Greece	GDF Suez	Thiva	SPX	2008	One bay in	New
Fengzhen	China	China Huaneng Group	Fengzhen	SPX	2006	One bay in	Retrofit

## 1.4 Organization of Report

The remainder of the report is organized as follows.

- Chapters 2 and 3 contain descriptions of existing full-scale ACC installations with wind barriers and of previous studies of wind protection schemes and their results, respectively.
- Chapter 4 describes the scope and approach of the current study, including the field tests, the physical modeling and the computational modeling.
- Chapter 5 presents the results of the field testing and modeling work and examines the comparisons among the several elements.
- Chapter 6 presents the results of the modeling work.

## CHAPTER 2: Existing Installations

Table 1 in Chapter 1 lists a number of plants at which ACCs are equipped with various kinds of wind barriers. A few of those are described briefly in the following sections to provide some understanding of the approaches that have been taken. Where possible, an indication of the effectiveness of the wind barriers in improving the thermal performance of the unit is indicated. The types include solid walls and porous screens; the locations are both under the ACCs extending from grade level up to or approaching the fan deck and extending from the fan deck down toward the ground covering one-third to one-half the height of the air inlet opening on the sides of the ACC. Of those descending from the fan deck level, some are on the outer perimeter of the ACC while others are located “one bay in” with the perimeter fans on the outside of the screens.

### 2.1 WyGen 1

WyGen 1, an 80 MWe coal-fired unit, is part of the Neil Simpson Complex of Black Hills Power and Light, located a few miles east of Gillette, Wyoming. Figure 7 shows an aerial view of the complex with WyGen 1 extending toward the north of the plant. At the time the unit was constructed there were only two streets of ACC cells on each unit, each with 5 cells. An additional cell was added to each of two original streets and then a third street was added later.

**Figure 7: Aerial View of Neil Simpson Complex**

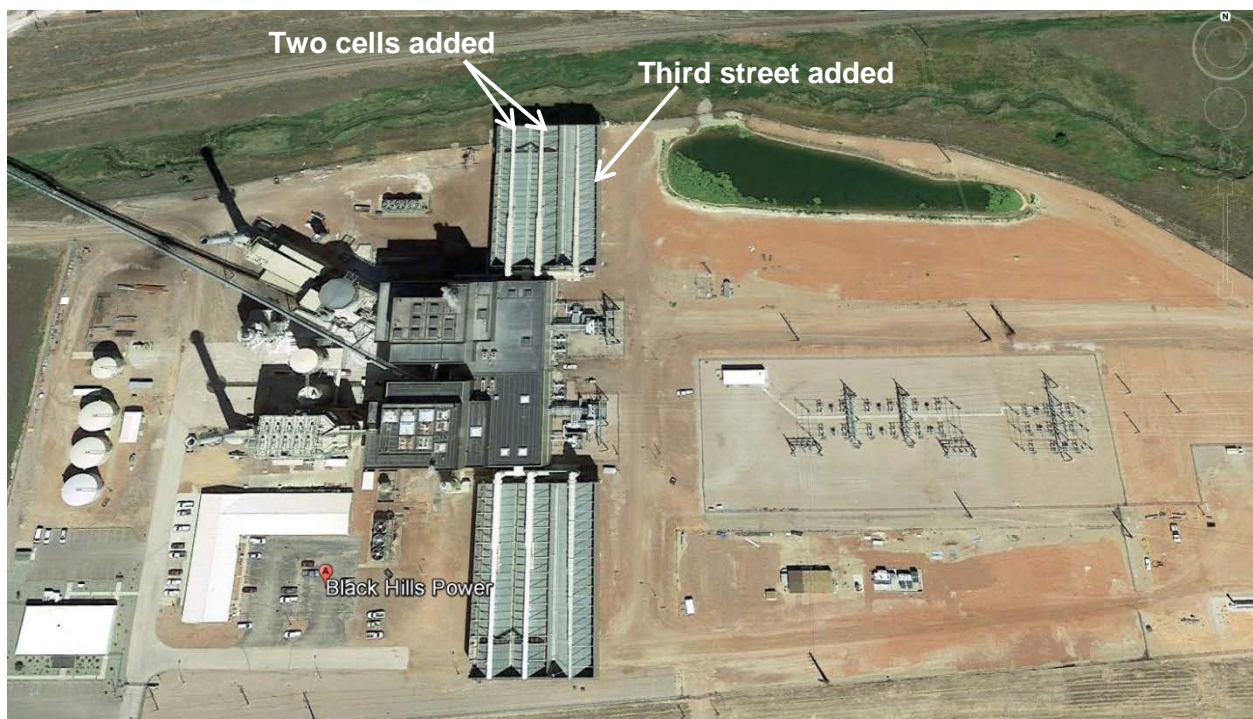


Figure 8 shows the original two streets plus the additional sixth cell at the end of each street. Figure 9 shows one part of the recirculation problem. When the wind blew from the north down the length of the ACC toward the wall of the boiler house, the plume was blown against the wall and a portion of it turned down and was entrained by the fans at the south end of the ACC. The installation of a wall which closed off the inlet area at the south end of the ACC prevented much of that south end recirculation. The cruciform wall under the length of the ACC between the two original streets and across the width of the ACC between Rows 2 and 3 (shown in Figure 10) further reduced recirculation primarily from cross winds coming from the east or west.

Figure 11 shows the improvement in performance resulting from the various modifications. The plot demonstrates that, prior to the summer of 2002; the unit performance was consistently below the design level, particularly at temperatures above 90 F. It is characteristic of that site that the higher temperatures were often accompanied with high winds. The two sets of performance data for June and July of 2002 show restored performance exceeding the design level. Unfortunately, since the addition of the two additional cells and the installation of the wind barriers were done at the same time, it is not possible to isolate the specific benefit of the wind barrier. However, it appears that the additional cells are responsible for the general increase in performance over the entire temperature range while the wind barriers contribute primarily to the elimination of the dramatic decrease in capacity at temperatures above 85 to 90° F.

**Figure 8: ACC Original Streets With Added Cells**



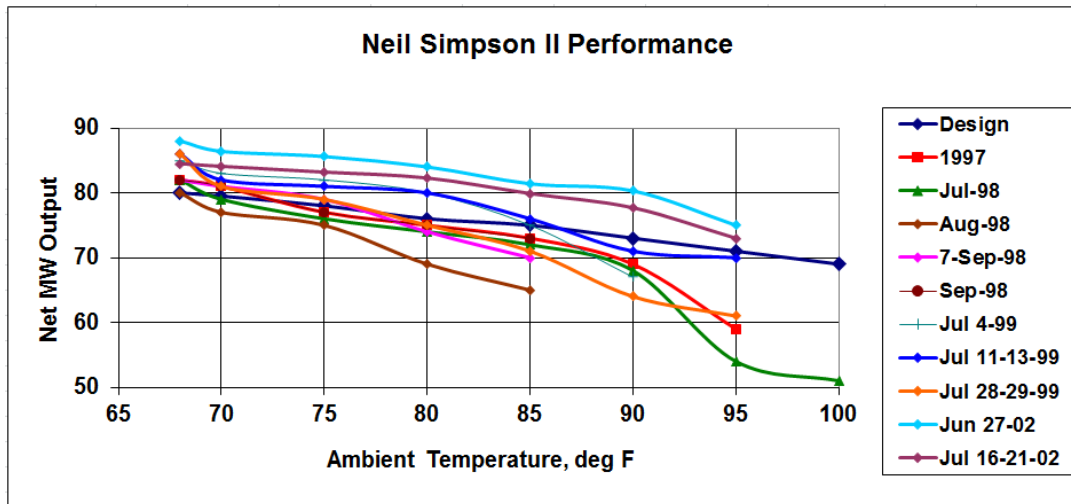
**Figure 9: Wind Barrier at End of ACC (Between ACC and Turbine Hall)**



**Figure 10: Cruciform Wind Wall under ACC**



**Figure 11: Effect of Modifications on ACC/Turbine Performance**



## 2.2 Desert Star Energy Center (formerly El Dorado Energy Center)

The Desert Star Energy Center, formerly the El Dorado Energy Center, is a 480 MW gas-fired, combined-cycle plant in a 2 x 1 configuration. The plant came on-line in 2000. Figure 12 gives an aerial view of the plant site showing the plant buildings to the north of the ACC. The areas to the east, south and west are essentially unobstructed for several miles in all directions. At the time of the field tests the solar panel field to the south and southwest of the ACC was not present. Prevailing winds in the summer are from the south and southwest and frequently reach speeds of 20 to 40 mph during hot afternoons with occasional gusts to 50 mph.

**Figure 12: Desert Star (Formerly El Dorado) Aerial View of Site**



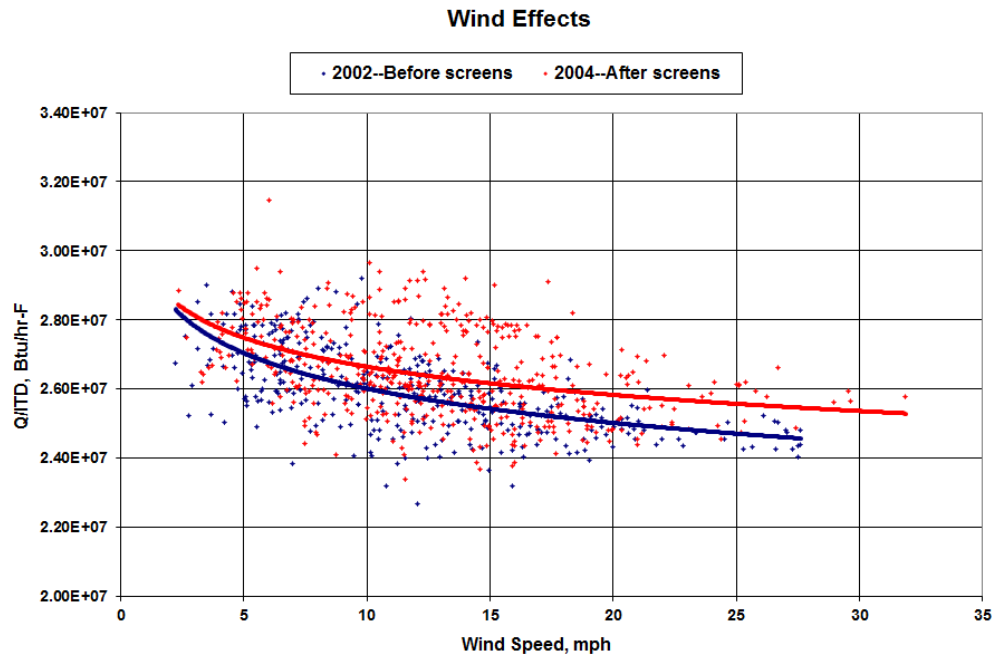
Figure 13 illustrates the windscreen under the ACC. The screen is in a cruciform arrangement running north/south between streets 3 and 4 and east/west between rows 3 and 4. The screens extend from the ground to the fan deck and are divided into four sections separated at the horizontal structural beams. The porosity of the screens varies from top to bottom with the top section being the most porous.

The effect of wind on the performance of the ACC and steam turbine without the screens in place was shown in Figure 1. Figure 14 shows the comparison of the performance before and after the screens were installed and confirms a significant improvement in performance. Unfortunately there were no detailed field measurements of the wind flow patterns or recirculation levels taken prior to the installation of the screens so it is not possible to identify the mechanisms which led to the improvement in detail.

**Figure 13: Desert Star ACC With Cruciform Windscreen**



**Figure 14: Effect of Screens on Desert Star ACC and Turbine Performance**



### **2.3 Walter M. Higgins Generating Station (formerly Bighorn)**

The Higgins plant, formerly Bighorn, is a 540 MW gas-fired, combined-cycle plant in a 2 x 1 configuration. The plant came on-line in 2004. Figure 15 shows an aerial view of the plant. The ACC is a 40 cell ACC arranged in two 20-cell clusters with 4 streets of 5 rows each. Figure 16 shows a porous wind-screen under the south cluster running north and south between streets 2 and 3. There is no screen in the crosswise direction. In addition to the wind screen there are panels or “wings” located at the northwest corner of the north cluster as shown in Figure 17 and another at the southwest corner of the south cluster.

The prevailing winds in the summer are from the south and hence are often aligned parallel with the screen and the wings. Therefore, the screen and the wings often have little effect on the wind flow patterns under or around the ACC. In fact, the screen and the wings were installed for aesthetic rather than performance reasons to provide a more pleasing appearance as viewed from three casino hotels located west of the plant. However, detailed measurement of wind patterns taken in 2005 (Maulbetsch & DiFilippo 2013) did indicate some effect for winds not directly from the south, providing some protection of downwind cells for winds from either the southeast or southwest. It is, however, difficult to infer any reliable, quantitative information about the effect of the screen at this site.

**Figure 15: Higgins (Formerly Big Horn) Aerial View of Site**



**Figure 16: Higgins ACC with Screen under ACC**



**Figure 17: Higgins ACC With “Wings”**



## **2.4 Gateway**

The Gateway Generating Station is a 600 MW gas-fired, combined-cycle plant in a 2 x 1 configuration. Figure 18 shows an aerial view of the plant. The ACC is seen at the south end of plant site. The plant came on-line in early 2009.

**Figure 18: Gateway – Aerial View of Site**



The ACC is a 36 cell unit, arranged in six streets of six rows each. It is equipped with a windscreen, shown in Figure 19, which extends downward from the fan deck about half way to

the ground. The screen is placed “one bay in” with the perimeter cells outside of the screened area. The screens extend to the perimeter of the ACC at each end, however, so each of the four corner cells is screened on the two interior sides.

The screens were included as part of the original design, so no comparative performance information without the screens is available. To our knowledge, no unusual performance variations have been noted during windy periods. However, the power station plans to study a more optimal arrangement, as this area is in a valley with high wind occurrence as noted by the preponderance of wind turbines installed just to the north of the plant.

**Figure 19: Gateway ACC With “Fan Deck” Windscreen—“One Bay In”**



## **2.5 Caithness**

The Caithness Energy Center is a 350 MW gas-fired, combined-cycle plant in a 1 x 1 configuration. The ACC is an 18 cell unit with three streets and six rows. Figure 20 shows an aerial view of the site with the ACC centrally located near the west boundary. The plant came on line in August, 2009.

**Figure 20: Caithness Energy Center Site Aerial View**



Figure 21 shows the windscreen which extends downward from the fan deck. The screen is located at the perimeter of the ACC as opposed to the “one-bay-in” arrangement described for the Gateway ACC.

The screens at Caithness can be retracted in the event of very high (hurricane force) winds which, with the screens deployed, might exceed the structural limit of the ACC. The screens themselves are designed for 120 mph wind speed. To our knowledge, this is the only installation in the US with retractable screens. For this reason, this site was selected for field testing as a part of the current study since comparative data with the screens fully retracted, fully deployed and at intermediate positions could be obtained. A more detailed description of the site, the ACC and the windscreen will be provided in Chapter 4 of this report.

**Figure 21: Caithness ACC with “Fan Deck” Windscreen at Perimeter**



## **2.6 Power Plants in England**

Several power plants in England have been retrofitted with wind screens for the purpose of improving thermal performance and mitigating physical stress on the ACC's mechanical components from wind. Aerial views of the two plants are given in Figures 22 (Coryton) and 24 (Kings Lynn).

Coryton is a gas-fired, combined-cycle plant in a 2 x 1 configuration with a capacity of approximately 750 MW. It is located in southeast of England. It came on line in 2002 and was retrofitted with windscreens in 2004.

The ACC is a 40 cell unit arranged in 8 streets with 5 cells per street. The screens were installed on the full perimeter of the ACC extending down from the fan deck. The inlet is 60 feet tall. The screens on the SW side extend down 50 feet from the fan deck. The two modules on the NW and SE sides extend down 26 feet from the deck all other cells extend down 13 feet from the deck. While no detailed measurements of wind flow patterns under or around the ACC were made, comparisons of turbine exhaust pressure before and after the installation of the windscreens over a range of wind speeds from similar directions with the plant operating a full load were made. The results are shown in Figure 23.

The installation of the windscreens resulted in a reduction in turbine exhaust pressure and a corresponding increase in turbine efficiency at wind speeds above about 5 km/h (~ 3 mph) for winds from directions from the southeast to the west (~ 110° to 290° where 180° designates a southerly wind). At 30 km/h (~ 18 mph), the turbine exhaust pressure at full load was reduced

by .015 bar (~ 0.44 in Hga). At wind speeds below 5 km/h (~ 3 mph) there is a slight increase in turbine exhaust pressure corresponding to a slight disbenefit to turbine performance.

**Figure 22: Coryton Aerial View**



Kings Lynn, shown in Figure 24, is a gas-fired, combined-cycle plant in a 1 x 1 configuration with a capacity of approximately 325 MW. It is located in central England near the east coast. It came on line in 1997 and was retrofitted with windscreens in 1998.

The ACC is a 16 cell unit arranged in 4 streets with 4 cells per street. The screens were installed in a cruciform pattern underneath the ACC extending from grade level up to the fan shroud. One screen ran the length of the ACC between streets 2 and 3; the other ran across the ACC underneath Row 3. The screens were installed to improve thermal performance issues, and the cruciform arrangement was chosen by the customer. While no detailed measurements of wind flow patterns under or around the ACC were made, comparisons of turbine exhaust pressure

before and after the installation of the windscreens over a range of wind speeds from similar directions with the plant operating a full load were made.

**Figure 23: Effect of Screens at Coryton**

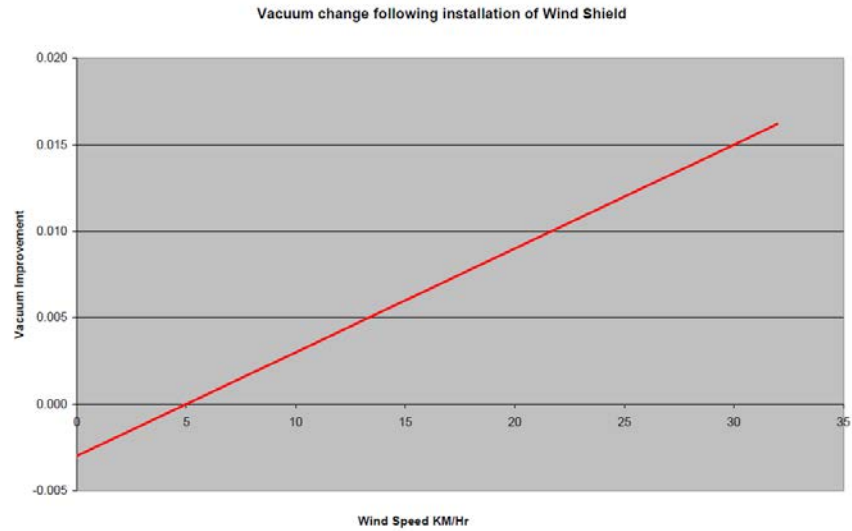


**Figure 24: Kings Lynn Aerial View**

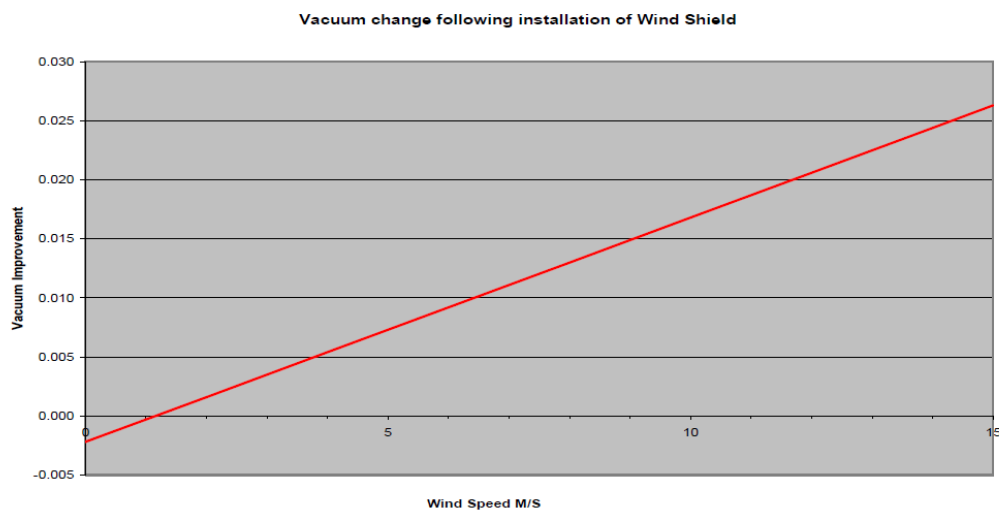


The installation of the windscreens resulted in a reduction in turbine exhaust pressure and a corresponding increase in turbine efficiency at wind speeds above about 1 m/s (~ 2.2 mph) for winds from directions from the southeast to the west (~ 110° to 290° where 180° designates a southerly wind). At 15 m/s (~ 34 mph), the turbine exhaust pressure at full load was reduced by

.026 bar (~ 0.77 in Hga). At wind speeds below about 1 m/s (2.2mph) there is a slight increase in turbine exhaust pressure corresponding to a slight disbenefit to turbine performance. The results are shown in Figure 25.

A few years after the screens were installed they were moved toward the windward side. Smoke testing was also done to determine the airflow patterns and to determine if further performance improvements could be achieved. The smoke testing showed that the perimeter fans on the windward sides were not moving the smoke filled air into the fans. In 2011 the wind screens were modified further, and motorized wind screens were added on the perimeter at the windward end and fixed perimeter screens were added on the two other sides. The cruciform screens were also replaced as they had been damaged during some unrelated maintenance activity. Some improved thermal performance was noted as well as a reduction in mechanical equipment maintenance costs. Other UK installations, such as Spalding, had OEM supplied cruciform solid wind walls augmented with fixed perimeter screens to improve performance and to reduce maintenance costs of gear reducers and motors.

**Figure 25: Effect of Screens at Kings Lynn**



## 2.7 Power Plants in Mexico

A power plant in Mexico, San Luis de la Paz has experimented with a wide variety of combinations of wind screens and wind barriers. An aerial view of the plant site, showing the “three street” ACC closely bounded by other plant structures, is shown in Figure 26.

**Figure 26: Aerial View of San Luis de la Paz Dry Cooled Power Plant**



Figures 27 through 30 show the variety of wind mitigation approaches that were investigated. While no specific data on the relative effectiveness of the different approaches are available, some improvement in thermal performance and reduction in mechanical stress are believed to have been achieved.

**Figure 27: Wide Field View of Various Wind Mitigation Devices**



**Figure 28: Close-Up of Perimeter Screens and Louvers**

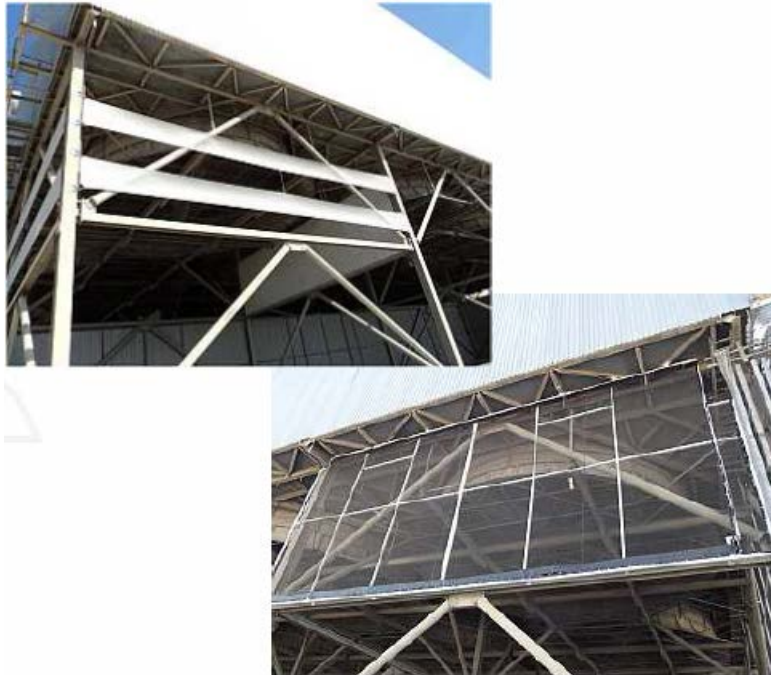


**Figure 29: Close-up of Perimeter Screen and Cruciform Barrier Wall**



**Figure 30: Close-up of Barrier Walls: Up From Ground and Down From Fan Deck**



## **2.8 Power Plants in Canada**

North Battleford is a natural gas fired power plant located in the province of Saskatchewan in Canada. A ten cell ACC at North Battleford shown in Figure 31 was fitted with perimeter screens. The location of the ACC on the plant site is shown in Figure 31.

**Figure 31: ACC With Screens at North Battleford**



The screens were installed in response to undesirable levels of vibration measured on the fan motors which had resulted in frequent motor trips. Figure 33 shows the effectiveness of the screens in reducing the wind speeds under the ACC over a wide range of wind speeds. Figure 34 shows the resultant reduction in vibration levels. It is reported that the occurrence of fan motor trips has been eliminated.

**Figure 32: North Battleford Site Plan**

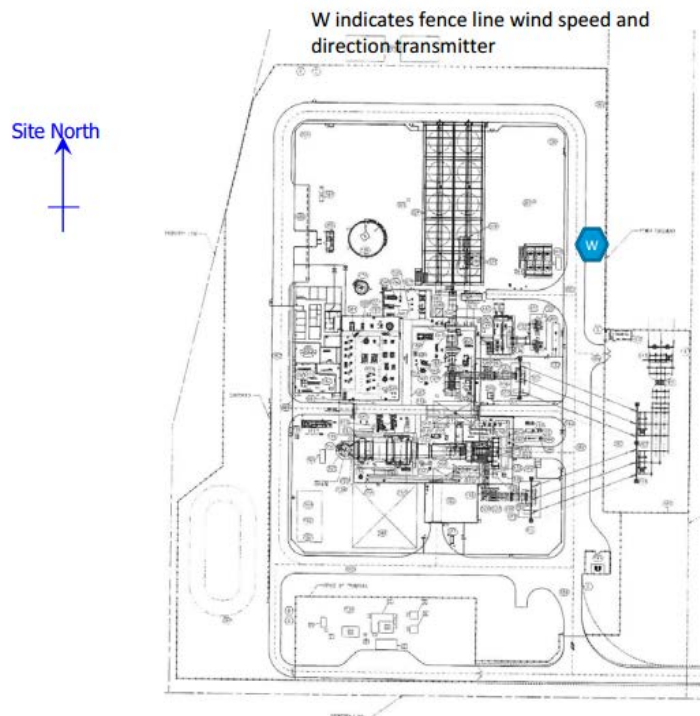


**Figure 33: Velocity Reduction With Wind Screens**

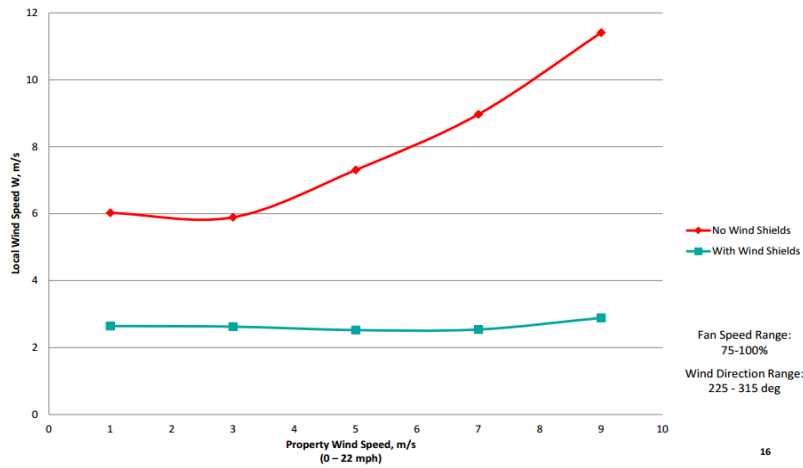
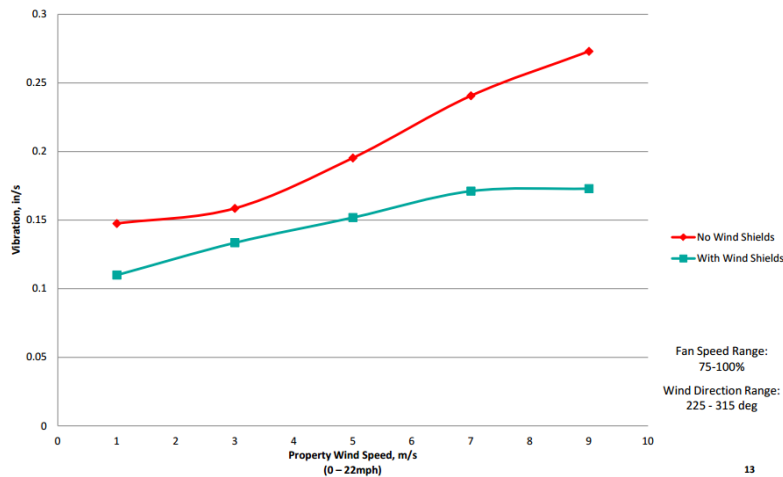


**Figure 34: Vibration Reduction With Screens**



## 2.9 SPX Louver Concept

An alternative approach to the mitigation of wind effects was tested by SPX (2010) under USDOE sponsorship. Figure 35 shows the installation of a louver arrangement on an ACC at Black Hills Power and Light's WyGen III unit.

The concept involved a slanted "lip" extending outward from the bottom of the windwall to divert the downdraft coming off the windwall which can act as a wind curtain preventing incoming horizontal airflow from turning into the fan inlets on the windward side of the ACC and a louver located in the open air inlet area of the ACC turned upward to direct incoming air at that level up toward the fan inlets.

The effect of this arrangement was to provide a slight increase in ACC thermal performance in the turbine exhaust pressure over a range of wind speeds as shown in Figure 36 and a corresponding slight decrease in turbine exhaust pressure in Figure 37.

**Figure 35: ACC With Louvers at WyGen III**

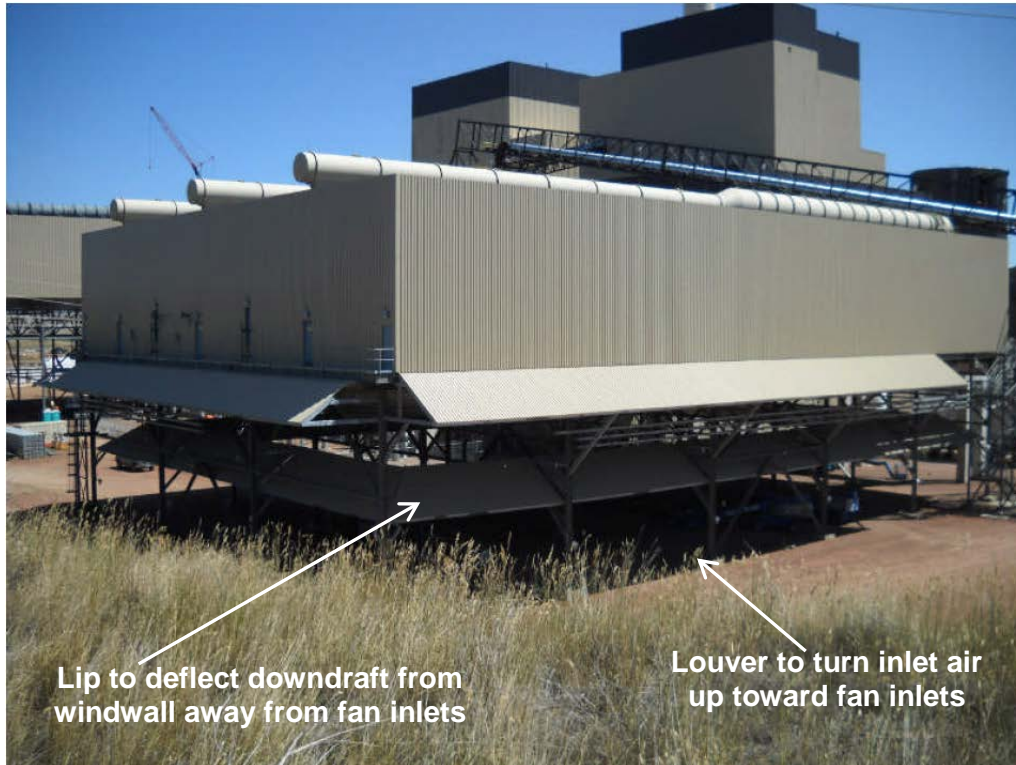


**Figure 36: ACC Thermal Performance Comparison**

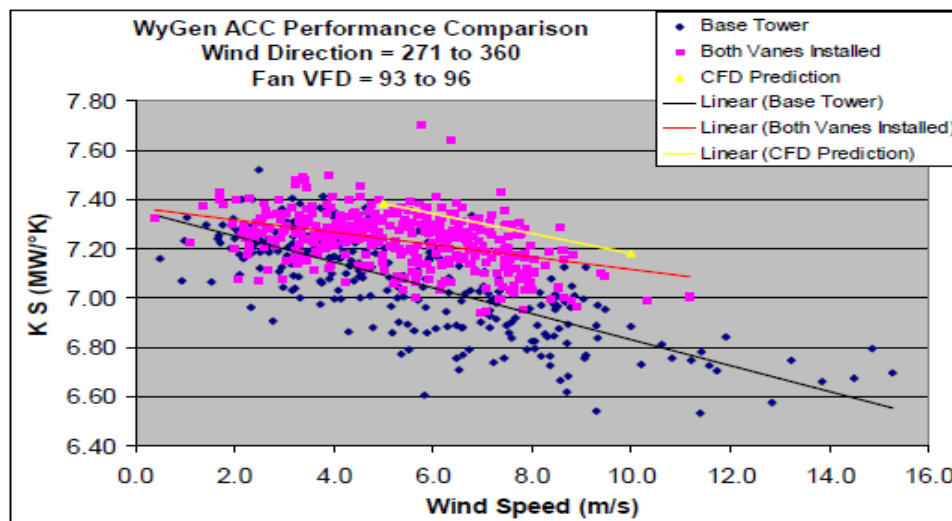
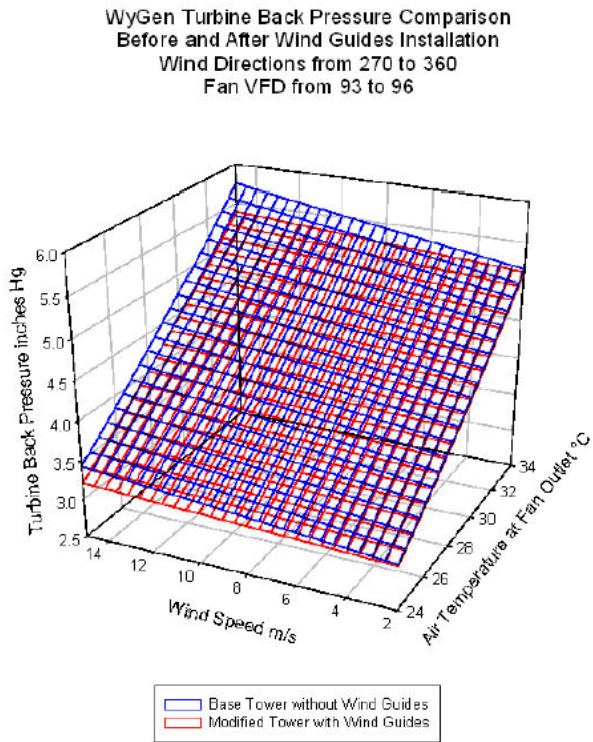


**Figure 37: Reduction in Turbine Exhaust Pressure**



## **Chapter 3: Prior Work**

### **3.1 General**

A number of studies have been conducted on the effect of wind on ACC thermal performance and fan stress. Some the earlier work is reported in Duvenhage and Kröger (1996) and discussed briefly by Maulbetsch and DiFilippo (2006). More recent work, of particular relevance to this study, consists of three separate but coordinated studies of the effect of wind on the ACC at Desert Star (formerly El Dorado). The ACC and the site are described earlier in this report in Section 2.2

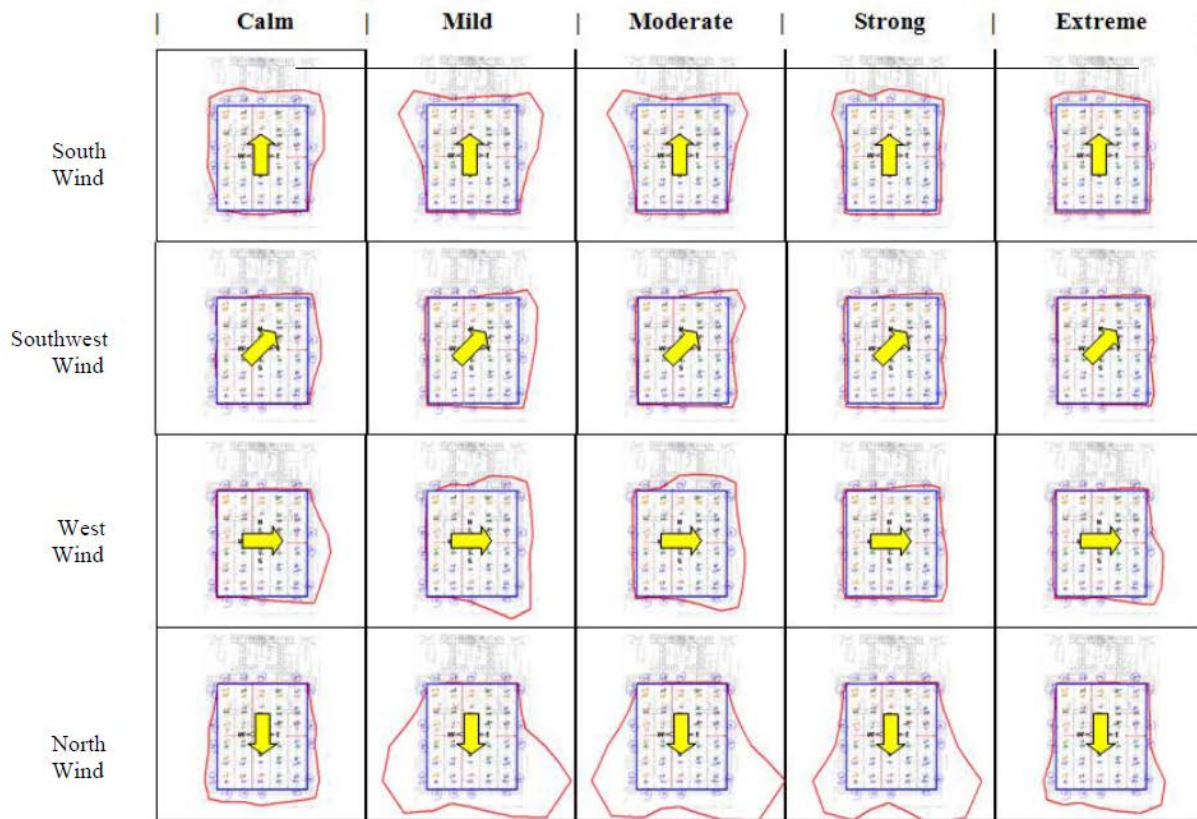
The studies included field testing by Maulbetsch and DiFilippo (2013), physical modeling by University of California at Davis (Kim et al. 2011) and computational fluid dynamic modeling (CFD) by the Kroger and Owen (2011).

The windscreen was installed at the time the field tests were held, so no direct measurement of the effect of the presence of the screens on ACC performance could be measured other than what is inferred from the results shown in Figure 14. Similarly, the wind tunnel tests, while including tests of alternative wind protection schemes, did not test the ACC with no wind protection screens or barriers of any kind in place. The CFD analyses did include cases with no windscreens and indicate a significant effect on the wind flow patterns under and around the ACC and some effect on ACC thermal performance and turbine exhaust pressure. The information of most relevance to this study is the degree to which the results of the field tests, the physical model tests and the CFD model results showed similar trends with wind conditions.

### **3.2 Recirculation Patterns**

The emphasis of the physical model study was the measurement of recirculation patterns for a range of wind speeds over a full set of incident wind directions. The results are indicated schematically in Figure 38. Qualitative comparisons can be made with field measurements as illustrated in Figure 3.2. Measurements of inlet temperatures for each cell at the El Dorado ACC on June 30, 2005 showed high recirculation in Cells 1 and 2 (downwind corner), moderate recirculation in Cells 4, 5 and 6 (crosswind side) and some recirculation in Cells 11, 12 and 24, which is qualitatively similar to the patterns shown in Figure 38 for the grouping of conditions of “moderate” to strong” wind speeds from “south” and “southwest”. There was no indication of recirculation in Cell 25 in the wind tunnel results. Similar comparison at different wind speeds and for different wind directions often, but not always, showed reasonable qualitative agreement.

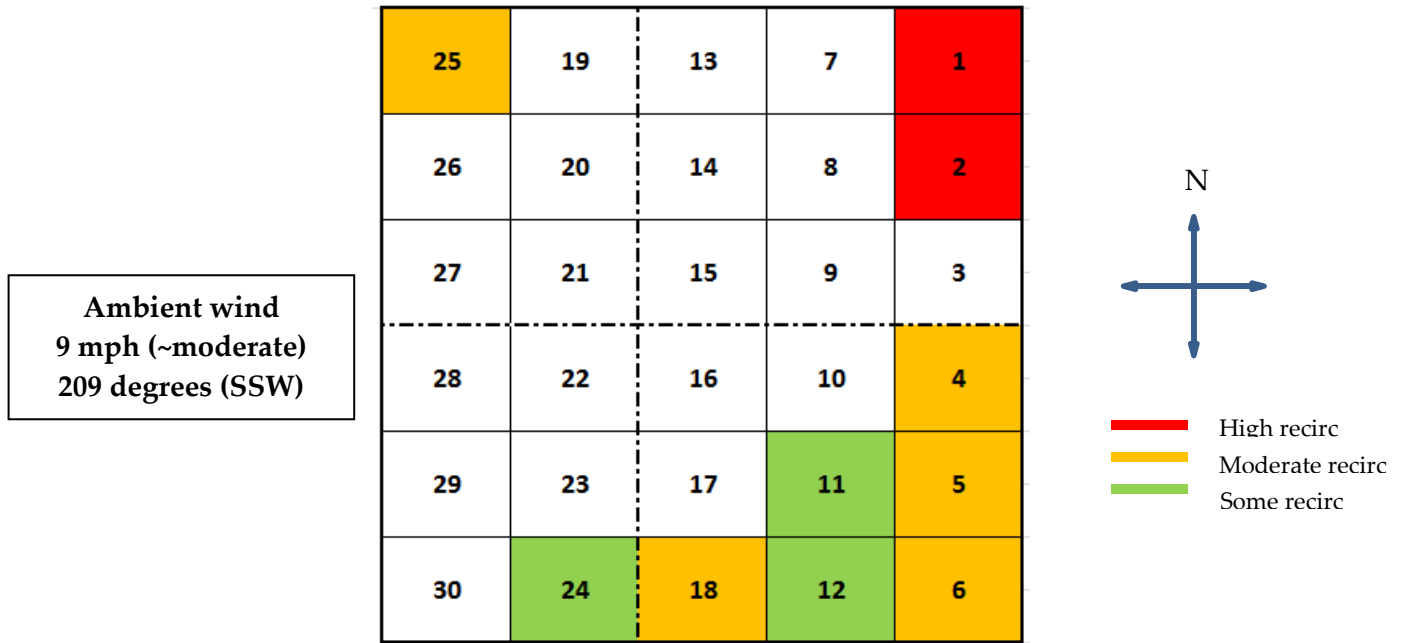
**Figure 38: Recirculation Patterns Measured in ABL Wind Tunnel**



Source: Kim et al. 2011

More general comparisons can be made which demonstrate good correspondence in the trends of recirculation versus wind speed and direction between the field measurements and the wind tunnel tests. The schematics in Figure 38 can be interpreted as giving an estimate of the overall or total recirculation in addition to the distribution of recirculation around the perimeter of the ACC. The area between the rectangular blue lines showing the outline of the ACC and the curved redlines showing the magnitude of the recirculation at each point around the periphery is a rough indication of the total or average recirculation. Viewed this way, it appears that, while shifts in wind direction at a given wind speed have a discernible effect on the distribution of recirculation around the ACC, the average recirculation does not show a compelling dependence on wind direction with the exception of winds from the north. The significant increase in recirculation with winds from the north is presumably due to strong disturbances of the incoming wind as it passes over the large plant structures of the turbine building and the heat recovery steam generators located directly north of, and close to, the ACC.

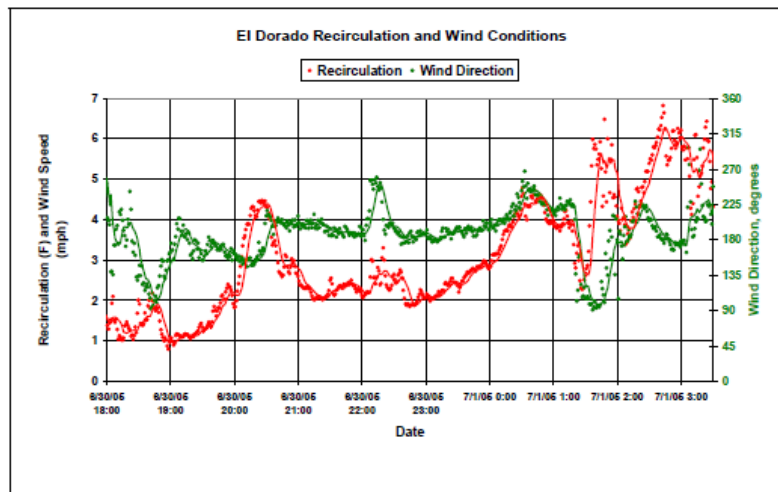
Figure 39: Field Measurements Compared to “Moderate/Southwest”



Source Maulbetsch and DiFilippo 2013

The absence of a strong correlation between recirculation and wind direction in the field measurements is shown in Figure 40. The singular effect of northerly winds was not apparent from the field measurements, but there were virtually no occurrences of northerly wind during the entire test period.

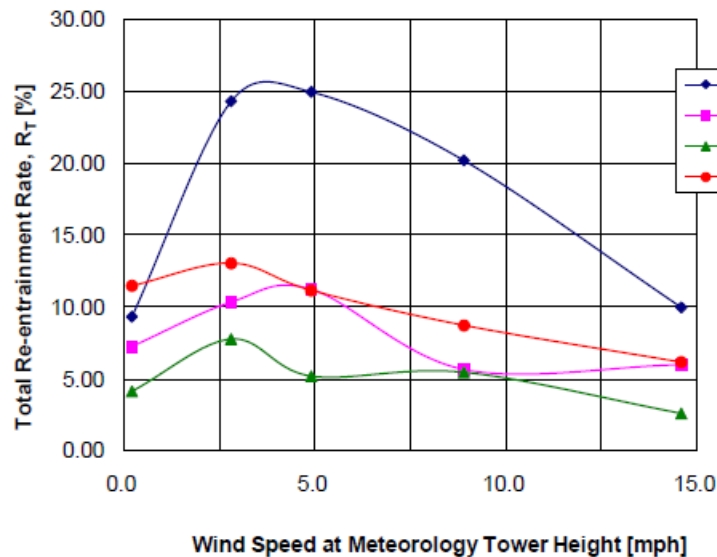
Figure 40: Recirculation and Wind Direction Measurements at El Dorado



Source Maulbetsch and DiFilippo (2013)

The effect of wind speed on average recirculation is more interesting. The schematics in Figure 38 indicate, for all wind directions, an increase in recirculation with wind speed from “calm” to “moderate” followed by a decrease from “moderate” to “extreme”. Specific confirmatory plots from the wind tunnel measurements are shown in Figure 41.

**Figure 41: Re-Entrainment vs. Wind Speed in Wind Tunnel**



Source: Kroger and Owen (2011)

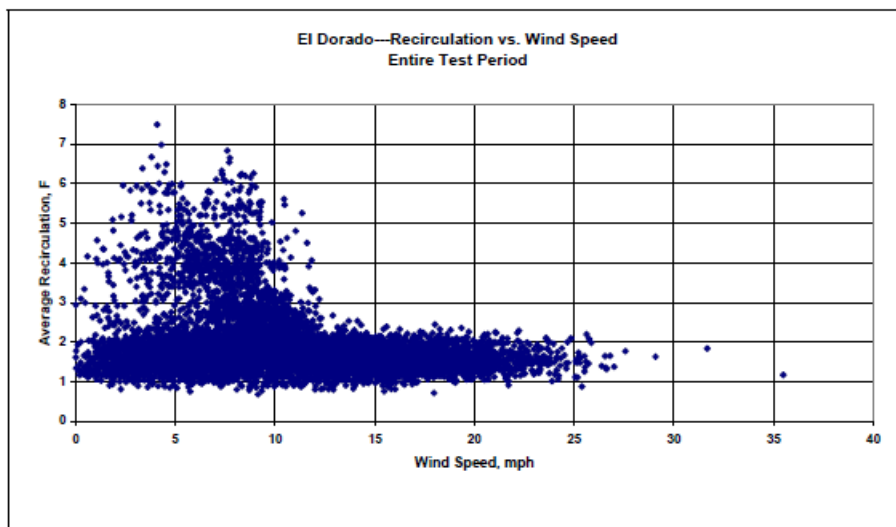
Figure 42 shows the average recirculation vs. wind speed for all wind directions as measured in the field at El Dorado. Although the peak persists to higher wind speeds in the field measurements, the general trend of the data is identical. It is noteworthy that related CFD measurements performed for the El Dorado site (Kroger & Owen 2011) did not show this trend but rather predicted an increasing recirculation with increasing wind speed and postulated a different explanation for the peak at low to moderate wind speeds. This discrepancy will be discussed in the following section.

## 3.2 Computational Analysis

CFD analyses were conducted at the University of Stellenbosch and reported in Kroger & Owen (2011). The model of the ACC unit itself replicated the dimensional and configurational aspects of the El Dorado ACC including the number of cells, the arrangement into streets and rows, the cell dimensions and the height above the ground. The several elements of the ACC were modeled separately. Each ACC cell model included a fan/fan shroud model, a heat exchanger model and a plenum chamber. The fan and shroud dimensions were those of the actual unit. The heat exchanger was modeled as a rectangular, porous element mounted horizontally above the fan on top of a rectangular plenum chamber with vertical sides instead of the sloping, A - frame sides of the actual unit. The effect of modeling the actual A - frame heat exchanger with this simplified representation was found to have a negligible effect on the numerically predicted

ACC fan performance, and it did not significantly affect the nature of the flow in the vicinity of the ACC.

**Figure 42: Re-Entrainment vs. Wind Speed in El Dorado Field Measurements**

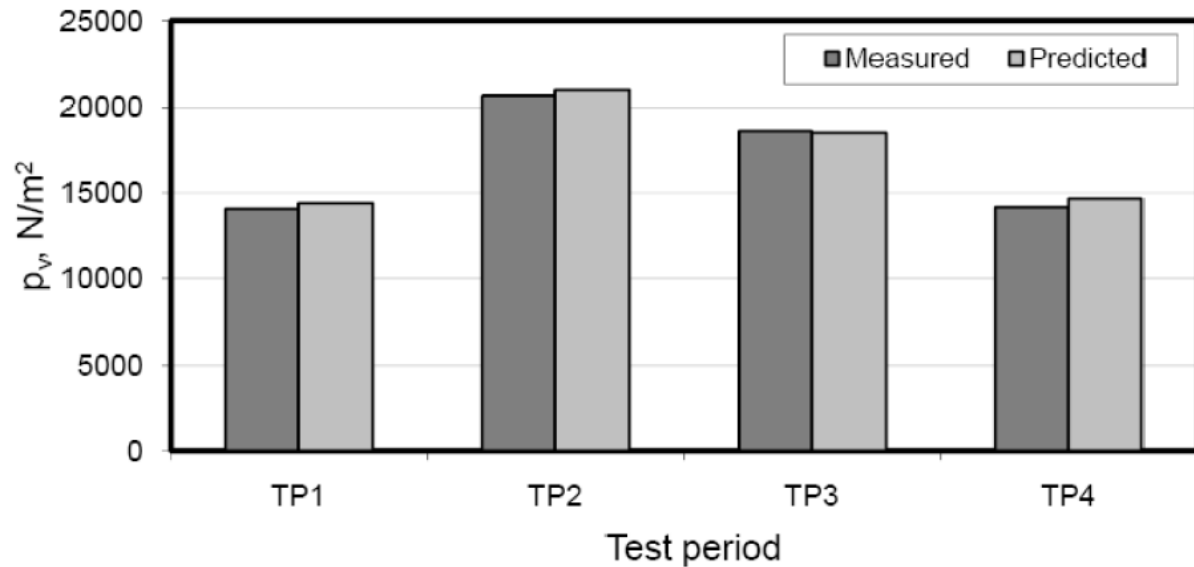


Source Maulbetsch and DiFilippo (2013)

The numerical model of the fan used the “pressure jump” model (FLUENT 2006) calibrated to match the actual fan performance specifications. The heat exchanger model uses FLUENT’s “porous zone continuum” condition (FLUENT 2006) adjusted to match the pressure loss characteristics of the finned tube bundle in the El Dorado ACC. An energy source term was added to the energy conservation equation to account for the heat transfer to the air passing through the condenser.

The model was tested under “ideal”, no-wind conditions with uniform, parallel flow at the fan inlet and no cross-wind to induce recirculation. The agreement between the numerical model results and the theoretically determined values based on El Dorado design information was excellent. The model predictions of the overall ACC performance were made against the measured performance. The chosen performance measure was the steam turbine exhaust pressure at the four operating points. Figure 43 shows the comparison between the data reported from the plant and the field test project and the predicted values of the turbine exhaust pressure for those points.

**Figure 43: Validation of CFD Results Against Plant Data**

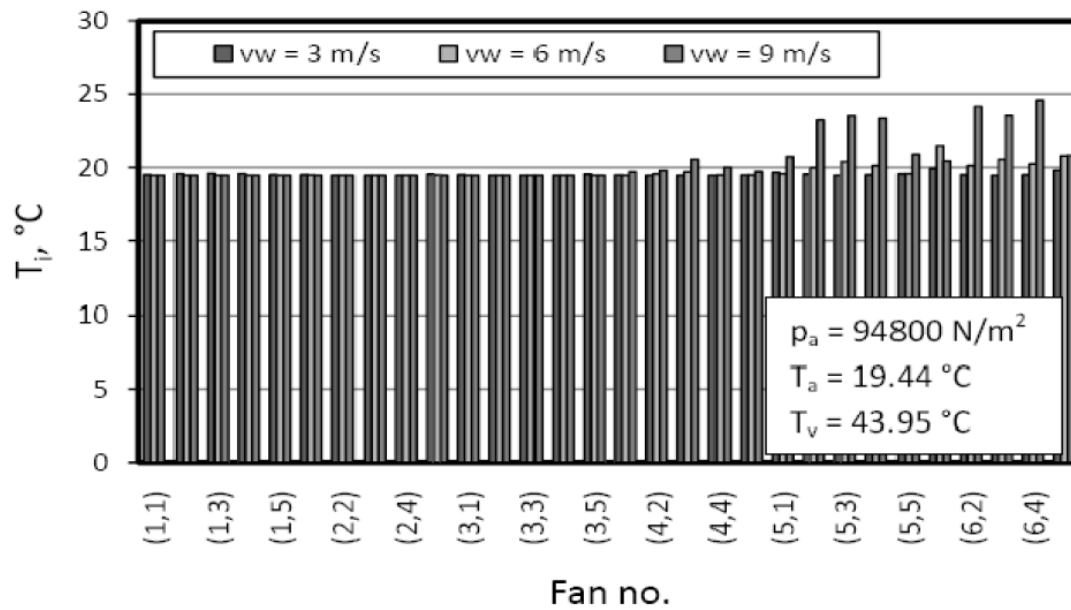


Source: Kroger and Owen (2011)

While the general agreement with plant performance data was excellent, the agreement with the details of ACC operation was explored in order to understand the mechanisms of recirculation and fan performance degradation to determine how the results might be extended to other sites and operating conditions.

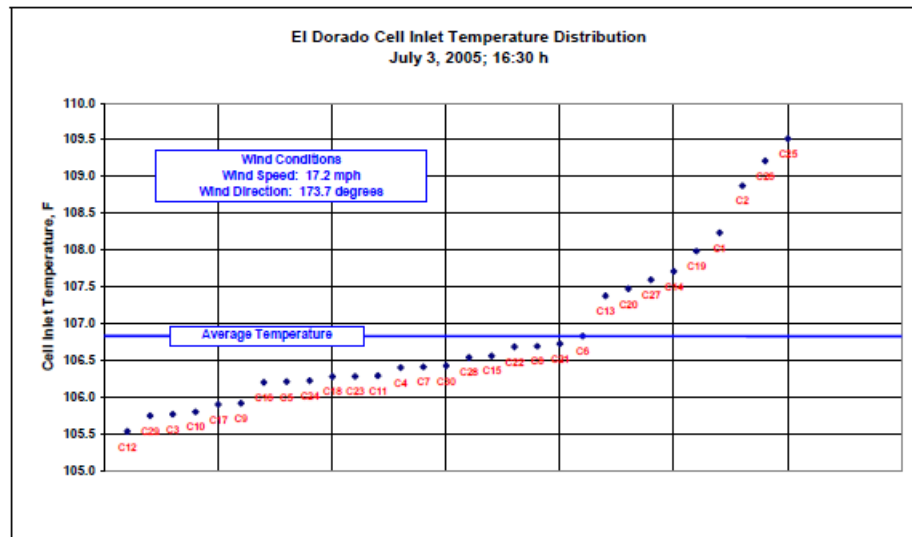
Figure 44 shows the calculated inlet air temperatures to each of the 30 cells for three wind speeds 3, 6 and 9 m/s (6.7, 13.4 and 20.2 mph) and a southerly wind direction. Temperatures above the ambient temperature of 19.44 C indicate recirculation. Figure 44 shows the measured inlet temperatures from field data at conditions a 17 mph wind speed and a nearly southerly wind direction of 173.7°. Figure 45 displays the comparison between the recirculation patterns predicted by the CFD model and those measured in the field. The correspondence in the general pattern is satisfactory. The magnitude of the inlet temperature due to recirculation in, for example, Cell 25 is measured as 4. F in the field measurements and calculated to be about 1 C (1.8 F) at 6 m/s (13.4 mph) and about 4 C (7.2 F) at 9 m/s (20.2 mph). The field measurements at 17.2 mph are at close to 16.8 mph which is the average wind speed of the two calculated inlet temperatures. The average of the two inlet temperatures is 4.5 F and the agreement is considered satisfactory.

Figure 44: CFD Predicted Cell Inlet Temperatures <sup>1</sup>



Source: Kroger and Owen (2011)

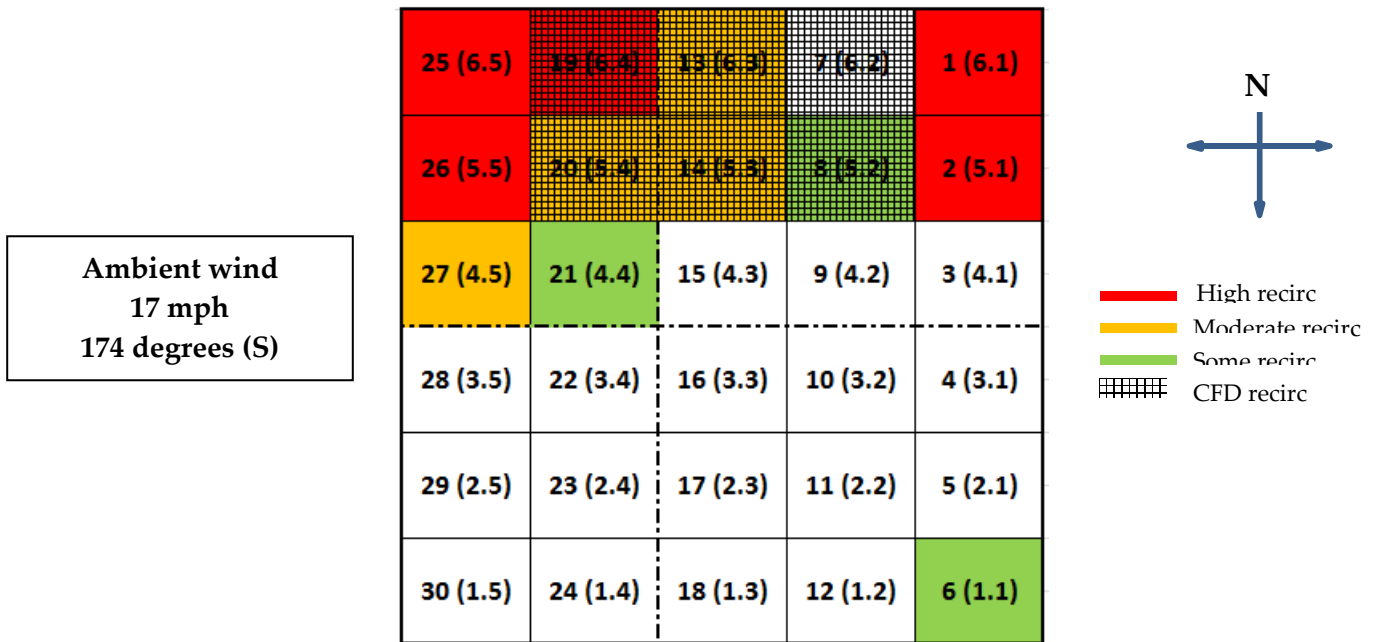
Figure 45: Inlet Air Temperature Measurements From Field Tests at El Dorado



Source: Maulbetsch and DiFillipo 2013

<sup>1</sup> Note the different cell numbering convention. Corresponding designations are shown in Figure 46 below.

Figure 46: Comparison of Field Measurements and CFD Predictions of Recirculation



# CHAPTER 4:

## Approach

### 4.1 Introduction

The study adopted a three-pronged approach to obtaining the information and analyzing it in order to understand the means by which wind barriers mitigate the effect of wind on ACC performance and fan blade stress level. The three elements were field testing, physical modeling in a wind tunnel and mathematical simulation using computational fluid dynamics (CFD) methods. The field tests were used to guide calibrate and validate the physical and computational models; the models in turn, when validated, were used to develop guidance for the specification design and installation of wind barriers and other sites. The equipment and methodology for the conduct of the field test, the physical modeling and the CFD modeling are described in the following sections.

### 4.2 Field Testing

Field testing was conducted with the two objectives of (1) determining the effect of windscreens on ACC airflow and performance and (2) obtaining direct measurements of fan blade vibrations and stresses and how they are mitigated by windscreens.

The tests were conducted at the Caithness Energy Center. It was selected since it is the only ACC in the US of which we are aware that is equipped with retractable windscreens enabling comparative tests of the effects of wind on ACC performance and physical stress with and without screens under essentially identical conditions.

**Figure 47: Aerial View of Caithness Site and Surroundings**



Field measurements of site ambient conditions, air temperatures into individual cells, fan inlet velocity distributions, cell static pressure levels, motor currents and stresses on individual fan blades were made on the Caithness ACC under varying wind conditions. Measurements were taken at 65 points continuously for over one year. While data were reported for analysis at one minute intervals, they were actually recorded at 4 millisecond intervals and archived for high resolution examination if desired.

The measurements were adequate to:

- Characterize the ambient wind conditions at the site,
- Measure the air temperature at the inlet to each cell and at other selected locations,
- Measure the air velocity distribution approaching and crossing the inlet air plane of selected cells,
- Determine the wind patterns at selected locations under and on the perimeter of the ACC,
- Measure the static pressure distribution under selected cells, measure the fan motor current in selected cells and
- Monitor the varying stresses on the individual fan blades of one fan.

A schematic of the instrumentation at the 65 measurement points is given in Figure 49.

Appendix A contains a detailed description of the instrumentation and data acquisition system.

#### 4.2.1 Plant Data

In addition to the data obtained from project instrumentation, data at one minute intervals were collected from the Caithness control room on:

- Plant output (gross)
- Steam turbine output
- Steam turbine exhaust pressure
- Steam flow to the ACC
- Fan status for all 18 fans individually (2 = full speed; 1 = half speed; 0 = off)
- Site meteorological data<sup>2</sup>, which includes
- Temperature
- Wind speed
- Wind direction

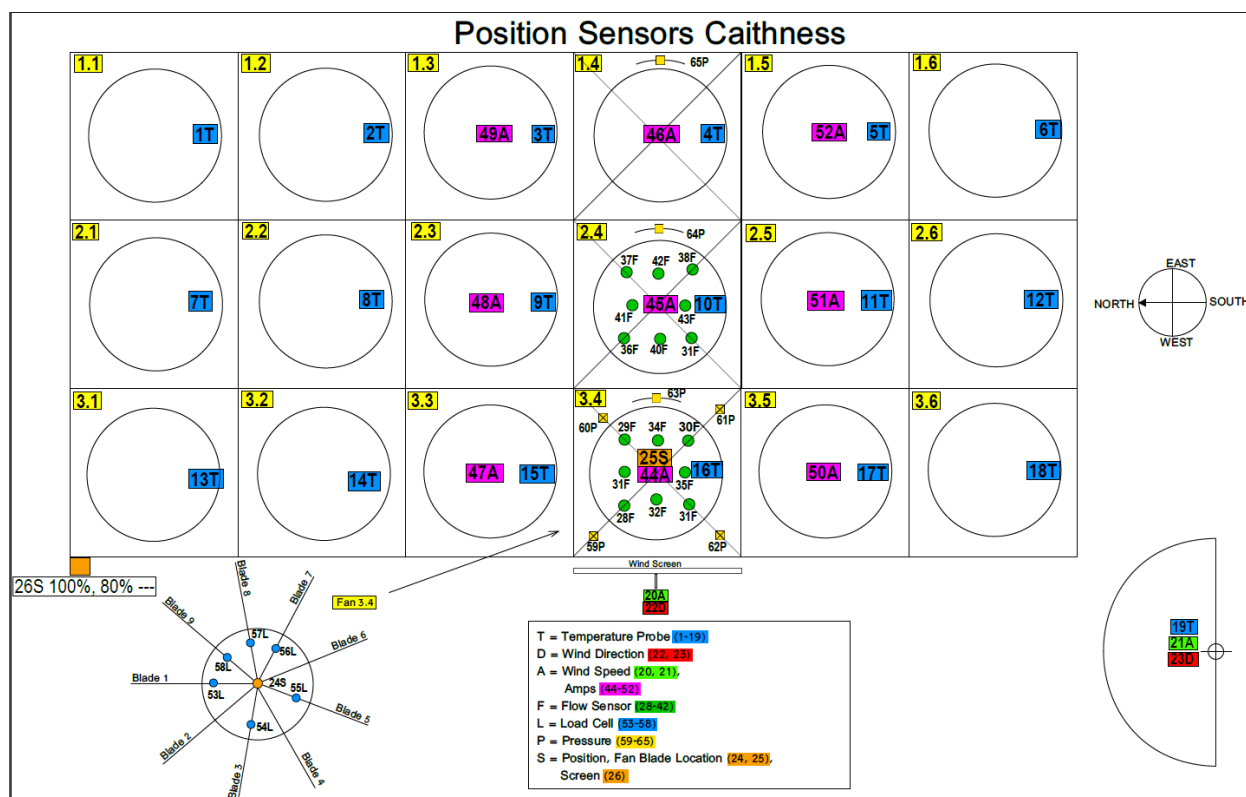
---

<sup>2</sup> Measured at the top of the gas turbine building as shown in Figure 48.

**Figure 48: Close in Aerial View of Caithness Site, ACC, and Other Structures**



**Figure 49: Schematic of Instrumentation and Measurement Points**



#### 4.2.2 Airport Weather Data

Meteorological data were also obtained from National Weather Service Centers at two neighboring airports (Shirley and Brookhaven). The locations in relation to the plant are shown in Figure 50.

### 4.3 Physical (Wind Tunnel) Modeling

The physical modeling was conducted in the Atmospheric Boundary Layer (ABL) wind tunnel at the University of California at Davis. A schematic of the facility is shown in Figure 51.

A 1:130 scale model of the Caithness ACC and the surrounding site structures was constructed based on dimensions from a CAD/CAM representation of the ACC, shown in Figure 52, and other plant drawings provided by Caithness. A photograph of the model as installed in the tunnel is shown in Figure 53.

The free-stream velocity in the tunnel can be varied up to approximately 4 m/s corresponding to a modeled, on-site wind speed of 10.0 m/s (~22. mph). Wind direction can be varied by rotating the wind tunnel turntable upon which the site model is placed.

Figure 50: Locations of Neighboring Airports

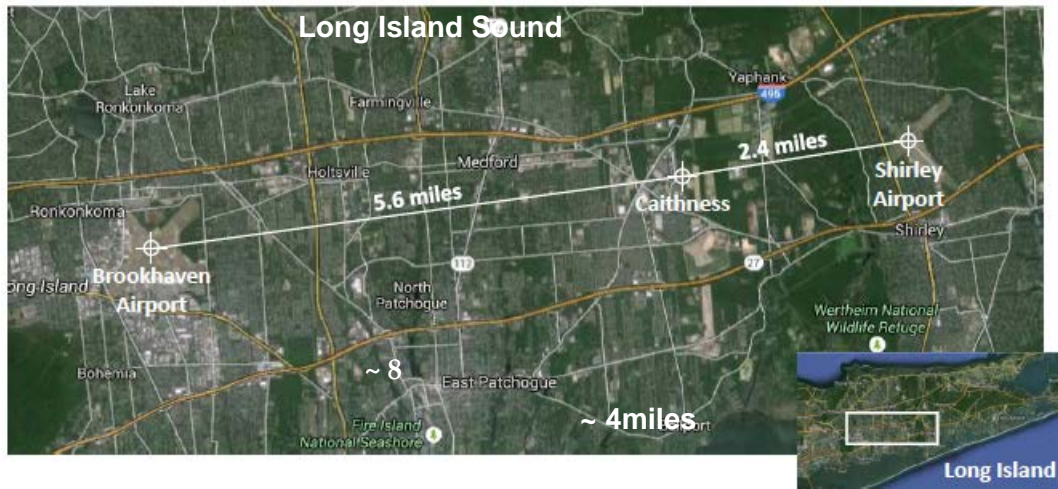
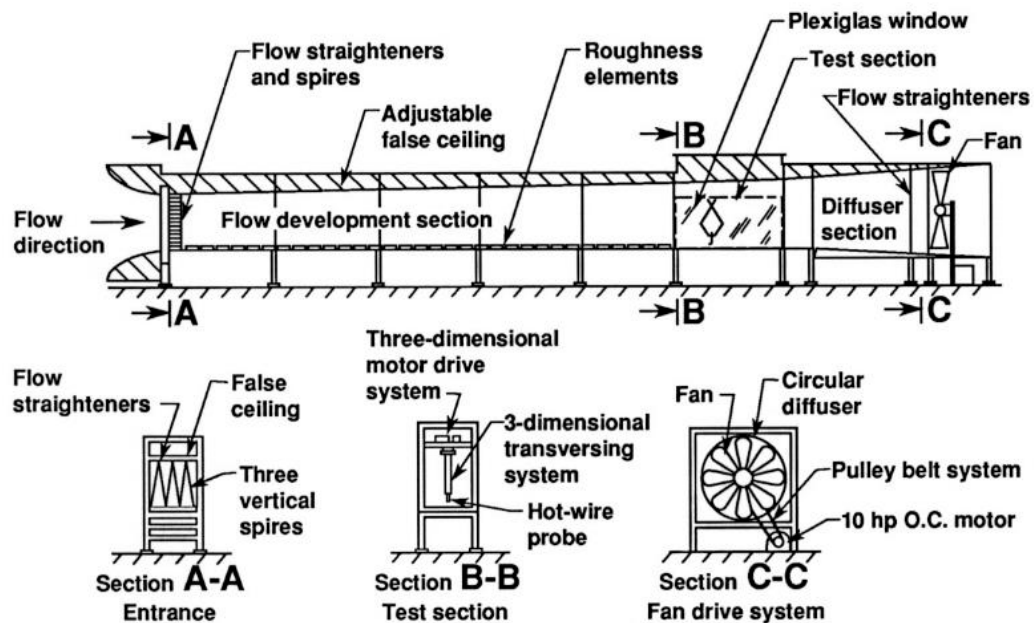
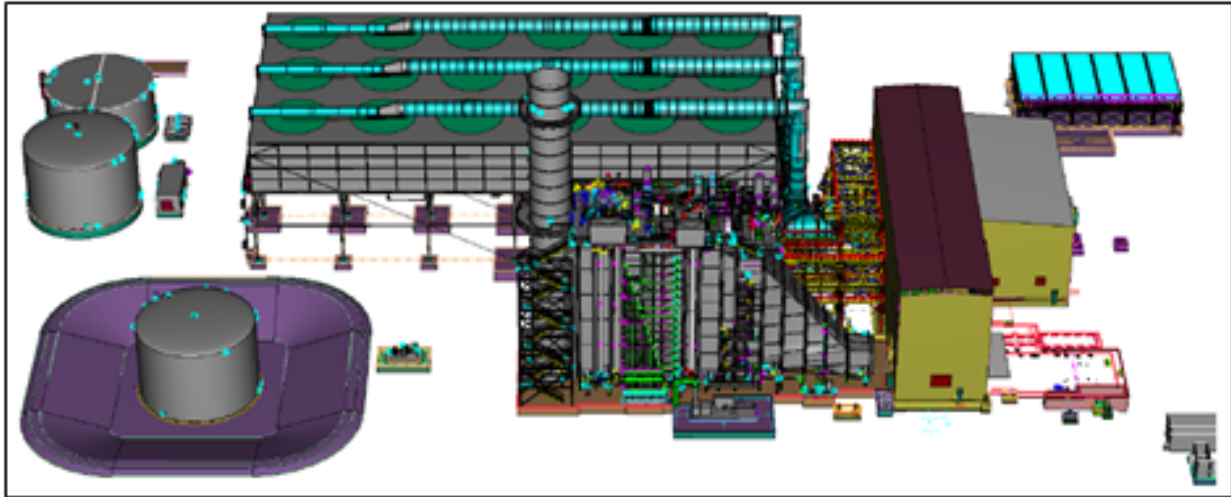


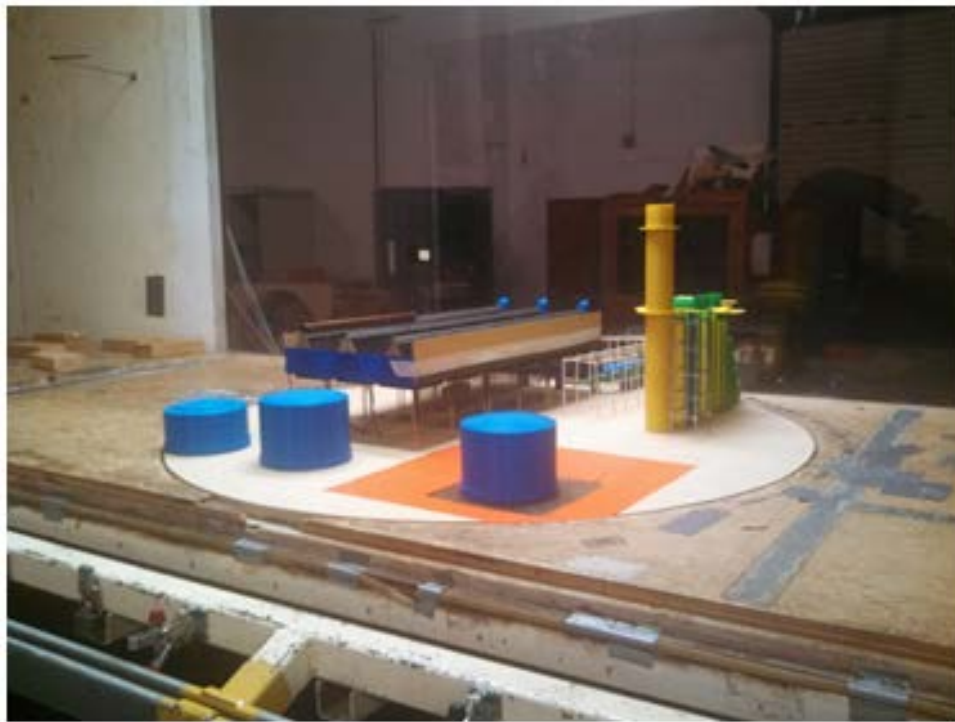
Figure 51: Schematic Diagram of the UC Davis Atmospheric Boundary Layer Wind Tunnel



**Figure 52: CAD Model of Caithness Site**

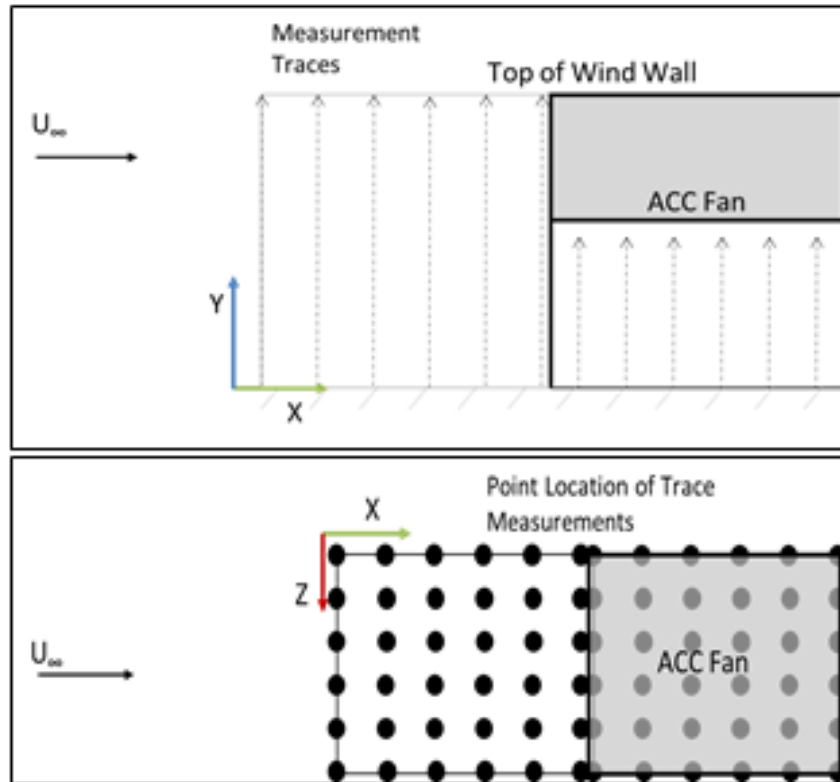


**Figure 53: 1:130 Scale Model Installed in UC Davis ABL Tunnel**



Wind tunnel measurements of mean velocity and turbulence characteristics are made using hot-wire anemometry. The majority of the measurements were taken upwind of and underneath the model at the position corresponding to Row 4 (Cells 3.4, 2.4 and 1.4) of the Caithness ACC where most of the field instrumentation was concentrated. (See Figures 4.2 and 4.3) Figure 54 shows the wind tunnel measurement locations in front of and underneath Cell 3.4.

**Figure 54: Wind Tunnel Measurement Locations**



Measurements were taken with no screens, full screens and partial screens in place. Some supplementary measurements were made in the vicinity of the water tank on which the field wind station was located. (See Figure 48) In addition, video recordings of smoke traces injected upwind of the inlet area to Cell 3.4 were made to provide a visual representation of the flow behavior with and without screens. The results obtained are displayed and discussed in Section 6.

A detailed description of the facility and instrumentation and the data acquisition system is included as Appendix B.

#### **4.4 CFD Modeling**

A computer model of the Caithness ACC and site was constructed including any adjacent structures that potentially had an impact on the ACC flow; specifically, the three fuel/water tanks, the entire HRSG structure with exhaust stack, the generator building, and the control shed below the ACC.

The model of ACC included, in addition to the A-frame heat exchanger bundles and the fans, the surrounding wind walls, deck floor, fan shrouds, steam headers, cell divider walls beneath the A-frames and the wind screens. The support structures, walk ways, fan motors, and stairs were not considered significant aerodynamic elements and, therefore, not modeled. The wind screens

were modeled using the boundary conditions imposed upon the main ACC grid, where the upper portion of the grid contained the wind walls and enclosed the A-frame and fan grids. The dimensions and relative locations of all of these structures and ACC elements were determined using the original site CAD model and architectural site plans.

Models of varying complexity were run:

- The complete, or “Full Site”, Configuration utilized a total of 71 volume grids, with a total of ~40 million grid points. A top view of the surface grids in this configuration is shown in Figure 55. An isometric view of the site geometry is shown in Figure 56.
- A “Reduced Site” configuration represented the minimum geometric components that still represented the site and retained all of the ACC components and eliminated the HRSG, generator building, shed, steam headers and two of the three water tanks. The “reduced Site” configuration utilized 48 million volume grids with a total of 25 million grid points. An isometric view of the grid components in this configuration is shown in Figure 57.
- Single Cell Configuration - Even with the “Reduced Site” configuration, the turn around time required to generate each solution still proved impractical when validating the proper pressure change boundary conditions encountered in the system. Due to the sensitivity of these small changes in pressure on the order of ~10-30 Pa over the screen and ~100 Pa across the fan and A-frames, very small changes had a large effect on the resultant flow rates and behavior through the system. Determining these values accurately were found to be critical in properly modeling the site. So in order to perform a proper parametric study to validate these proper values an even more streamlined approach was necessary.

**Figure 55: Zoomed in Top View of the Overset Surface Grid Components of the Full Site Configuration**

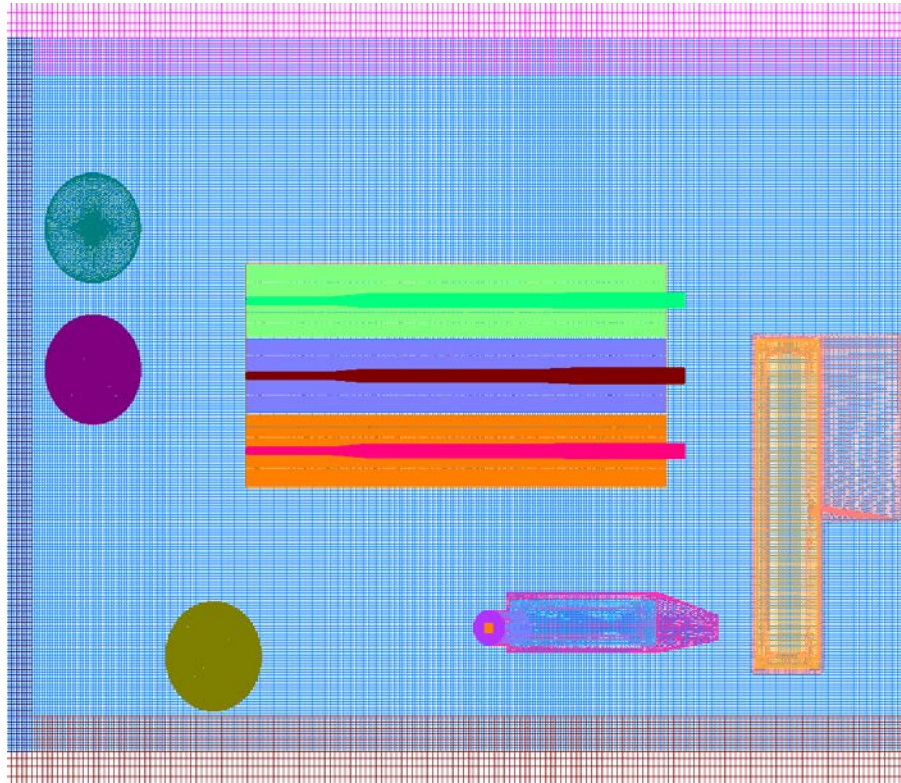


**Figure 56: Surface Geometry of CFD Model of the Plant Site (Full Site Configuration)**

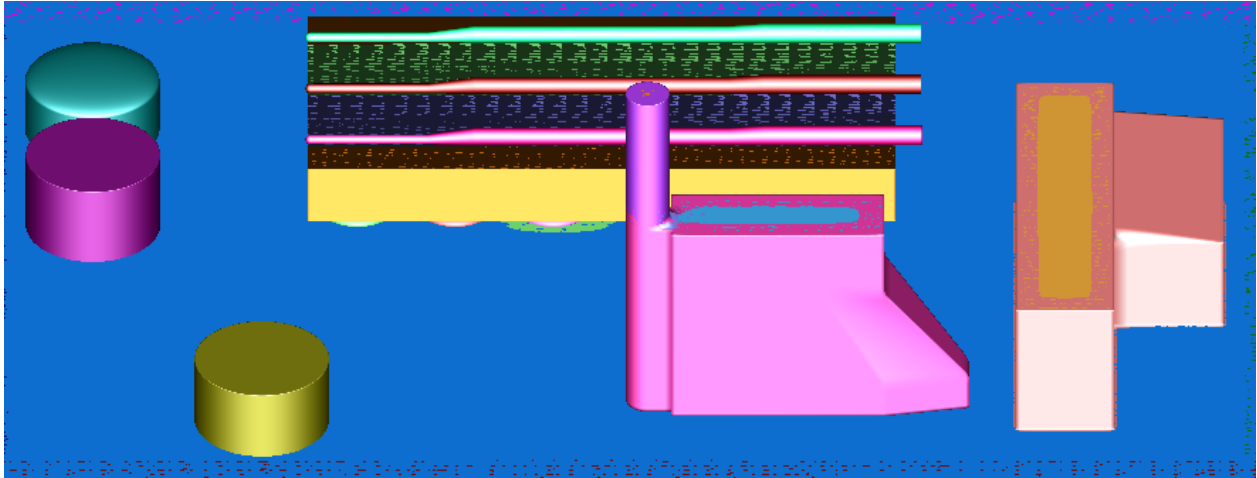
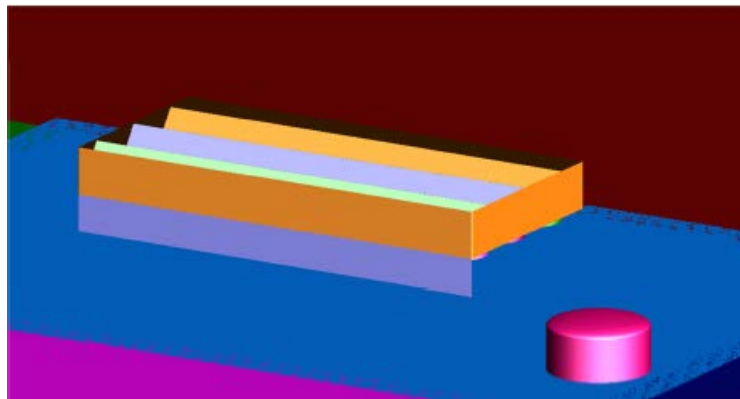


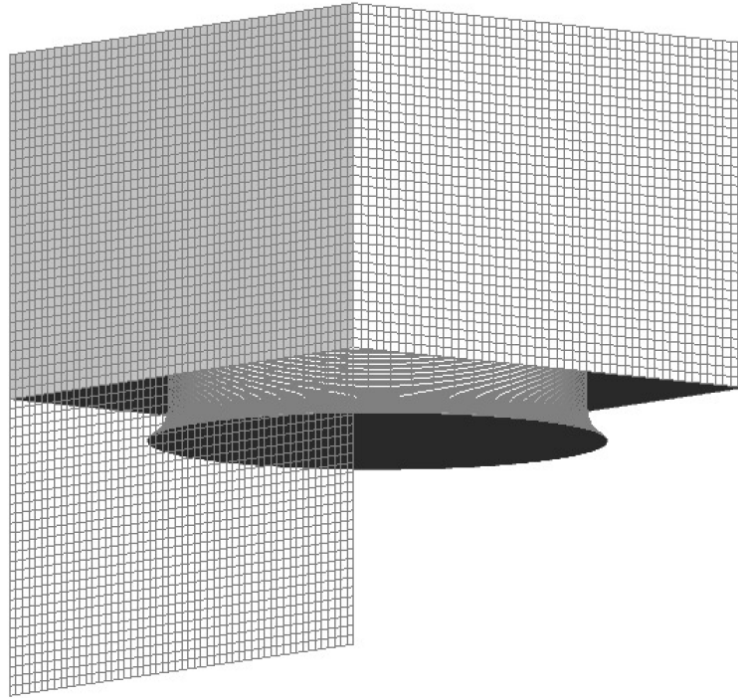
**Figure 57: Surface Geometry of CFD Model of the Reduced Site Configuration**



As in the Reduced Site Configuration, the “Single Cell Configuration” retained the “Full Site” geometry, but all of the surrounding elements were removed, and only a single fan and corresponding sections of a cell and A-frame was retained. While only a single cell’s grid remained, using a periodic boundary condition at the north and south walls of the cell created a domain that effectively represented an infinitely long column of cells. This would more closely resemble the flow around a cell near the middle of an ACC than a single isolated cell in space.

The “Single Cell” Configuration utilized a total of 5 volume grids, with a total of ~1.6 million grid points. This represented only 4 percent of the total problem size of the “Full Site” configuration. A view of the single cell grid is shown in Figure 58.

**Figure 58: Overset Surface Grid Components of the Full Site Configuration**



Results from the CFD work are presented and discussed in Section 6. A detailed description of the approach, format and methodology of the complete CFD model is given in Appendix C.

# CHAPTER 5:

## Field Test Results

The results of the study are presented in three parts: field test results, physical modeling results and CFD results. The field test results are presented in this chapter; the results from the physical and CFD modelling are discussed in Chapter 6.

### 5.1 Field Test Introduction

The field tests were conducted over a 16 month period starting on November 18, 2013 and continuing until the conclusion of the project on March 31, 2015. The individual measurement points were identified in Chapter 4. The data were collected and reported to the Howden data storage facility at 4 millisecond intervals. They were then compressed into one minute averages and distributed to the rest of the study participants. As noted in the previous section, the data analyses conducted by Howden were based on 10 second averages. Plant data were reported at one minute intervals. In addition, readings from the National Weather Service facilities of ambient temperature, wind speed and wind direction at two nearby airports were collected.

The results of these tests will be discussed in the following sections in several separate topical areas. These are:

- The establishment of ambient conditions
- The effect of wind and wind screens on:
  - Fan performance and airflow to the ACC,
  - ACC operating points,
  - ACC thermal performance and,
  - Wind-induced stress on fan blades.

### 5.2 Establishment of Far-Field Ambient Conditions

The important ambient conditions are ambient temperature, wind speed and wind direction. Ambient humidity has a minor effect on airflow and fan power through its effect on air density at constant temperature. However, this effect was deemed to be unimportant in comparison to other effects, was not measured on-site and was disregarded in the data reduction and analysis.

#### 5.1.1 Ambient Temperature

Air temperature is measured on site in three separate locations:

- Under the ACC by the plant with three co-located thermal probes on the support column at the intersection of Cells 1-1, 1-2, 2-1 and 2-2 about six feet above grade. (See Figure 59) The measurements are reported by the plant as a single value.

- On the top of the water tank located at the southwest corner of the ACC at a height of about five feet above the top of the tank (See Figure 60).
- At the inlet to each of the 18 cells with a thermal probe attached to the fan bridge inside the cell (See Figure 61).

**Figure 59: Plant Temperature Probes Under ACC**



**Figure 60: Temperature Measurement on Top of Water Tank**



**Figure 61: Temperature Probe on Fan Bridge Inside Cell (Typical)**



Figure 62 displays a comparison of the temperature readings in all three locations for the 24 hours of August 9, 2014. The “in-cell” reading was taken as the lowest of all 18 inlet temperature readings to eliminate, to the maximum extent possible, the effect of any recirculation on the measured temperature, which would cause it to differ from ambient.

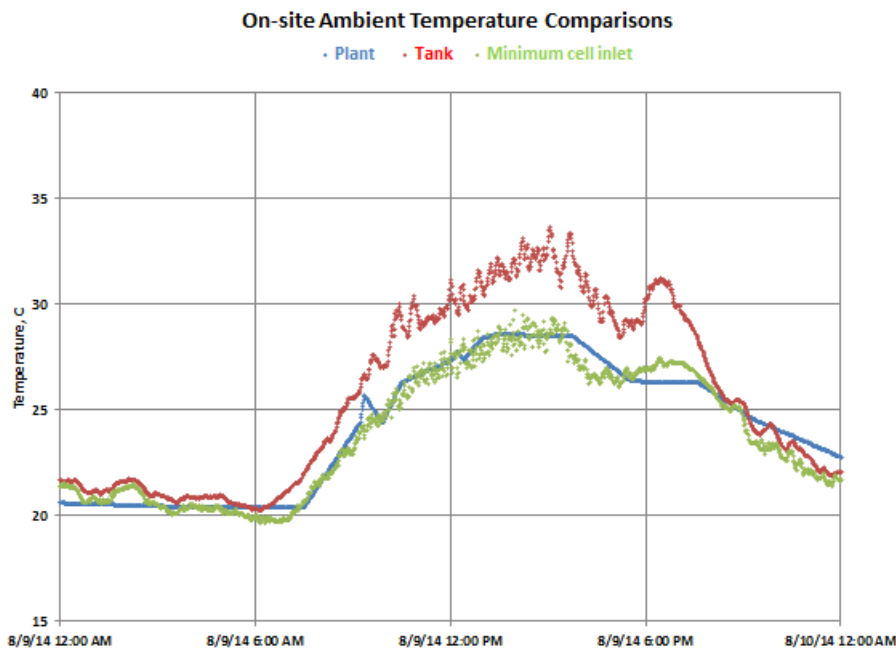
This example, for August 9, 2014, was arbitrarily selected for illustrative purposes, but is fully representative of readings throughout the test period. The “minimum cell inlet” temperature is chosen as the best surrogate for the true “ambient” temperature for the following reasons.

- The plant readings, while generally consistent with the “minimum cell inlet” readings appear to have been smoothed in some way and do not show the short term fluctuations seen in both the tank and the in-cell readings.
- The tank readings appear to be influenced by solar radiation. They are quite consistent with the in-cell readings during the nighttime hours but diverge to substantially higher readings when the sun rises in the morning, returning to good agreement at sunset.

- The in-cell readings are shielded by the cell walls from direct solar incidence and the ambient air is drawn over the probes at high velocity which minimizes the influence of any radiative effect from the condenser bundles which are higher than the inlet temperature since they are rejecting heat to the air stream.

Therefore, all references to “ambient temperature” in the future discussions of the field data should be understood to mean the lowest of the inlet air temperature readings in each of the 18 cells.

**Figure 62: Comparison of On-Site Temperature Measurements**



### 5.1.2 Wind Speed and Direction

The on-site measurements of wind speed and direction are taken in three locations:

- Plant measurements are made with the plant wind station located on the top of the turbine building at the west end of the roof line (See location in Figure 48 and close-up in Figure 63).
- Project measurements were taken with directional propeller anemometers....one on the top of water tank at the southwest corner of the ACC (Figure 60) and on the west side of Cell 3.4, mounted on the upper, exterior structural beam in line with the center of the cell. (Figure 64) This is approximately at the level of the bottom of the windscreen when the screen is fully deployed.

**Figure 63: Plant Wind Vane on Top of Turbine Building**



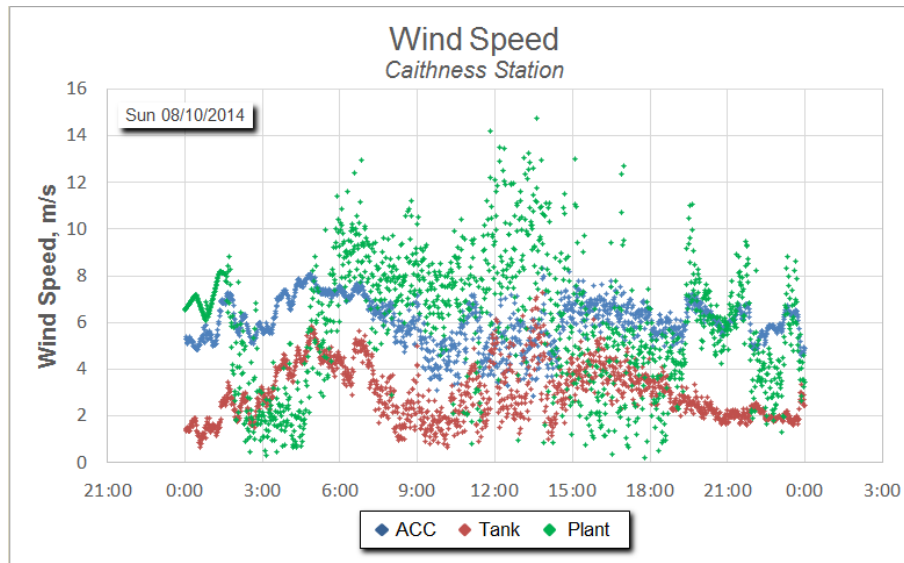
**Figure 64: Anemometer on the Side of Cell 3.4**



### 5.1.3 Comparisons among On-Site Measurements

Significant differences exist among the three on-site measurements of wind speed as seen in Figures 65 and 66.

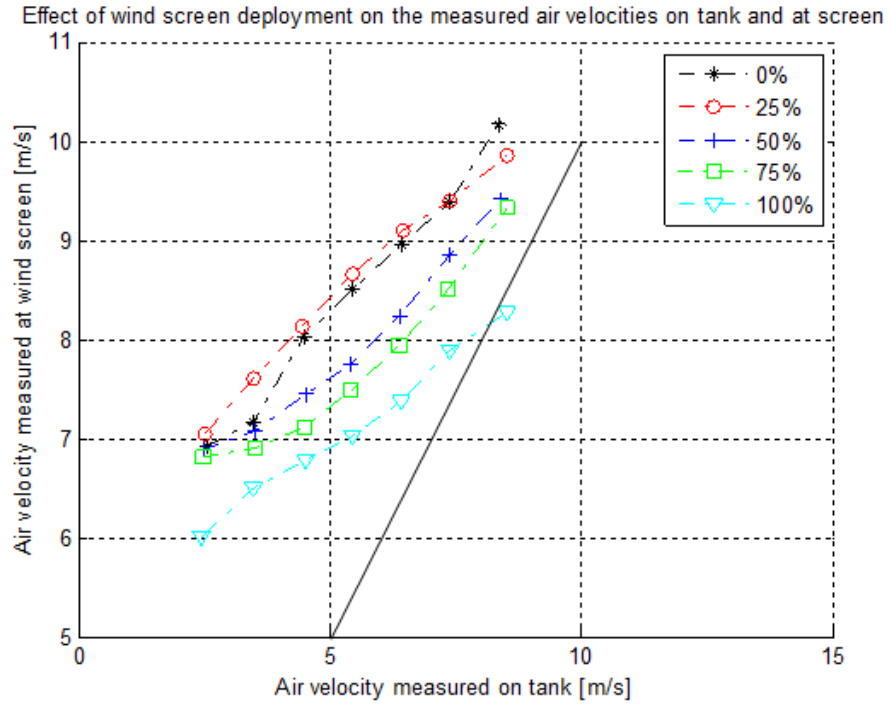
**Figure 65: On-Site Wind Speed Measurements on August 10, 2014**



The plant measurements at the top of the turbine hall show wide variations in wind speed from well above to well below either of the other measurements. These differences are assumed to be due to the effect of the building itself on airflow patterns at the roofline.

Wind speed measurements on the tank and at the side of Cell 3.4 follow similar trends but show a consistent difference with the measurements on the side of the ACC from 2 to 3 m/s higher at most times. These differences, measured with the screens fully deployed in Figure 65 were confirmed for fully deployed screens and extended to a range of screen positions in an interim report by Howden (Holters 2015). The results are shown in Figure 66. The difference in wind speed between the tank and the side of Cell 3.4 increases as the screen is retracted and is generally smaller at higher wind speeds. Note that Figure 65 displays instantaneous readings at one minute intervals while Figure 66 plots differences in readings taken over two months of operation and averages points within a small ( $\pm 0.5$  m/s) range of the velocities measured on the tank.

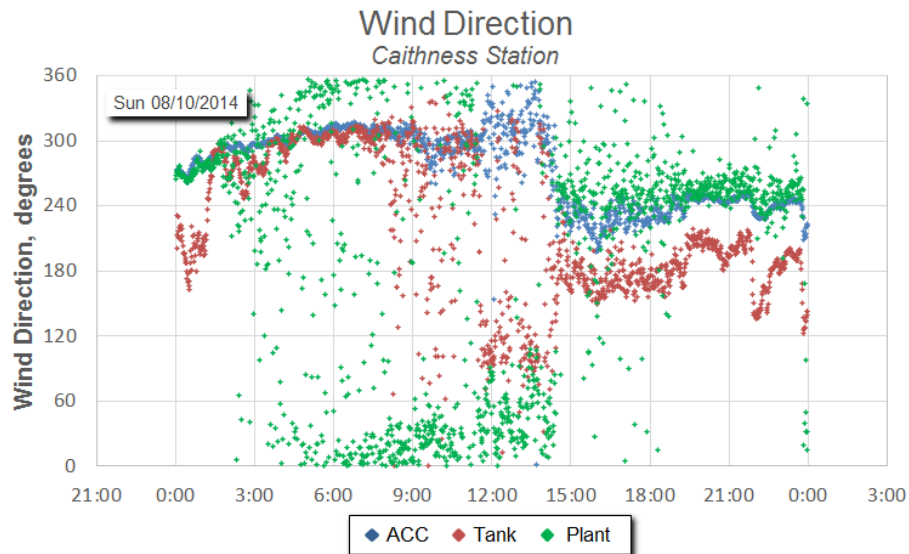
**Figure 66: Effect of Screen Position on Wind Speed Measurements**



Source: Holkers 2015

Figure 67 shows wind direction measurements taken at the same three locations on the same day as the wind speed measurements presented above.

**Figure 67: On-Site Wind Direction Measurements on August 10, 2014**



The plant measurements of direction again show high variability. During some periods (3 am to noon) there is good agreement between the measurements on the tank and those on the side of the ACC; throughout the afternoon (15:00h to midnight) these measurements follow similar trends but differ by about 45 degrees.

The following observations are relevant:

- The wind speed and direction measurements taken on the side of the ACC would be expected to be influenced by the air flow drawn in under the western windwall by the ACC, leading to a higher speed and a direction biased toward westerly winds compared to far-field ambient conditions. Therefore, when the true, far-field wind direction is westerly, or close to it, the agreement is reasonably good. When the true, far-field wind direction is other than westerly, it is not. This is consistent with the measurements shown in Figures 65 and 66.
- The plant measurements taken on top of the turbine hall would be affected by wind spilling over the roof line for winds coming from westerly directions (NNW to SSW) and interference from the ACC plume and the HRSG structure for winds coming from the south to northeasterly directions. This is likely to account for the high variability in both speed and direction and makes it difficult to utilize these measurements as a representation of far-field ambient conditions.

Therefore, the measurements taken on the top of the tank appear to be preferred among the three on-site measurement locations for characterizing ambient conditions. However, two issues require further consideration. These are:

1. A significant flow of air is drawn into the ACC from the surrounding area by the fans during normal operation. Some of this fan-induced airflow may pass around and over the tank and distort the incoming, far-field airflow and lead to erroneous determinations of both speed and direction. This would be of particular concern at very low ambient wind conditions.
2. The blockage of the tank itself may divert and accelerate the incoming ambient air up and over the top of the tank leading to an erroneously high measured wind speed.

These issues are addressed from several points of view:

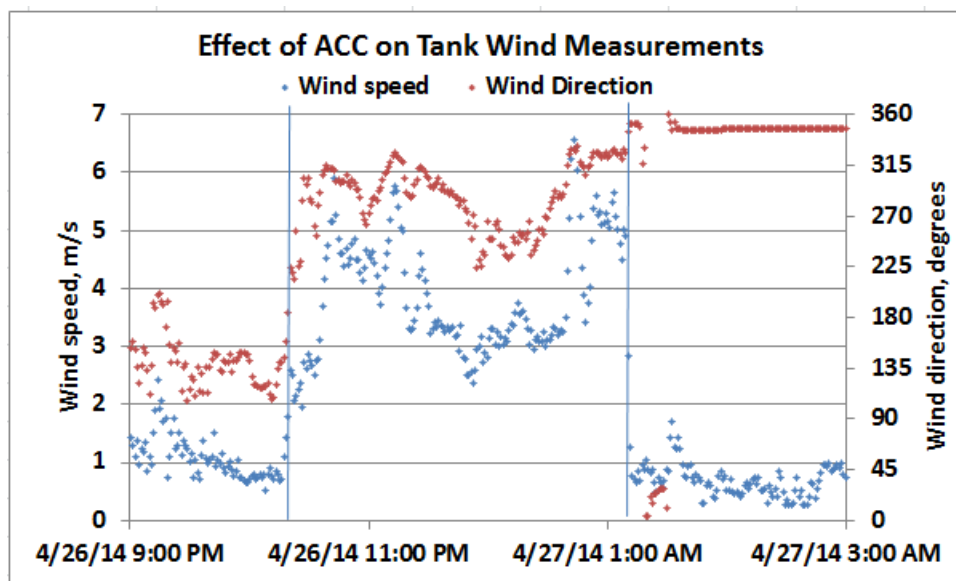
- Direct comparison of tank wind measurements with and without the ACC fans in operation;
- Comparison of tank wind data with wind data reported from nearby airports; and
- Wind tunnel measurements

#### 5.1.4 Comparisons with Fans on and Off

From April 19 through May 4, 2014, the plant was off-line for an annual maintenance outage. However, for a brief period from 10:30 pm on April 26 until 1:10 am on April 27, the ACC fans were turned on for the purpose of running a series of tests on the effect of screen deployment on

fan inlet velocity. The starting and subsequent stopping of the fans at the beginning and end of that test period provides an opportunity to observe any potential effect of ACC-induced airflow on ambient wind speed measurements taken at the tank. Figure 68 displays the wind speed and direction measurements taken before, during and after the period when the fans were running.

**Figure 68: Effect of ACC-Induced Wind**



Some observations are noteworthy.

- The measured wind speed increases, and then decreases, abruptly when the fans are turned on and then turned off. During the “fans-on” period, the measured wind speed exhibits considerable variability, which is difficult to attribute to ACC-induced airflow alone.
- The wind direction also indicates an abrupt shift when the fans are turned on, but the direction of the shift is difficult to understand. The tank measurement point is located just off the southwest corner of the ACC. Therefore, ACC induced airflow at the tank would be expected to be southwesterly. However, the ambient wind direction immediately prior to starting the fans is from the southeast and immediately after turning the fans on it appears to be from the west-northwest, and it is unclear how adding a southwesterly component to a southeast wind could result in northwesterly flow.
- Turning the fans off appears to have no effect on the measured ambient wind direction. Additionally, the readings appear to be unusually steady and remain so until midday on April 28. While this may, in fact, be the case, there may also be some problem with the wind direction measurements at that time, although they resume the more normal pattern on the following day.

- The reported ambient wind speed immediately before the fans are turned on, and immediately after they are turned off is very low at less than 1 m/s.

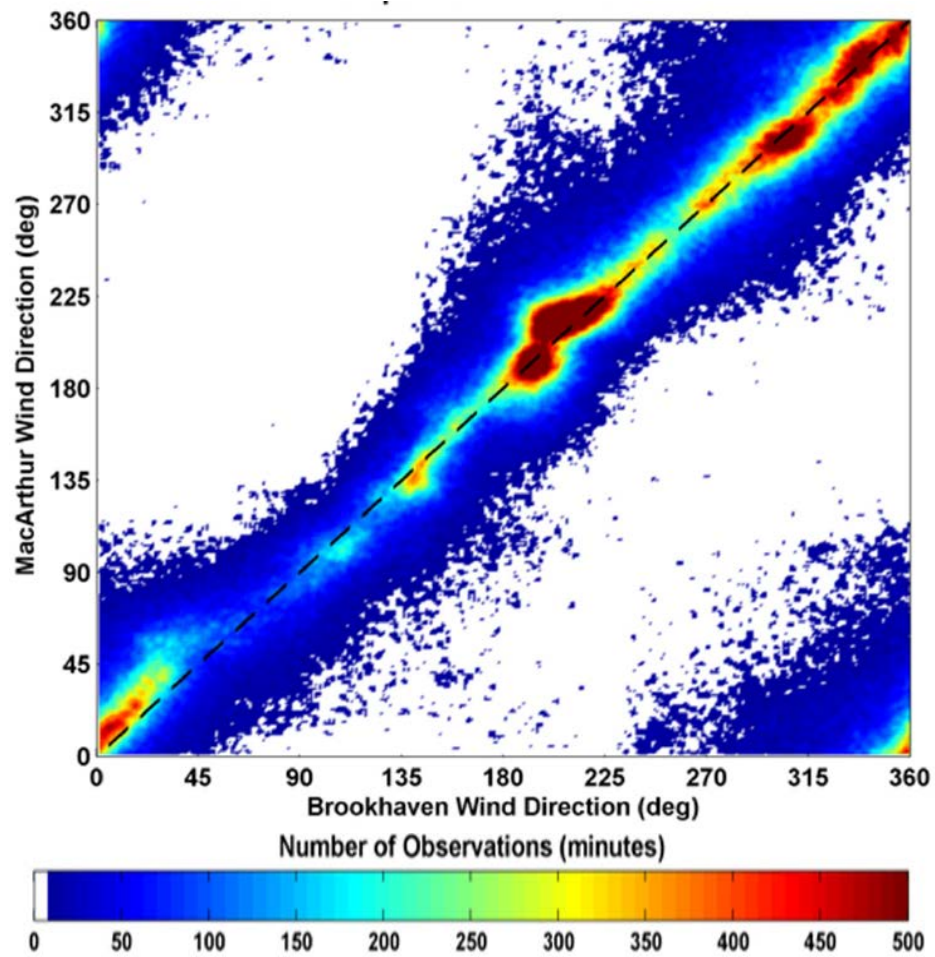
### 5.1.5 Comparison with Nearby Airports

Wind speed and direction data are available at two nearby airports, the New York/Shirley Brookhaven Airport and the New York/Long Island MacArthur Airport (National Atmospheric and Oceanic Administration 2014). Their location relative to the plant is shown in Figure 4. Data for air temperature and wind conditions at the two locations are available from National Weather Service records. An in-depth analysis of wind conditions on-site in comparison to information from the two airports was carried out by the group at UC Davis wind tunnel facility and reported by Parker *et al.* (2015). Figures 69 through 71 are excerpted from that publication.

The comparisons of wind speed and direction measurements between the two airports shown in Figures 69 and 70 indicate a reasonable agreement between the two for readings taken during the summer of 2014. For most of the time the winds were from either the northwest or the southwest. Note that points in the upper left and lower right hand corners of the graph indicate good agreement since both 0° and 360° indicate due North.

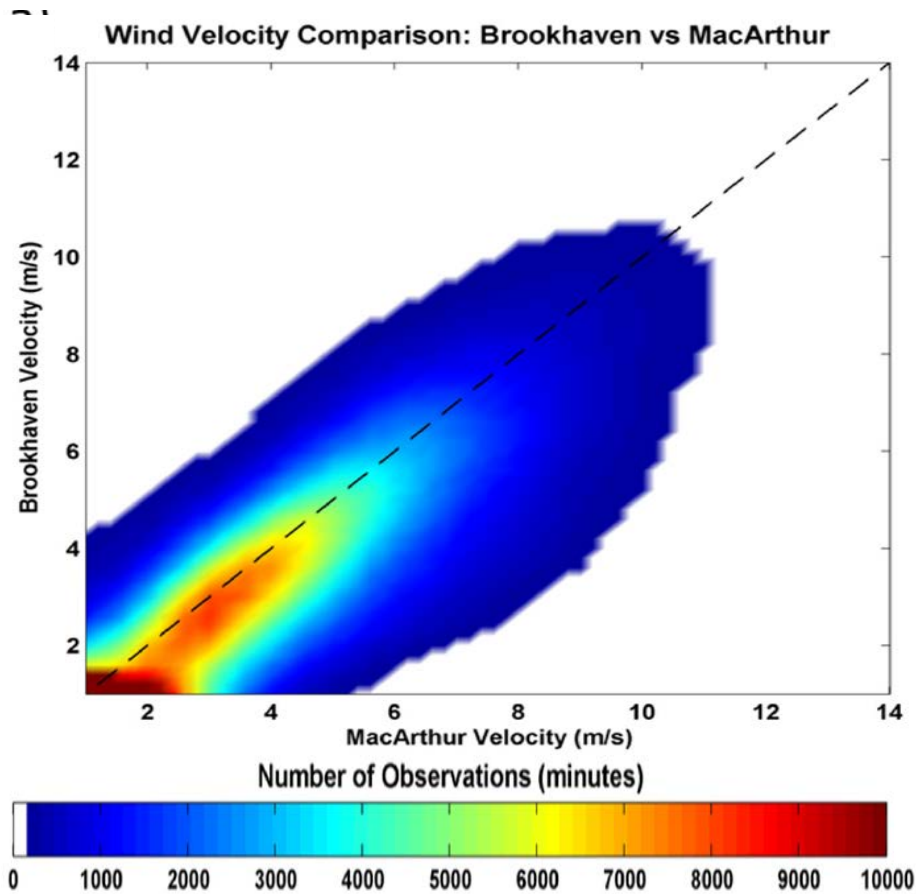
The wind speeds at MacArthur show a consistent tendency to be slightly higher than those at Brookhaven including at the very lowest speeds.

Figure 69: Comparison of Wind Direction Readings From Nearby Airports



Source: Parker *et al.*/2015

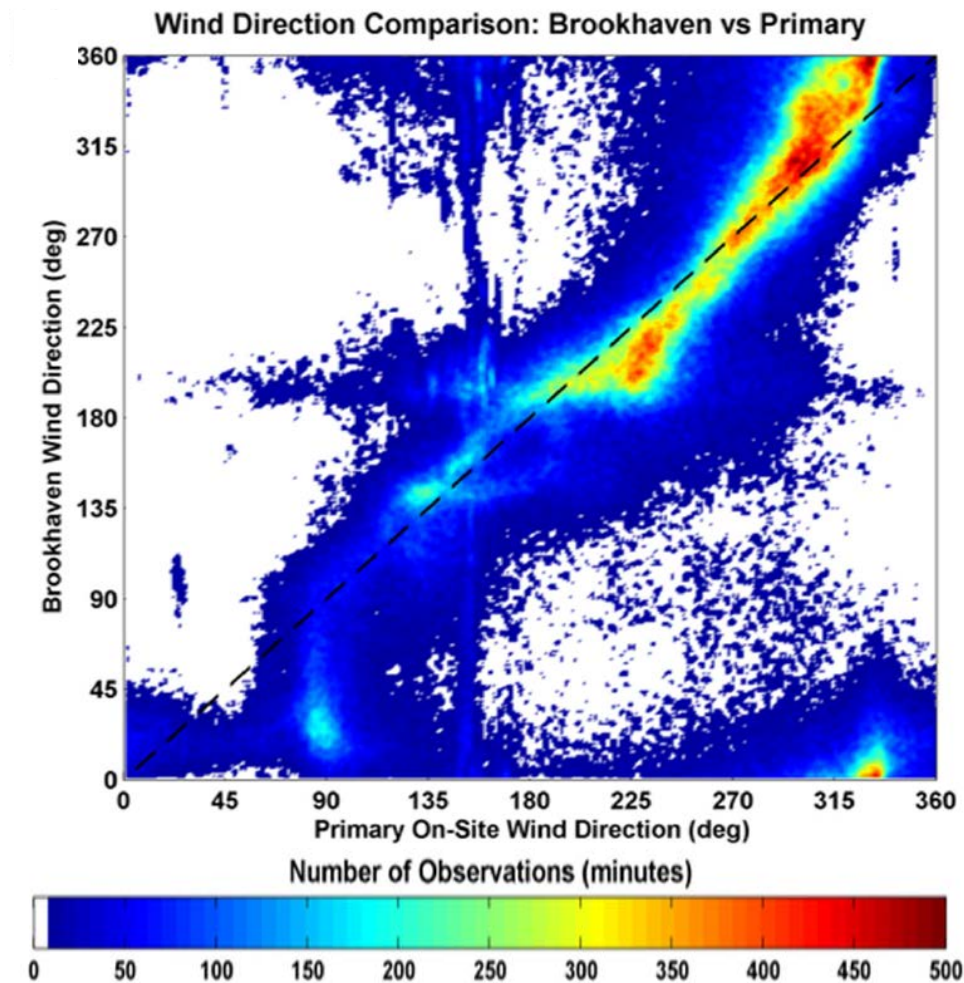
Figure 70: Comparison of Wind Speed Readings from Nearby Airports



Source: Parker et al. 2015

Figures 71 and 72 compares wind direction (Figure 71) and speed (Figure 72) measurements taken on the tank with those from Brookhaven airport. Figure 72 shows reasonable agreement, comparable to the agreement between the airports in Figure 69 for wind directions between about  $90^\circ$  and  $315^\circ$ . The anemometer on the tank records virtually no winds in the sector from northwest to east due to the blockage from the ACC, turbine hall and HRSG. Winds recorded as being from the northeast at Brookhaven are variously recorded as from nearly all directions by the tank; winds from the northwest quadrant at Brookhaven are recorded as more from the southwest and even the southeast at the tank. The cluster of predominant winds measured at Brookhaven between  $180^\circ$  to  $220^\circ$  tend to be recorded with a wider range of directions at the site, due presumably to local interferences and diversional effects.

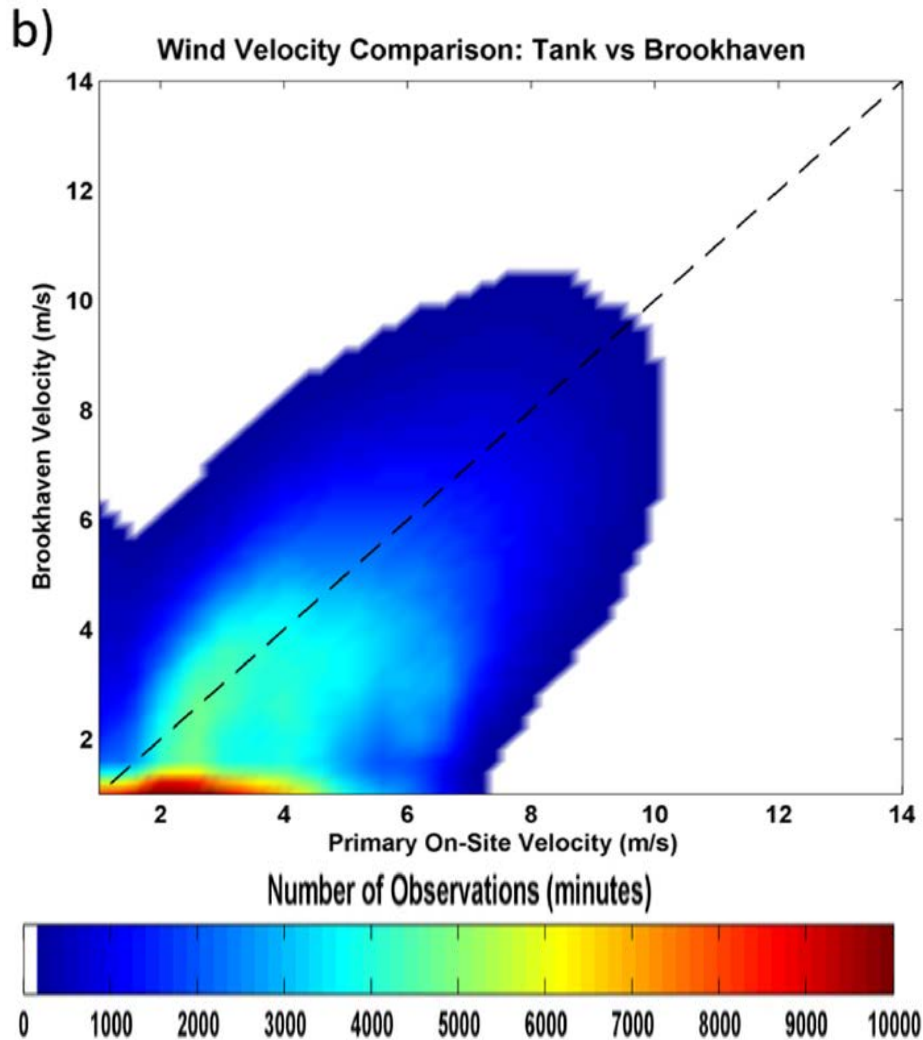
Figure 71: Wind Direction Comparison-On-Site Tank vs. Brookhaven Airport



Source: Parker *et al.* 2015

Wind speed comparisons between the tank and Brookhaven in Figure 72 indicate general agreement with considerable scatter with one important distinction. Very low wind speeds at Brookhaven often correspond to higher speeds at the tank. This same difference was seen between MacArthur and Brookhaven but to a lesser degree. Therefore, while this may indicate a general shift in wind speed with location across the terrain between the two airports, it may also suggest an influence of conditions at the site which influence the incoming wind and lead to measured wind speeds that differ from the true, far-field, ambient wind speed. Two possible effects are the ACC-induced airflow past the tank or a blockage effect of the tank itself which accelerates the wind over the top of the tank where the anemometer is located.

Figure 72: Wind Speed Comparison----On-Site Tank vs. Brookhaven Airport



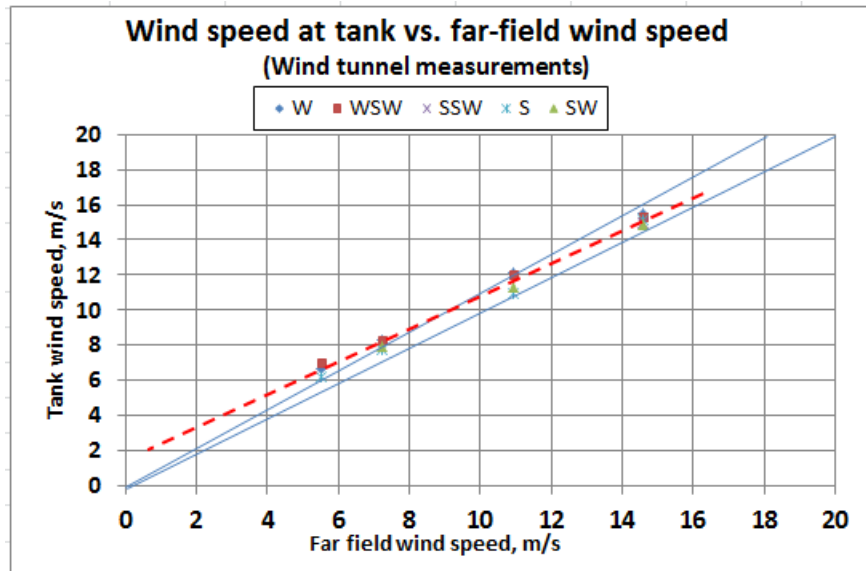
Source: Parker *et al.* 2015

### 5.1.6 Wind Tunnel Simulation

The questions of the influence of both the ACC-induced airflow and the tank blockage were investigated in the wind tunnel. A detailed description of the wind tunnel measurements and the results inferred from them regarding the importance of ACC-induced wind and tank blockage are given in Section 6 as part of the discussion of the physical modeling results.

The essential results are shown here, for convenience of reference, in Figure 73. They indicate that the measured results over most of the wind speed range for directions between south and northwest are within 10 percent of the far field wind speed. At the lowest wind speeds of 2 to 3 m/s the extrapolated results suggest a maximum difference of measured wind speed at the tank in excess of the far field wind speed with all fans at full speed is at most about 1.0 to 1.5 m/s. This is reasonably consistent with the low wind speed differences between the Brookhaven measurements and the tank measurements at the lowest wind speeds shown above.

**Figure 73: Tank Measurements vs. Far Field Wind Speed---Wind Tunnel Measurements**



With respect to the results presented later in this section, a re-plotting of the data using a correction based on wind speed and direction of the magnitude inferred from the plot in Figure 72 would make little difference to the relative shape or level of the correlation lines or data clusters or the essential conclusions stated. Therefore, in the following presentation and discussion of the field test results, the wind speed measured at the tank will be used as an adequate representation of the “ambient” wind speed. However, the possibility exists that winds reported at the lower wind speeds (< 4 m/s) might actually represent calm or almost windless days.

## 5.2 ACC Airflow

Previous studies have concluded that the major effect of wind on the performance of ACCs is a degradation of fan performance and a reduction of the air flow into the ACC (Maulbetsch and DiFillipo 2013; Kroger, D.G. and M. Owen 2011). A major emphasis of the field tests in this study was, therefore, on determining the effects of wind speed, wind direction and screen position on the airflow into selected cells. To this end, extensive instrumentation, as described in Chapter 4, was mounted in Cells 3.4 and 2.4 with less extensive, confirmatory measurements in Cells 1.4, 1.3 to 3.3 and 4.1 to 4.3.

In order to interpret the comparative results appropriately, some baseline information is required. The fan selection sheet provided by Howden for the Model 34ELF9 fans (34 foot diameter; 9 blades; blade pitch of 5.5°) currently installed at Caithness, specifies a performance point of airflow of 576.7 m<sup>3</sup>/s and static pressure of 110 Pa for undisturbed inlet conditions, at an inlet temperature of 33.3°C and a fan speed of 93.2 rpm. This volumetric airflow implies an average inlet velocity at the inlet to the fan shroud, where the diameter is 11.66m for an inlet area of 106.8m<sup>2</sup>/s, of approximately 5.4m/s.

However, the field measurements obtained over a year of operation consistently record average inlet air velocities in the neighborhood of 7. m/s or less, implying a volumetric airflow of approximately 750 m<sup>3</sup>/s and static pressures which vary from 40 to 70 Pa depending on wind conditions. This condition is “off the curve” of Howden’s “Selection Graph” shown in Figure 74 for the Model 34ELF9 at a 5.5° blade pitch. Additionally, a single test of this fan in Cell 1.5 at Caithness performed by Howden on May 12, 2012 gave an even higher volumetric airflow of 889 m<sup>3</sup>/s.

Studies of the recommended procedure for measuring the volumetric airflow through large diameter axial fans (Holkers 2015) state that 40 anemometers be used arranged along radii at right angles to cover four quadrants with 10 anemometers at equal area locations along the four radii. For the current study, limitations on available instrumentation and data acquisition capacity did not permit that many measurement points. As noted in Section 4 and Appendix A, eight anemometers per fan were used placed on two concentric rings at 90° intervals at ring diameters of 3.1 and 4.14 m, corresponding to 1/3 and 2/3 of the distance from the hub to the blade tip. To confirm that an average of these measurements can be considered representative of the actual flow, the results of a test performed by Howden in 2012 using the “40 anemometer” procedure are shown in Table 2.

The test was performed on Cell 3.3 at Caithness, the cell immediately adjacent to the primary test cell in this study. The fan characteristics differ only in that the blade pitch at the time of the Howden test was 6.8° and 5.5° for the current study.

**Table 2: Results of Howden Fan Test; Cell 3.3; December 5, 2012**

Cell 3.3		Air velocity [m/s]			
		Segment			
i	D <sub>i</sub>	1	2	3	4
	[m]	V <sub>air,i</sub>	V <sub>air,i</sub>	V <sub>air,i</sub>	V <sub>air,i</sub>
1	4.623	6.1	7.9	7.7	5.1
2	3.655	6.7	6.9	8.2	6.8
3	2.990	7.6	6.3	10.9	6.8
4	2.450	8.5	6.6	11.3	8.0
5	1.983	9.1	6.7	8.4	9.0
6	1.566	9.2	6.3	10.0	9.9
7	1.185	9.9	5.2	10.3	9.7
8	0.833	8.3	5.1	9.1	9.0
9	0.503	12.9	5.8	6.9	5.4
10	0.193	2.9	0.6	6.4	2.2

The average of readings in the four segments at each radial location was determined and a curve of velocity vs. radius was developed. The inlet air velocity inferred from averaging the measurements at the locations of the anemometer rings in the current study agreed well with the average of all 40 measurements. This suggests that the placement of the anemometers in the

current study was appropriate. Therefore, the inlet velocity measurements and the static pressure readings obtained throughout the study will be taken as representative of the fans in Cells 3.4 and 2.4 as currently configured and operated.

### 5.2.1 Effect of Screen Position on Inlet Air Velocity to Fans

The eight anemometers in Cell 3.4 and 2.4 are averaged and the average inlet velocity is used to represent the inlet airflow to each cell. These average inlet velocities are plotted against ambient wind speed as measured on the tank at each of five screen positions. The five wind screen positions are 100 percent (fully deployed), 75 percent, 50 percent, 25 percent and 0 percent (fully retracted).

The data are reduced and presented in two ways.

#### 5.2.1.1 Averaged Data Presentation Format

The first analysis, developed by the Howden group, is displayed in Figures 75 through 77. All the readings during the period from the end of June to early September for wind directions from Northwest to Southwest ( $270^\circ \pm 45^\circ$ ) were binned into 7, 1 m/s wind speed ranges (2 to 3, 3 to 4, etc. up to  $>8$ ). Table 5.2 lists the number of data points for each speed range and screen position. Note that there are very few points at wind speeds above 8 m/s.

**Figure 74: Howden Fan Curve for Caithness Fans**

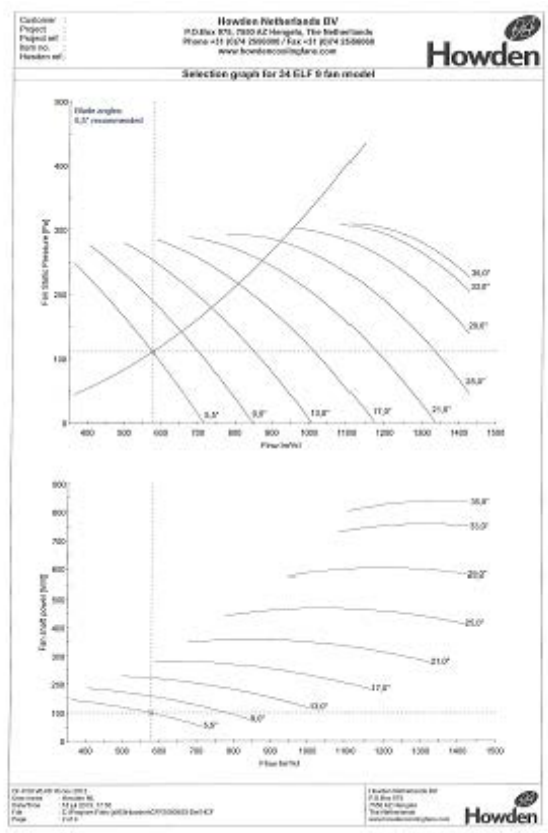


**Table 3: Distribution of Data Points Plotted in Figures 74 through 76**

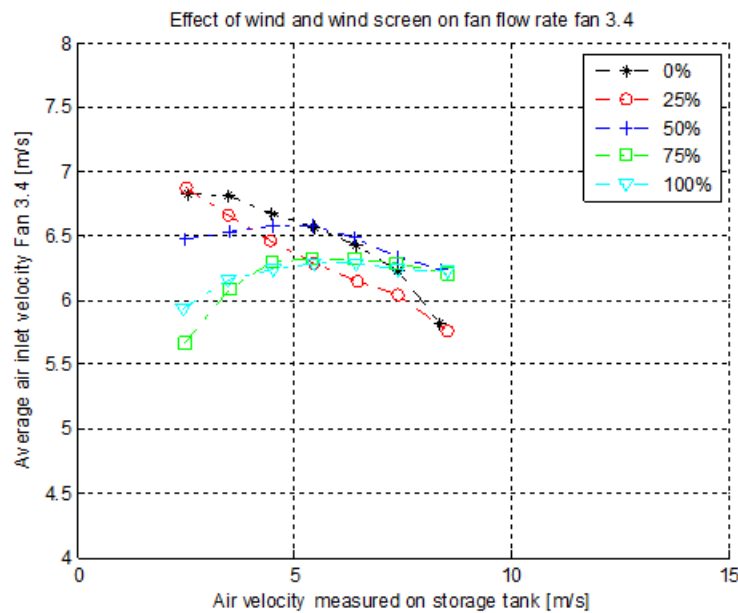
Air velocity [m/s]	Screen position				
	0%	25%	50%	75%	100%
$2 < v < 3$	3994	7980	7670	3048	11312
$3 < v < 4$	5915	6279	5581	3205	7876
$4 < v < 5$	3182	4475	9031	3727	6405
$5 < v < 6$	1786	2427	6199	2332	4610
$6 < v < 7$	629	1135	1588	649	1884
$7 < v < 8$	153	407	269	103	542
$v > 8$	25	131	41	9	146

Figure 75 presents the average velocities in Cell 3.4 for the 5 screen positions. Figure 76 presents the same plot for Cell 2.4 and Figure 77, for the average velocities in both cells.

The most dramatic effects are apparent in Figure 75 for the upwind, edge cell (Cell 3.4). For lower wind speeds of less than about 5.5 to 6.0 m/s (~ 12 to 13.5 mph), the deployment of the wind screen at all levels reduces the average inlet velocity below the value for the fully retracted case. For all wind speeds above 2.5 m/s, the average inlet velocity for the two least deployed cases (0 percent and 25 percent) decreases monotonically with increasing wind speed while the average inlet velocity for the more deployed cases (50 percent, 75 percent and 100 percent) increases from wind speeds of 2.5 m/s up to wind speeds of about 5.5 to 6. m/s and then decreases slightly or levels off for further increases in wind speed. At the highest wind speed of 8 m/s (~ 18 mph), screens at 50 percent, 75 percent and 100 percent deployment show essentially identical results of an approximately 9 percent increase in average inlet velocity over the retracted case.

Two items are noteworthy. First, over the full range of wind speeds, the 50 percent case exhibits the best overall performance. It produces the least reduction in average inlet velocity in comparison to the fully retracted setting at the lower speeds and better performance than the higher deployment settings over the entire range. Second, the curve for the 25 percent deployment case exhibits significantly different characteristics than the other cases. Unlike the 50 percent, 75 percent and 100 percent cases, the average inlet velocity decreases monotonically over the entire speed range. In comparison to the fully retracted case, the average inlet velocity is significantly lower at all speeds and the shape of the curve vs. wind speed is essentially linear unlike the 0 percent case. No reason for this behavior is known.

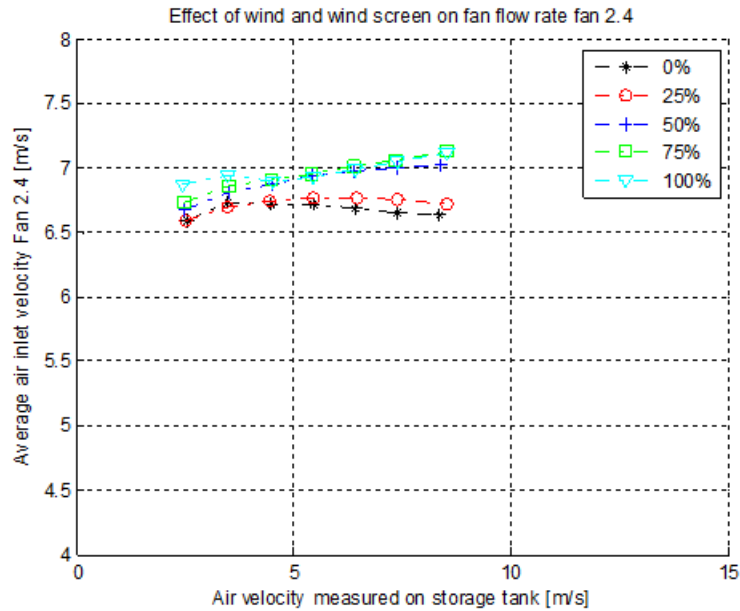
**Figure 75: Cell 3.4 Average Inlet Velocity for Varying Screen Position**



Source: Holkers 2015

Figure 76 displays the same curves for the next, downwind cell (Cell 2.4). The effect of wind speed on the average inlet velocity is much less than for Cell 3.4 for all screen positions. Over the entire speed range, the more deployed cases (50 percent, 75 percent and 100 percent) result in higher average inlet velocities than the less deployed cases (0 percent and 25 percent). The higher deployment cases show a steady, monotonic increase over the entire range; the two lower cases show a leveling off with a slight decrease at wind speeds above about 7 m/s (~ 15.5 mph).

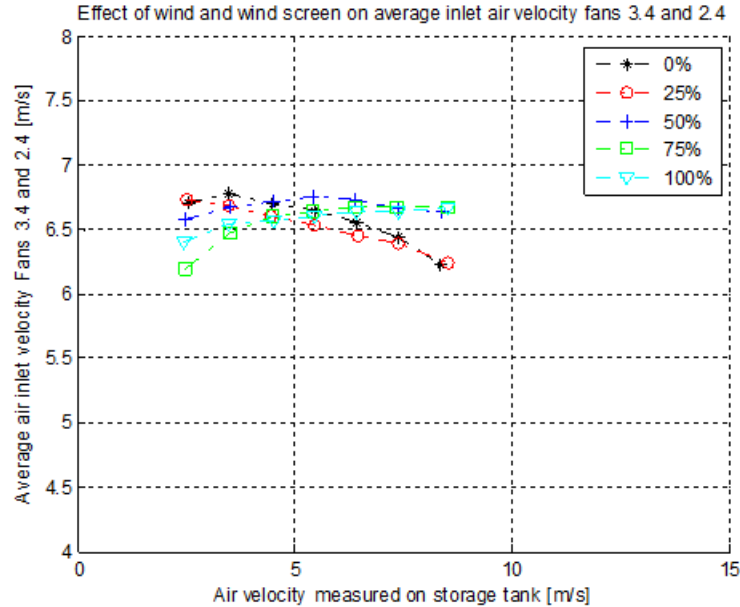
**Figure 76: Cell 2.4 Average Inlet Velocity for Varying Screen Position**



Source: Holkers 2015

Figure 77 indicates that the combined effect on the two cells essentially balances out. At wind speeds below 5 m/s (~ 11 mph), the screens reduce the average inlet velocity to the combined cells slightly; above 5 m/s (~ 11 mph), the higher deployments show a significant increase in comparison to the other two and they level out with wind speeds up to 8 m/s (~ 18 mph) at approximately a 5.5 percent increase in average inlet velocity compared to the fully retracted case. Again the 50 percent deployed condition gives the best performance on balance across the entire speed range.

**Figure 77: Cells 3.4 and 2.4 Average Inlet Velocity for Varying Screen Position**



Source: Holkers 2015

Some general observations can be made from comparisons of the previous three figures.

For the screens fully retracted:

- At the lowest wind speeds, the screen position has a much greater influence on the airflow into the windward cell (Cell 3.4) than it does on the downwind cell (Cell 2.4). For wind speeds up to about 4.5 m/s, the windward fan captures more incoming air than the downwind fan. At the lowest wind speed (2.5 m/s), the average inlet velocity into the windward cell is about 6.9 m/s; into the downwind cell, about 6.7 m/s.
- As the wind speed increases above 5 m/s, the incoming air increasingly bypasses the windward cell and is captured by the downwind cell. When the wind speed reaches 7.5 to 8 m/s, the average velocity in the windward cell has fallen to about 5.8 m/s, while the average downwind cell inlet velocity has remained essentially constant at about 6.6 to 6.7 m/s.

For the screens fully deployed:

- At the lower (2.5 to 5. m/s) wind speeds with the screens fully deployed, the airflow into the windward cell is partially impeded and the average inlet velocity is as low as 5.9 m/s, well below that with the screen retracted. In the downstream cell, it is about 6.9 m/s, well above that with the screen retracted, as incoming air is impeded from entering the windward cell is captured by the downwind cell.
- As wind speed increases above 5 m/s, the blockage effect on the windward cell is offset by reduced bypassing of the cell as the velocity of air passing through the screen is

reduced and the average inlet velocity into Cell 3.4 increases up to a wind speed of about 6 m/s and then levels off. The average inlet velocity into the downwind cell is only modestly affected by the deployment of the screen at the lowest wind speeds, but then, as the wind speed increases, the airflow into the downwind cell increases up to the highest wind speed of about 8 m/s.

For the two cells combined, the deployment of the screens to 50, 75 or 100 percent provides an increasingly significant improvement in total airflow into the two cells combined at wind speeds above about 6 m/s with an approximately 7 percent improvement at the highest wind speed of 8 m/s. The trend of the curves at that point suggests that the percentage improvement in total airflow would continue to increase at still higher wind speeds.

#### *5.2.1.2 Point-by-Point Presentation Format*

The second format for examining the data differs from the preceding slides in that narrower slices of wind direction are selected and all the points at one minute intervals are displayed rather than an average value for a particular range of wind speeds. This approach is intended both to understand the effect of wind direction more precisely and to display the fine structure of the measurements including the scatter and the intermediate trends of the variation in inlet velocity as a function of wind speed. The ambient wind directions are nominally NW, W, SW, S and SE with points from slices  $\pm 11.25^\circ$  around the nominal direction.

The presentation of results in this format requires a very large number of plots for which the descriptions and comparisons are voluminous. Therefore, a few examples are selected for illustrative purposes.

#### *Cell 3.4*

Figure 78 presents the average velocities in Cell 3.4 for the 100 percent and 0 percent screen positions. The northwest direction was chosen for two reasons.

First, since Cell 3.4 is on the west side of the ACC, the airflow patterns under and around the Cell 3.4 fan were expected to be most affected by winds with a significant component of velocity normal to the west face of the ACC (NW, W and SW) and less so by winds not directly impinging on the side of the cell (S and SE). Similarly, the effect of the screens should be more noticeable for winds with a westerly component.

Second, the northwest wind direction has a wider range of wind speeds than any of the other directions with speeds for the fully deployed case up to 10 m/s.

**Figure 78: Cell 3.4 Inlet Velocity With NW Winds and 100 Percent vs. 0 Percent Screens**

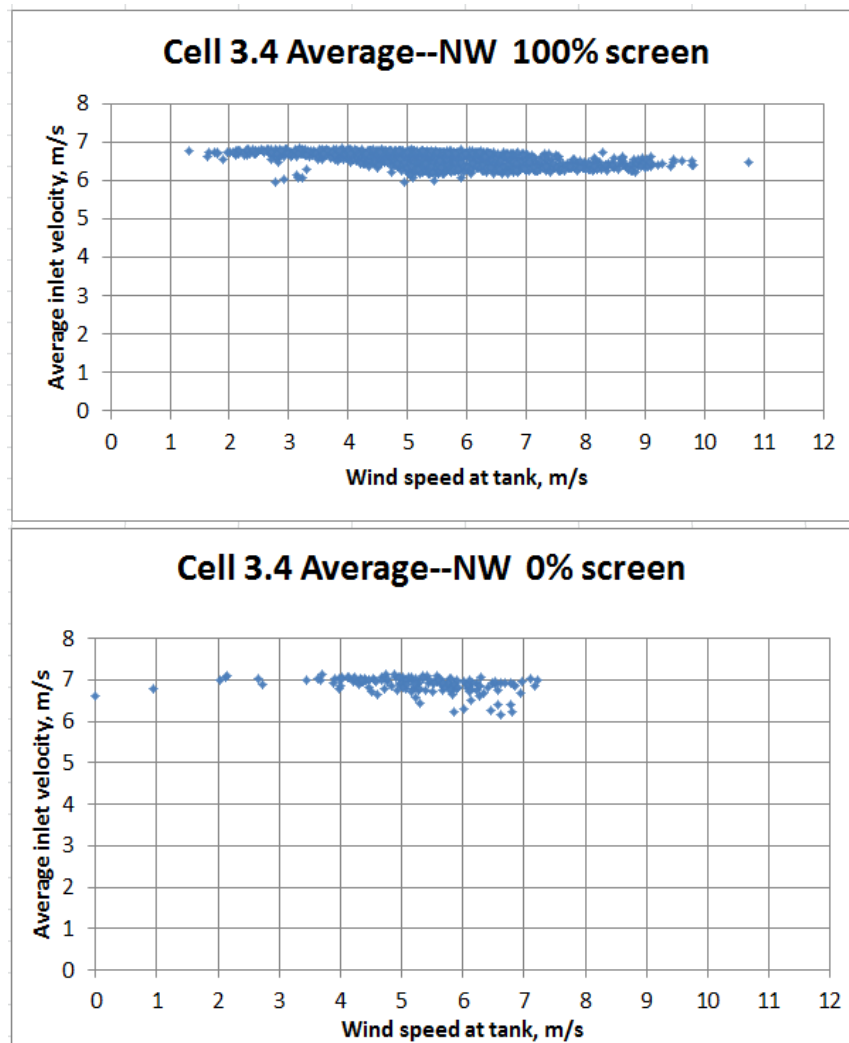
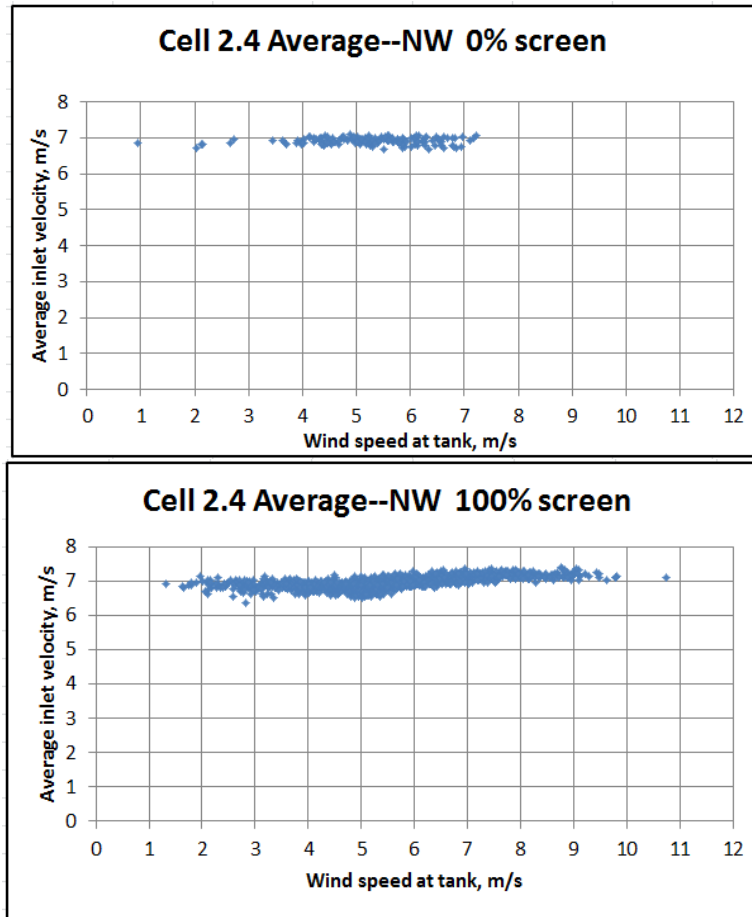


Figure 78 indicates a modest reduction in Cell 3.4 airflow with the screens full deployed compared to operation with the screens fully retracted. The average velocity for the screens fully deployed is reasonably constant between 6.5 and 6.9 m/s for wind speeds up to about 5 m/s and decreases slightly approximately 6.3 to 6.5 m/s for wind speeds up to 10 m/s. For the screens fully retracted, the average velocity is from 6.7 to 7.1 m/s for wind speeds up to about 5 to 6 m/s and then appears to decrease slightly above that. However, no winds above 7 m/s were experienced during this portion of the test period, so the performance at higher speeds is not known.

#### *Cell 2.4*

Figure 79 presents a similar plot for Cell 2.4. As shown in Figure 49, Cell 2.4 is in the middle street of the ACC directly to the east of Cell 3.4. Therefore the airflow patterns under and into the Cell 2.4 fan will be affected by the performance of the Cell 3.4 fan.

**Figure 79: Cell 2.4 Inlet Velocity With NW Winds and 100 Percent vs. 0 Percent Screens**

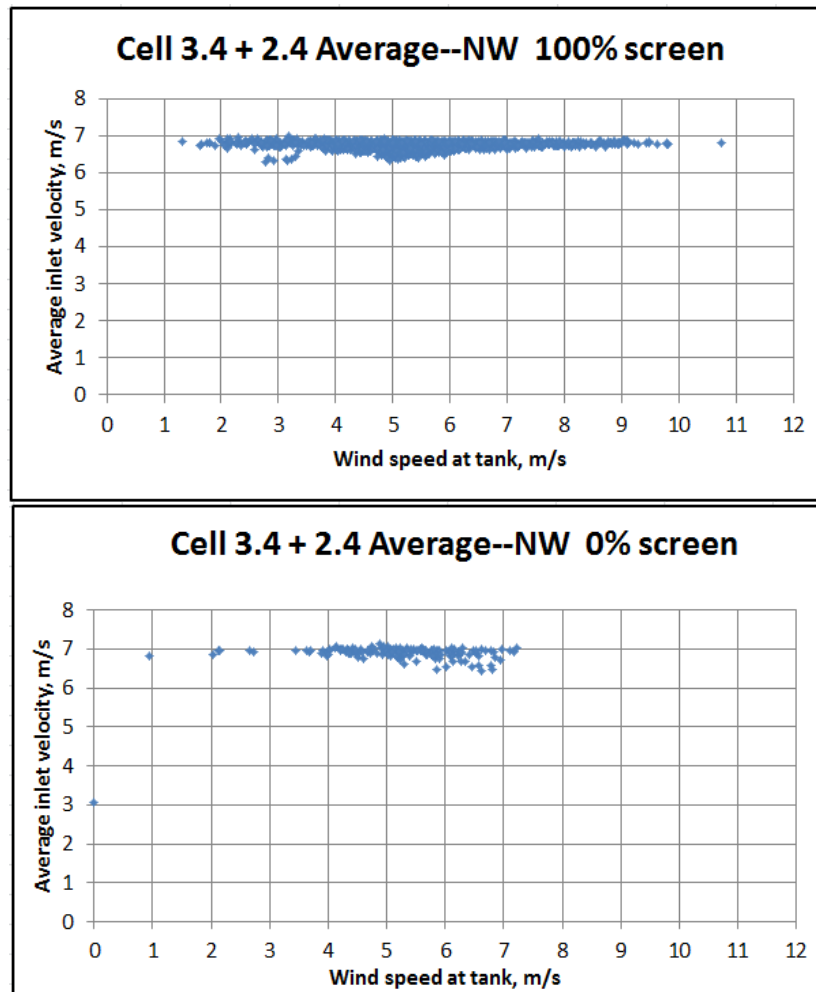


In contrast to the results for Cell 3.4, Figure 5.21 indicates a modest increase in Cell 2.4 airflow with the screens full deployed compared to operation with the screens fully retracted. The average velocity for the screens fully deployed is reasonably constant between 6.5 and 7.3 m/s for wind speeds up to about 10 m/s with no decrease and, in fact, a slight increase at the higher wind speeds above 6 m/s. For the screens fully retracted, the average velocity is very steady from about 6.7 to 7.1 m/s up to wind speeds of just over 7 m/s. However, no winds above 7.2 m/s were experienced during this portion of the test period, so the performance at higher speeds is not available for comparison to the fully deployed case.

#### *Cells 3.4 and 2.4 Combined*

Figure 80 displays the average of the inlet velocity measurements for *both* cells and represents the inlet airflow for the two cells combined.

**Figure 80: Cells 3.4 and 2.4 Inlet Velocity With NW Winds and 100 Percent Vs. 0 Percent Screens**



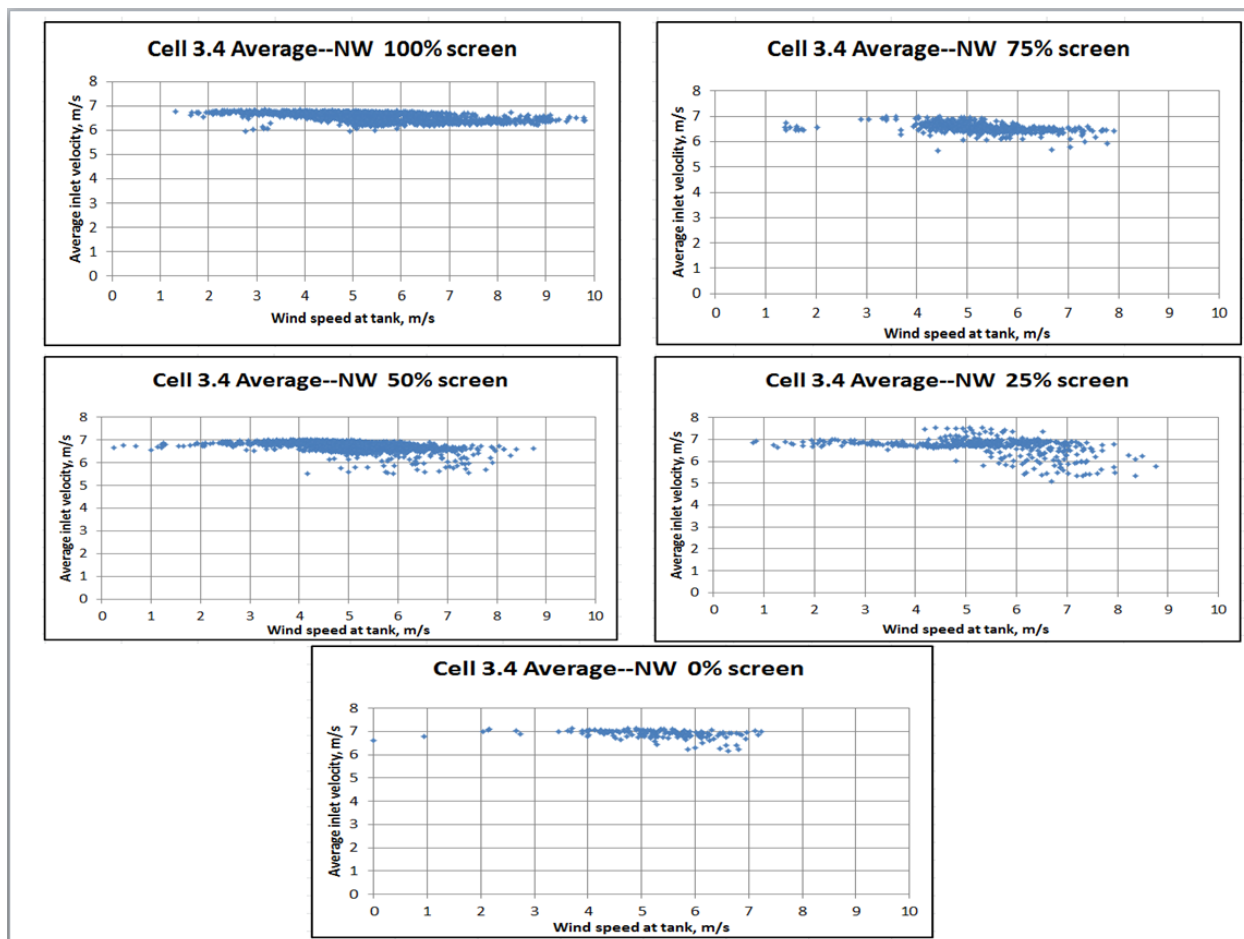
The general observation is that the total volumetric airflow for the two cells combined is, to a first approximation, the same whether the screens are fully deployed or fully retracted. The slight reduction in airflow from the deployment of the screens in Cell 3.4 is offset by a corresponding increase in the airflow to Cell 2.4.

Figures 81 through 83 show plots of average inlet velocity for Cells 3.4 and 2.4 individually (Figures 81 and 82) and the average inlet velocity for the two cells combined (Figure 83).

The most noticeable effect of screen position on Cell 3.4 is a reduction in the amount of variability in the inlet velocity at the higher wind speeds (between 6 and 10 m/s). The most variability is seen at the 25 percent position (the fully retracted case included almost no points at wind speeds above 6 m/s). This variability is steadily reduced with increasing screen deployment until, at the fully deployed condition; there is very little variability at wind speeds up to 10 m/s. As noted in the previous section, the maximum inlet velocity is slightly reduced at

the fully deployed position compared to the fully retracted position. This reduction is not seen up to 50 percent deployment and is first noted in the 75 percent case.

**Figure 81: Effect of Screen Position on Cell 3.4 Inlet Velocity (NW Wind Direction)**



The effect of screen position on Cell 2.4 inlet velocity (Figure 82) indicates a slight increase at screen deployments of 50 percent and above at wind speeds above 6 m/s. At the lower wind speeds (less than 5 m/s) there is essentially no effect.

Similarly, the average inlet velocity for the two cells combined (Figure 83) shows essentially no effect except for the reduction in scatter at the higher wind speeds which reflects the conditions in Cell 3.4. Again, any reduction in Cell 3.4 is compensated for with a slight increase in Cell 2.4.

Figure 82: Effect of Screen Position on Cell 2.4 Inlet Velocity (NW Wind Direction)

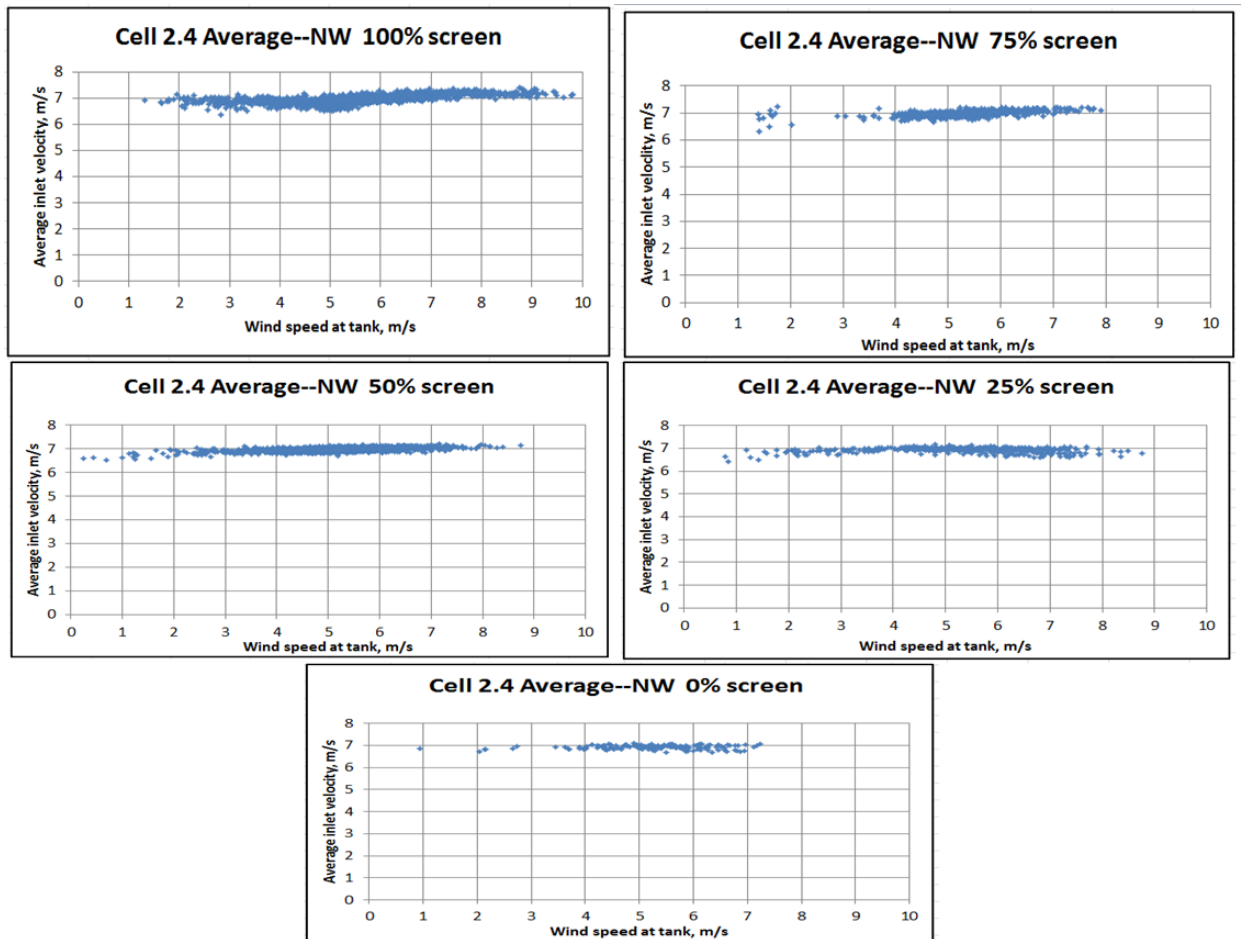
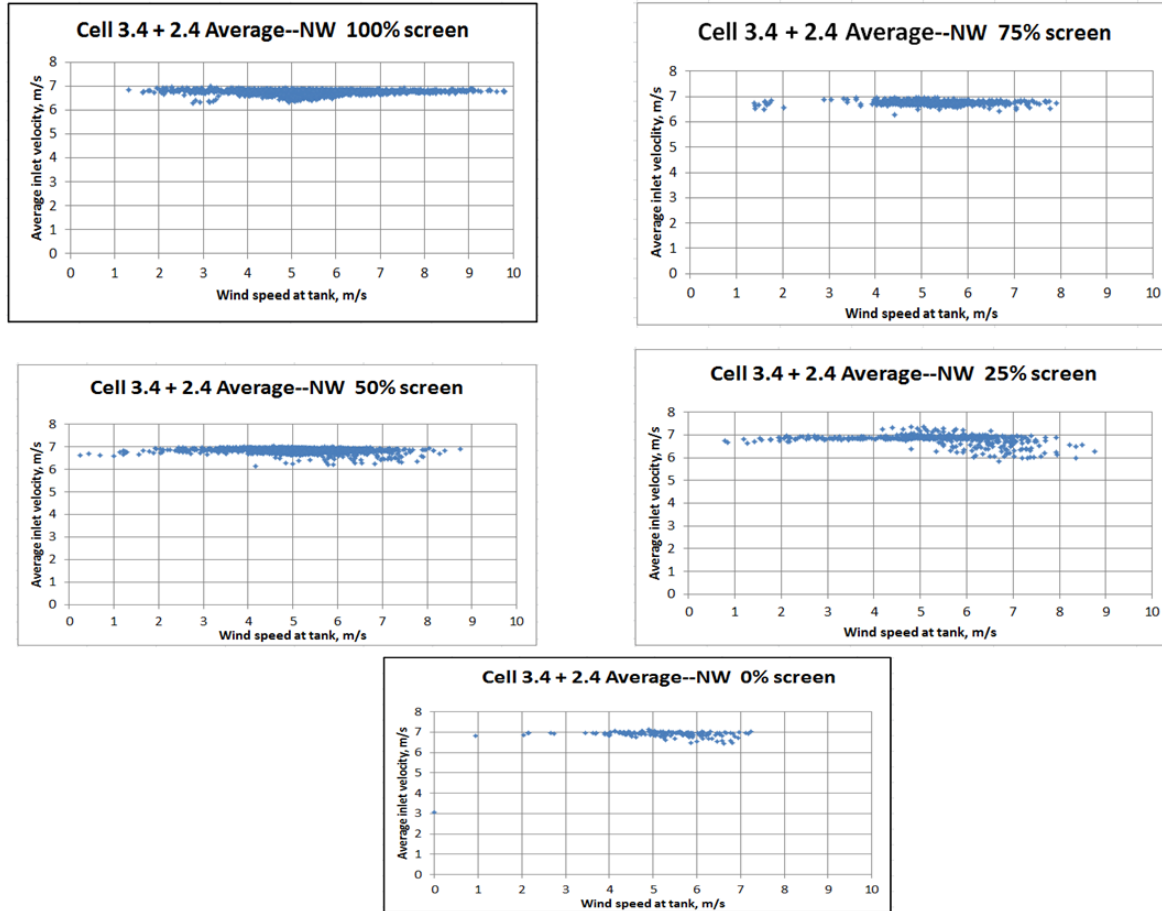


**Figure 83: Effect of Screen Position on Cells 3.4 and 2.4 Inlet Velocity (NW Wind Direction)**



### 5.2.1.3 Comparison of Alternative Presentation Formats

It is worthwhile to compare the conclusions drawn from the Howden plots of averaged values (Figures 75 through 77) with those from the all-points plots (Figures 78 through 80). The Howden plots average readings binned in 1 m/s intervals of all the data taken from the end of June through early September, 2014 for wind directions between NW and SW ( $315^{\circ}$  to  $225^{\circ}$ ). The all-points plots for points within  $\pm 11.25^{\circ}$  of the NW, W and SW directions are shown in Figures 5.20 (NW), 5.26 (W) and 5.27 (SW).

Figure 84: Cell 3.4 Inlet Velocity With W Winds and 100 Percent vs. 0 Percent Screens

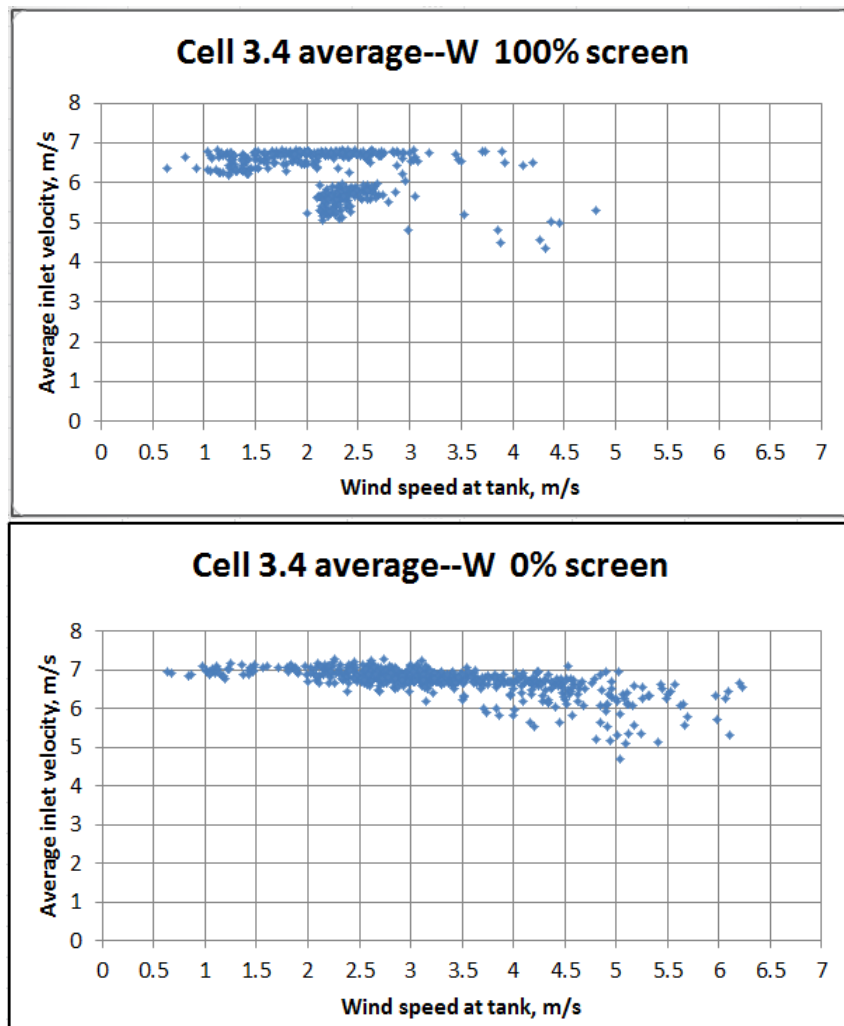
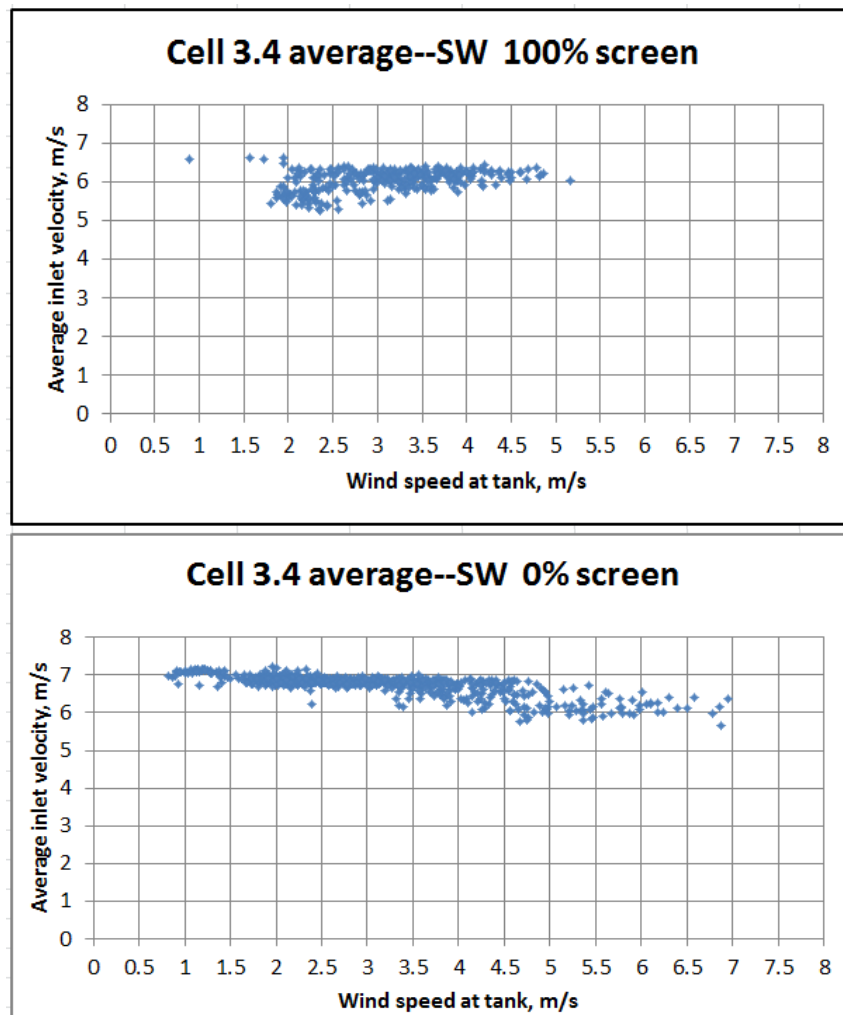


Figure 85: Cell 3.4 Inlet Velocity With SW Winds and 100 Percent vs. 0 Percent Screens



Three characteristics distinguishable from the Howden plots are compared. These are:

- The difference between the fully deployed and fully retracted cases at the very low wind speeds,
- The same difference at the higher wind speeds and
- The significant decrease in Cell 3.4 airflow with increasing wind speed.

#### *Low Wind Speeds*

The Howden plot on Figure 75 indicates that for wind speeds between 2 and 3 m/s the average Cell 3.4 inlet velocity is approximately 6.9 to 7. m/s with the screens fully retracted and 5.9 to 6. m/s with the screens fully deployed.

#### *High Wind Speeds*

The Howden plot in Figure 75 indicates:

- For wind speeds between 7. and 8. m/s
  - Fully retracted and fully deployed are nearly the same at ~6.25 m/s
- For wind speeds greater than 8. m/s
  - Fully retracted = ~5.75 m/s
  - Fully deployed = 6.25 m/s

The corresponding values shown in the all-point plots for the NW direction and the W and SW directions are summarized as follows:

- NW direction;
  - Fully retracted: no points above 7 m/s
  - Fully deployed: essentially constant at ~6.25 m/s from 6. to 10. m/s wind speed
- W direction;
  - Fully retracted: no points above 7 m/s wind speed; few above 6 m/s
  - Fully deployed: no points above 5 m/s wind speed
- SW direction;
  - Fully retracted: no points above 7 m/s; between 6. and 7. m/s, a few between 6 and 6.5 m/s inlet velocity
  - Fully deployed: no points above 5 m/s.

The point by point plots show almost no points with which to confirm or differ from the Howden results. The paucity of points is consistent with the tabulation of the Howden points in Table 5.2 which shows only 178 fully retracted points and only 688 fully deployed points above 7 m/s out of a total of over 114,000 points. The significant fall-off in inlet velocity between 7.5 m/s and >8 m/s for the fully retracted case is based on only 25 points.

#### *Cell 3.4 Inlet Velocity with Fully Retracted Screens*

Figure 75 shows a decrease in Cell 3.4 inlet velocity with increasing wind speed for fully retracted screens from approximately 6.9 m/s for wind speeds between 2 to 3 m/s down to 6.25 m/s at wind speed of 7 to 8 m/s and 5.8 m/s at windspeeds above 8 m/s. As noted above this latter value is based on very few points.

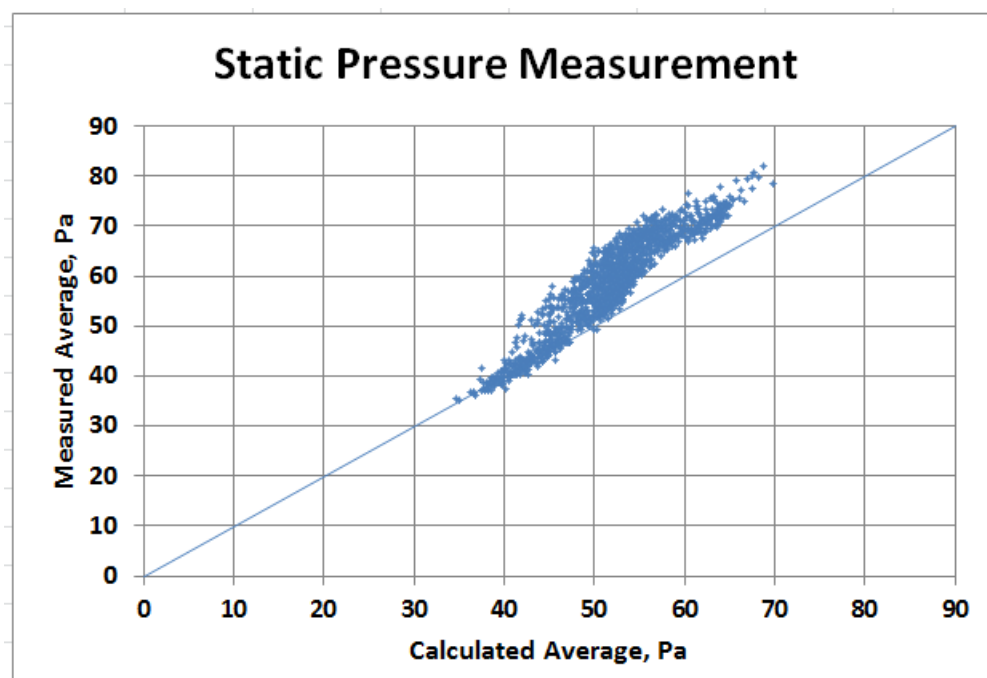
The all-points plots on Figures 78, 84 and 85 have, as noted above, very few points to compare with the Howden averages. However, the fully retracted points in the 2 to 3 m/s wind speed range compare well and the few points on Figure 78 for the highest available wind speed of 5 to 6 m/s suggest a reasonable correspondence with the Howden data.

We, therefore conclude that the general effect of wind speed is captured by the Howden averaging procedure displayed in Figures 75 to 77. However, there are effects of wind direction which are discernible in the all-point plots.

### 5.3 Static Pressure Variations

As discussed earlier in this section, static pressure rise across a fan is related to the volume airflow in accordance with fan operating curves as illustrated in Figure 74. Measurements of static pressure were made in Cells 3.4, 2.4 and 1.4. In Cell 3.4, measurements were made in each of the four cell corners as well as a measurement with a separate sensor that averaged the four corner measurements. It is noted that the measured average did not always agree well with the computed, numerical average of the four corner measurements as shown in Figure 86.

**Figure 86: Static Pressure Measurement Comparison**

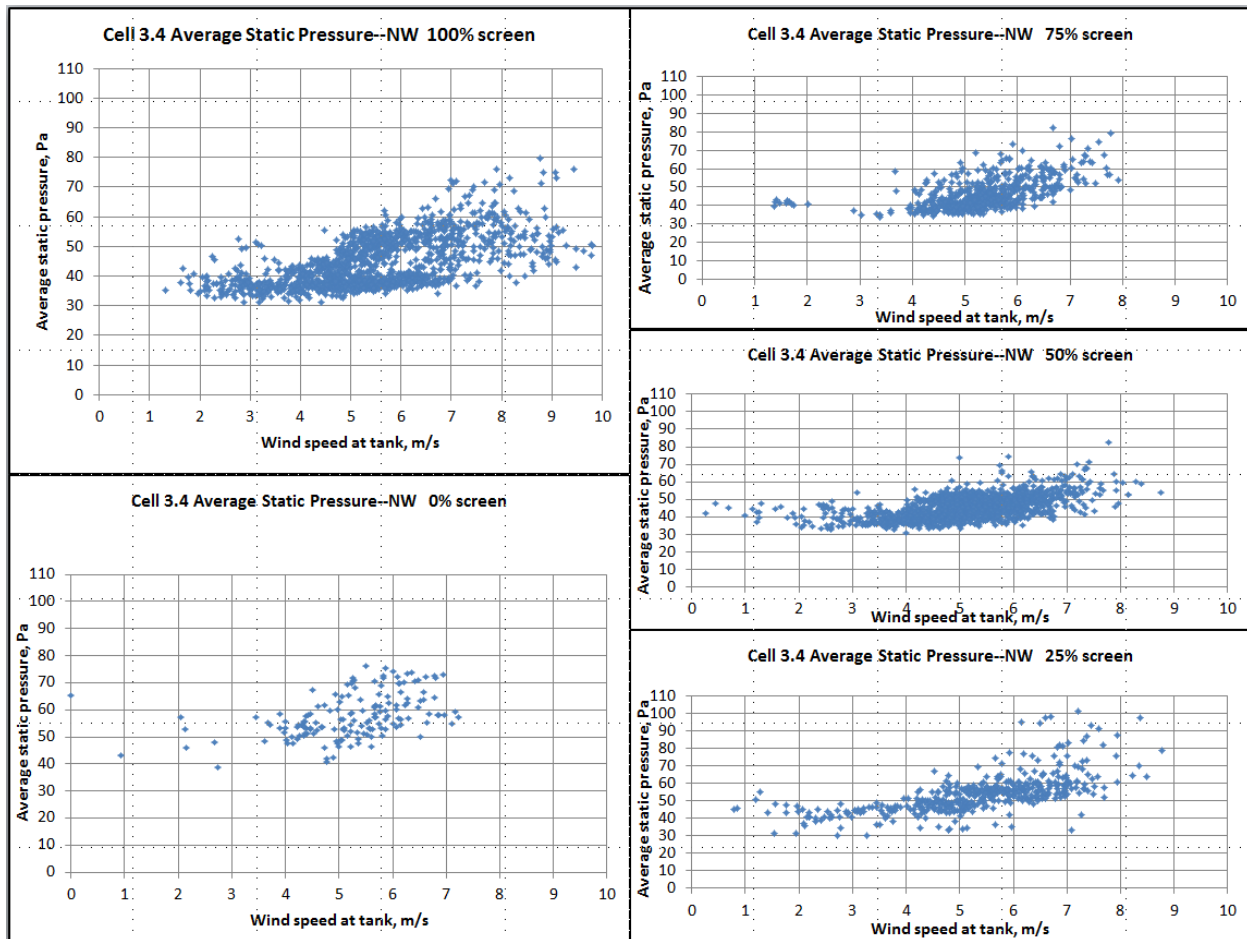


In the following plots, the measured average value for Cell 3.4 is plotted. In Cells 2.4 and 1.4 only a single measurement was made and will be assumed to represent an average (representative) value. Figure 87 displays the average static pressure in Cell 3.4 for the NW wind direction. The figure shows a plot for each of the five screen positions from fully deployed to fully retracted.

### 5.3.1 NW Wind Direction

For winds from the northwest, the variation of static pressure with wind speed is generally the same for all screen positions. It varies from 30 to 40 Pa at the low (< 5 m/s) wind speeds, rising to around 60 Pa at wind speeds in the 7 to 8 m/s range with a large amount of scatter in the readings. The fully retracted (0 percent) screen position shows slightly higher static pressures, but there are very few points at any wind speed, and they exhibit a great deal of scatter.

**Figure 87: Effect of Screen Position on Cell 3.4 Static Pressure (NW Wind Direction)**

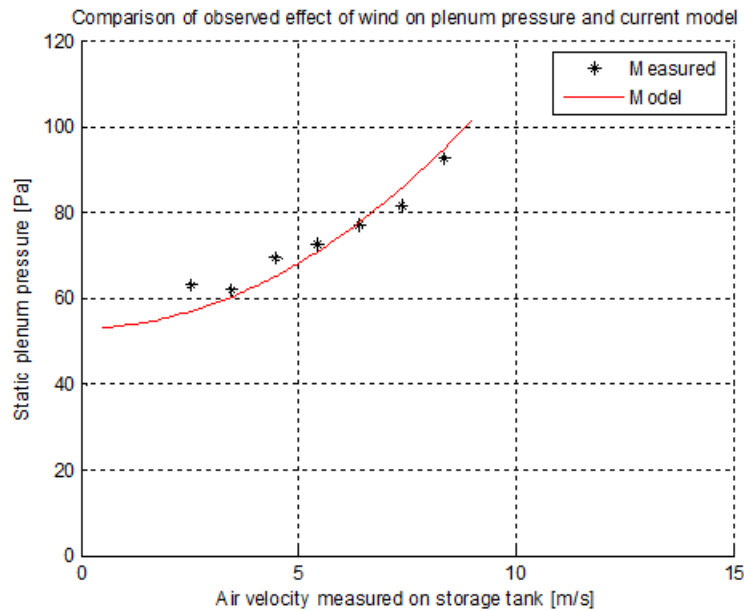


The correspondence of the patterns of static pressure variation is reasonably consistent with the patterns of airflow variation shown in Figure 83 with reductions in airflow corresponding to increases in static pressure. However, the quantitative correspondence is not in good agreement with what would be inferred from the fan curve displayed in Figure 74.

It is the opinion of the Howden technical members of this study team (who are the most experienced in field data acquisition on high flow/low static axial flow fans such as used on this ACC) that static pressure measurements are the more difficult measurements to make under field conditions. Therefore, it will be assumed that the inlet average velocity measurements are the more reliable representation of the fan operating conditions with varying wind speed.

A plot by Howden using the same binning and averaging approach that was used for the inlet velocity plots in Figures 75 through 77 is shown in Figure 88. The plot compares measured average static pressure vs. wind speed for the fully retracted case against their standard model for wind effects on static pressure. The agreement is deemed to be adequate.

**Figure 88: Static Pressure Variation With Wind Speed (Screens Fully Retracted)**



Source: Holkers 2015

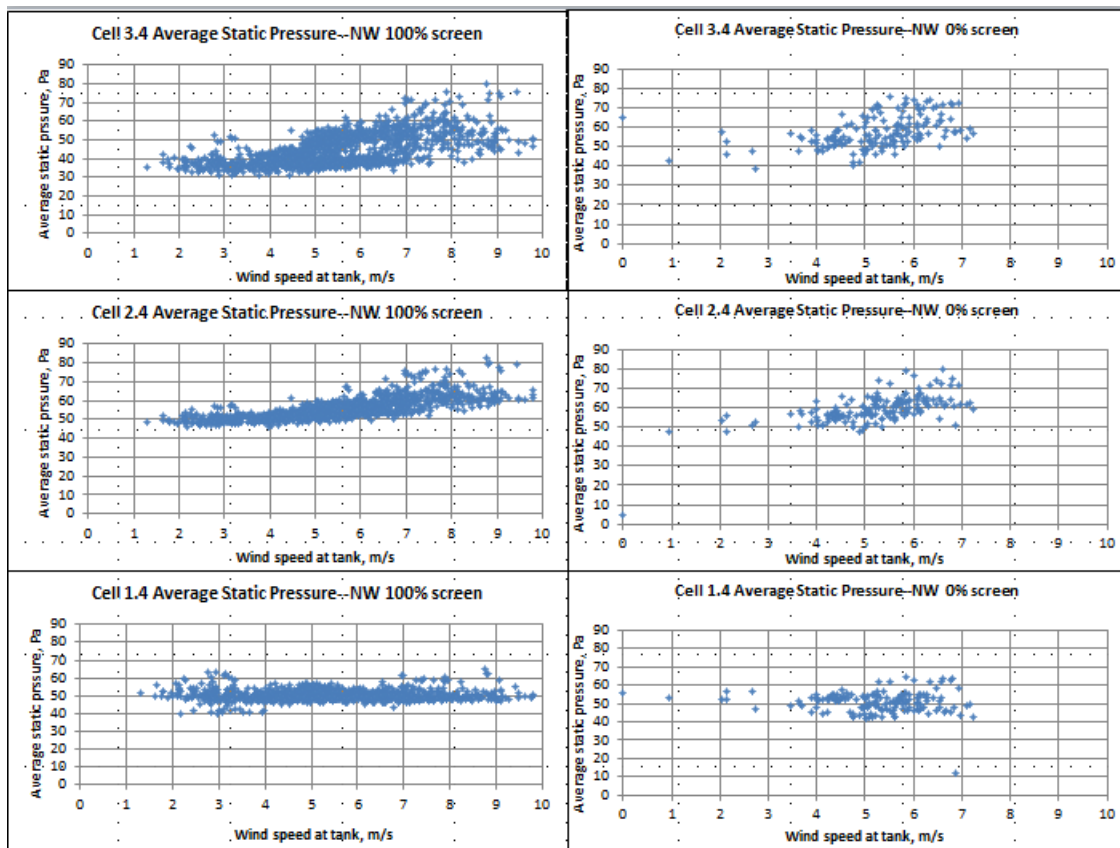
### 5.3.2 Effect of Cell Location

Figure 89 shows the difference in static pressure variation with wind speed between fully deployed and fully retracted screens for the three cells in row 3 (3.4, 2.4 and 1.4) for winds from the northwest. Cell 3.4 is the upwind cell with the winds impinging directly on the west side of the cell. Cell 1.4 is on the other (east) edge of the ACC and is fully shielded from any direct impact of the wind by the other two cells. Cell 2.4 is between them.

Cells 3.4 and 2.4 show increasing static pressure with increasing wind speed for both screen positions. Cell 1.4 is essentially unaffected by wind speed in both screen positions as might be expected since Cell 1.4 is well shielded from northwest winds.

The range of static pressures for each of the cells is essentially the same regardless of screen position, although the fully retracted cases generally increase to higher pressures at lower wind speeds than do the fully deployed cases. Cell 3.4 shows lower static pressures (~ 30Pa) at the lowest wind speeds than do Cells 2.4 and 1.4, which are above 40 Pa even at the lowest wind speeds.

**Figure 89: Effect of Screen Position on Cells 3.4, 2.4 and 1.4 (NW Wind Direction)**



## 5.4 Motor Current Variations

Motor current, which at constant motor input voltage and fan/motor efficiency is an indirect measure of fan power, was measured in 9 cells as indicated in Figure 50. In principle, it should be possible to relate the measured motor current to the air flow and static pressure rise through the fan. Figures AA through DD present some example relationships between motor current, wind speed, screen position and other fan operating conditions for winds from the northwest.

Figure 90 shows that over nearly the entire range of wind speeds the motor current (fan power) is essentially the same whether the screens are fully retracted or fully deployed. Figure 91 extends that conclusion to the intermediate screen positions with the exception of the 25 percent case. However, as was noted in the earlier discussions of inlet air velocity, the 25 percent case is often singular, perhaps because there are few data points at that screen position. Figure 92 and 93 show that the fully retracted operating points have generally higher motor currents for the same airflow but a lower motor current for the same static pressure rise.

Figure 90: Motor Current vs. Wind Speed for Fully Retracted/Deployed Screens

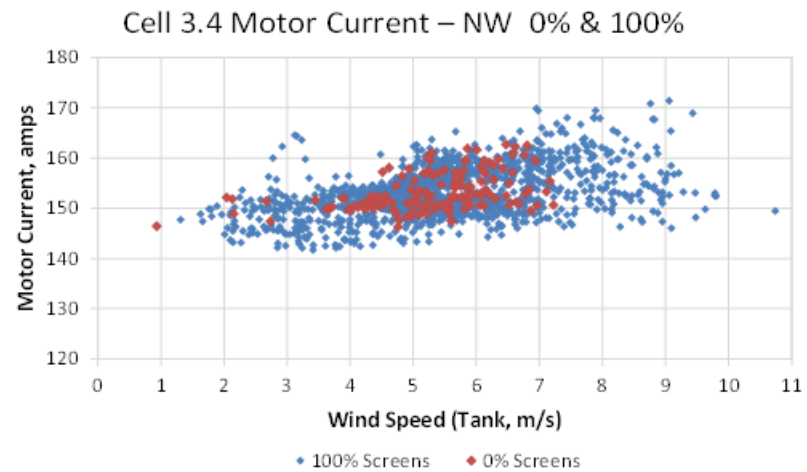
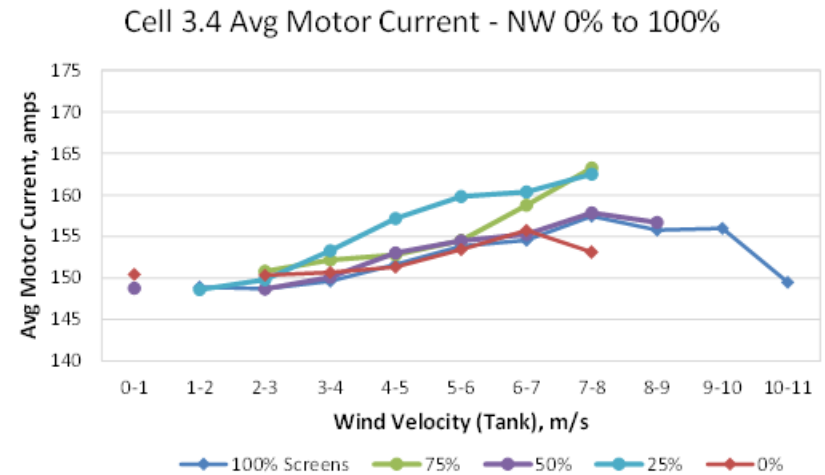
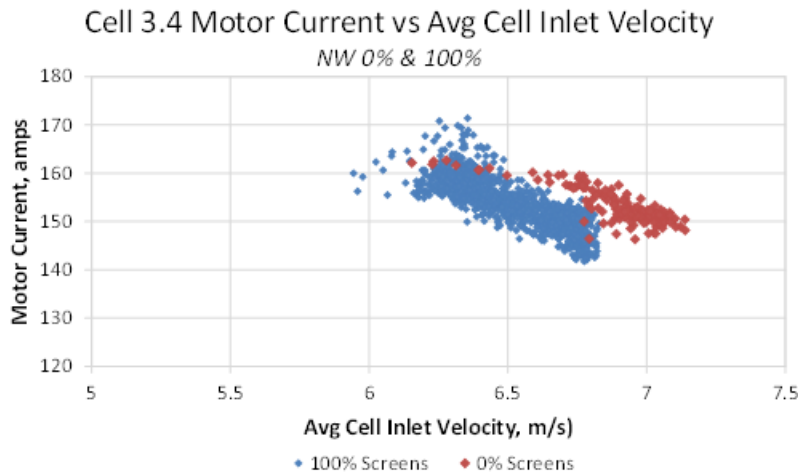


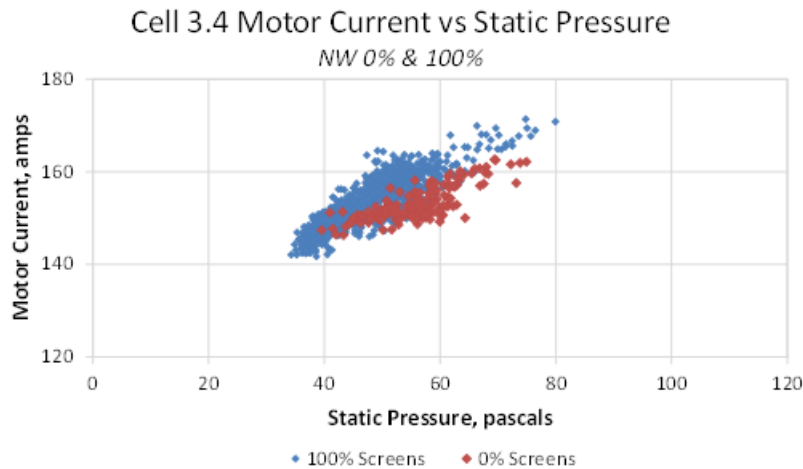
Figure 91: Motor Current vs. Wind Speed for 5 Screen Positions



**Figure 92: Motor Current vs. Fan Inlet Velocity**



**Figure 93: Motor Current vs. Static Pressure**



In general, however, the motor current results were often inconsistent and difficult to interpret. No consistent relationship could be developed between the measured motor currents and fan power as estimated with the independent measurements of average inlet velocity and static pressure rise.

## 5.5 Recirculation

While the more important effect of ambient wind on ACC performance is believed to be the degradation of fan performance and the consequent reduction in air flow through the ACC, the effect of recirculation which results in an inlet temperature to the ACC which is higher than the far-field ambient temperature can also have a deleterious effect. To the extent that wind screens could reduce the amount of recirculation, this would constitute a beneficial effect.

As discussed in an earlier section, average recirculation for the purposes of this study is defined as the average cell inlet temperature minus the minimum cell inlet temperature. In addition to the average recirculation, which would be the primary indication of ACC performance reduction, it is also of interest to identify the maximum recirculation, which is defined as the maximum cell inlet temperature minus the minimum cell inlet temperature.

Figure 94 displays a side-by-side comparison of both the average and maximum recirculation for northwest winds for fully deployed and fully retracted screens. While the much smaller number of points for the fully retracted cases makes comparison difficult, there is no obvious difference between the two screen positions. The average recirculation for both the fully retracted and fully deployed cases ranges from 0.5 to 2.5 C with the maximum occurring at intermediate wind speeds around 4 to 5 m/s. The maximum recirculation ranges from 1 to 10 C for the fully deployed cases with the higher values at low to intermediate wind speeds. The fully retracted cases shows a similar pattern with wind speed and, although the higher values of “maximum” recirculation are lower for the fully retracted case, this is likely due to the paucity of points at the wind speed associated with the higher recirculation.

Figures 95 and 96 show average and maximum recirculation values vs. wind speed for each of the 5 screen positions. It is difficult to discern any effect of screen position on either the magnitude of recirculation or its dependence on wind speed.

The highest average recirculation occurs at slightly lower wind speeds in the fully retracted condition and the highest levels of maximum recirculation are seen for the fully deployed condition. However, the number of data points related to both of these observations is very small and they are not considered robust. On balance, there appears to be no effect of the windscreen on recirculation for the ambient and operating conditions experienced at Caithness.

## 5.6 ACC Performance---Q/ITD

The most comprehensive indication of the effect of wind protection is a measure of the overall thermal performance of the ACC. A commonly used performance metric in the ACC industry is the total heat load,  $Q$  (kWth) divided by the initial temperature difference, ITD (K) (defined as the condensing temperature minus the ambient temperature) or  $Q/ITD$ . The heat load is calculated using plant data for the total steam flow to the ACC multiplied by the latent heat of vaporization,  $h_{fg}$  (J/kg) adjusted by the design value for turbine exit steam quality.

$$Q = W_{\text{steam}} * h_{fg} * x_{\text{exit}}$$

The ITD is determined from the condensing temperature corresponding to the turbine exhaust pressure from plant data and the ambient temperature as indicated by the minimum cell inlet temperature. Figure 97 displays the ACC thermal performance vs. wind speed for the five screen positions with wind from the northwest. The range of thermal performance is essentially the same at all five screen positions with a slightly higher performance at the fully retracted position at the lower wind speeds which is consistent with the reduction in airflow to the windward cells at the low wind speeds. All the cases show some points with reduced thermal

performance at wind speeds between 4 and 6 m/s which is consistent with the increased levels of average recirculation at that same wind speed range shown in Figure 96.

**Figure 94: Effect of Screen Position on Average and Maximum Recirculation—NW Wind Direction**

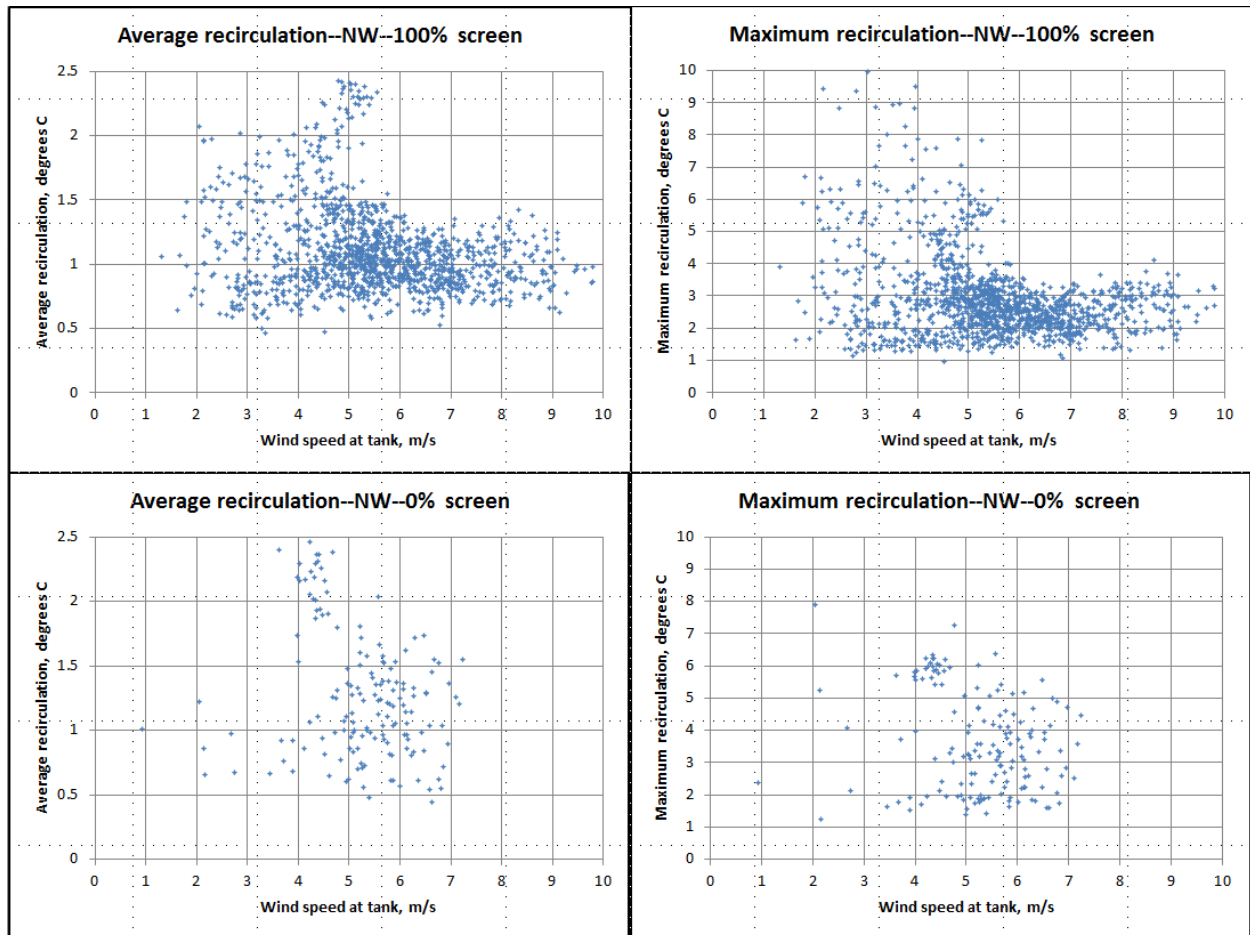


Figure 95: Effect of Screen Position on Average Recirculation—NW Wind Direction

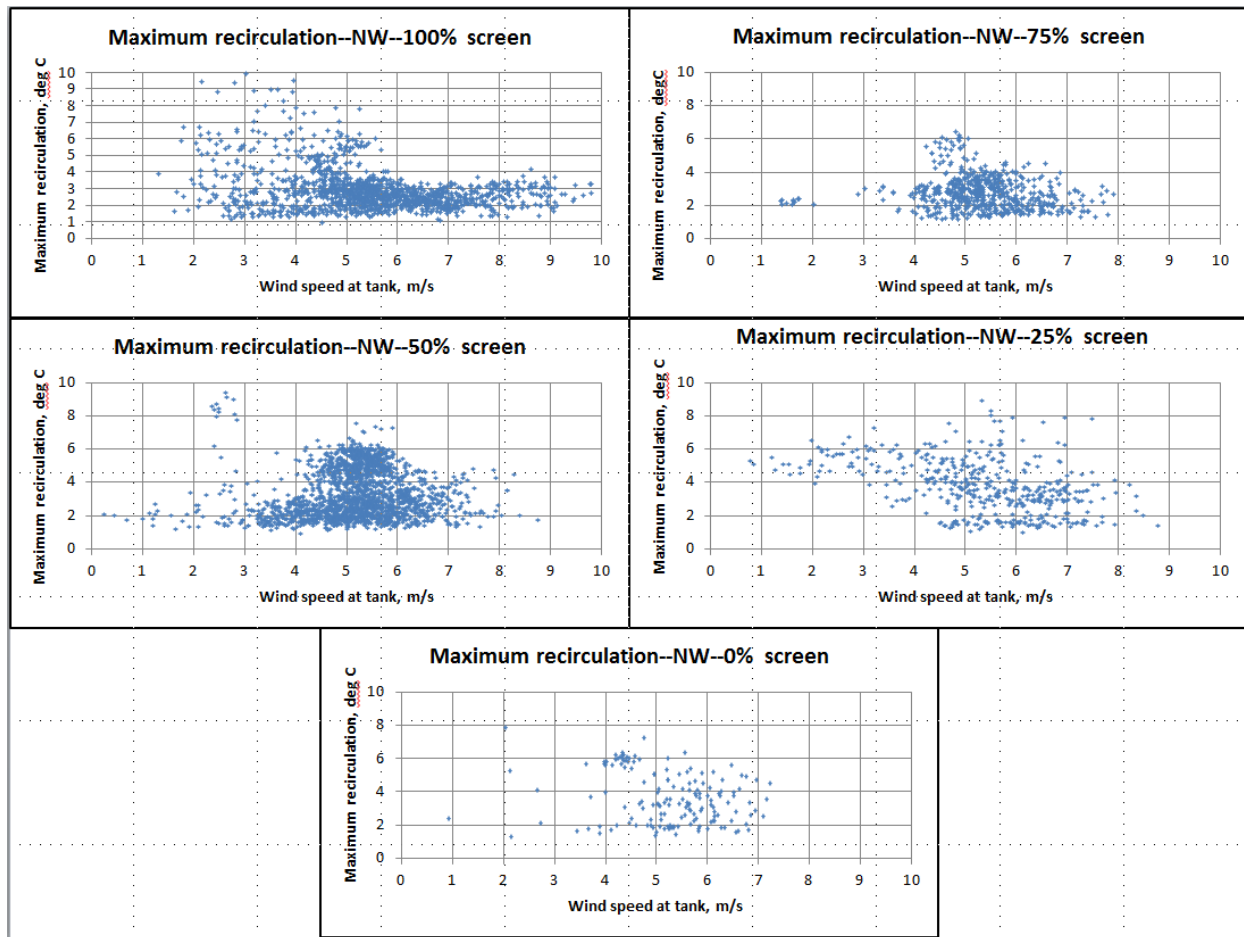
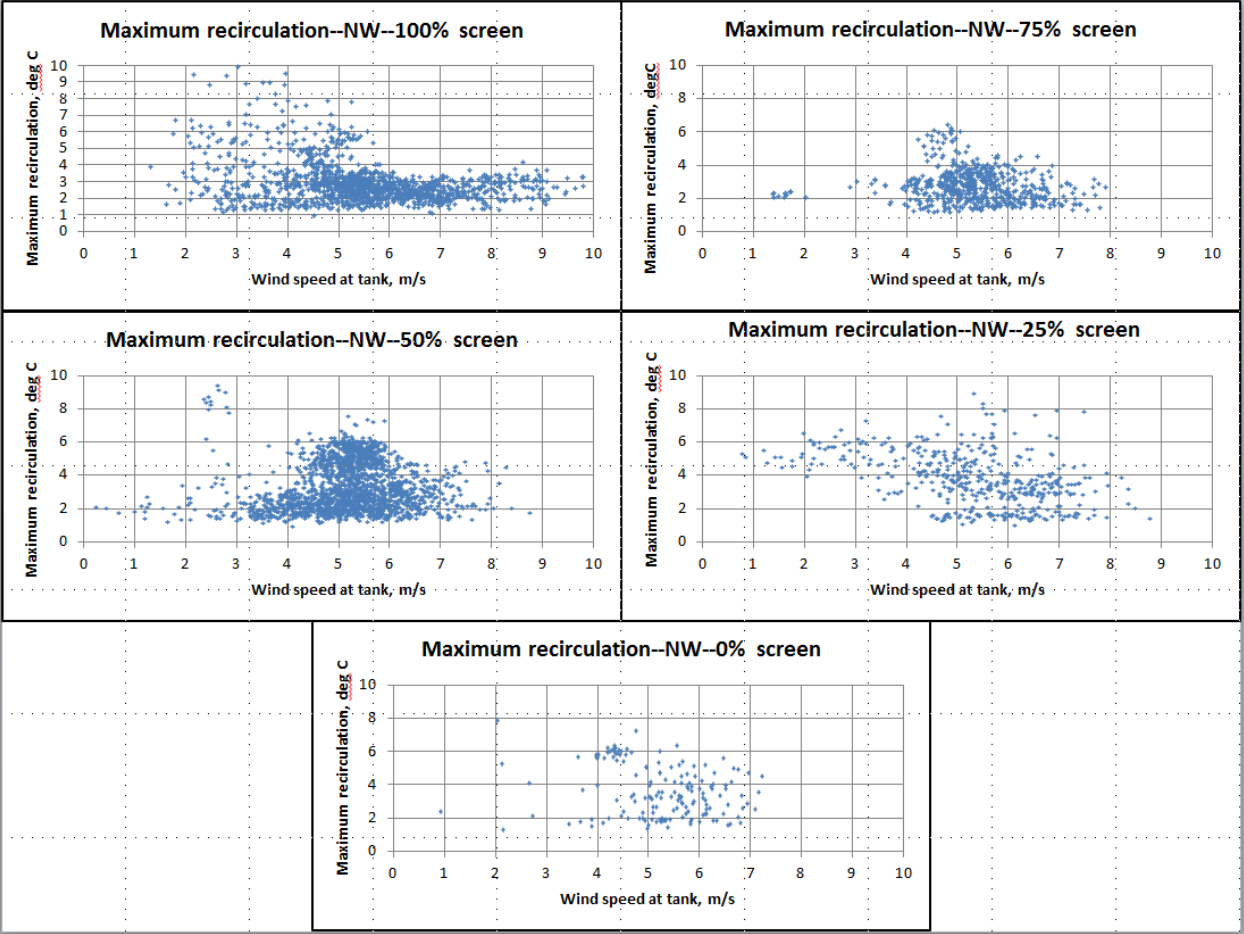
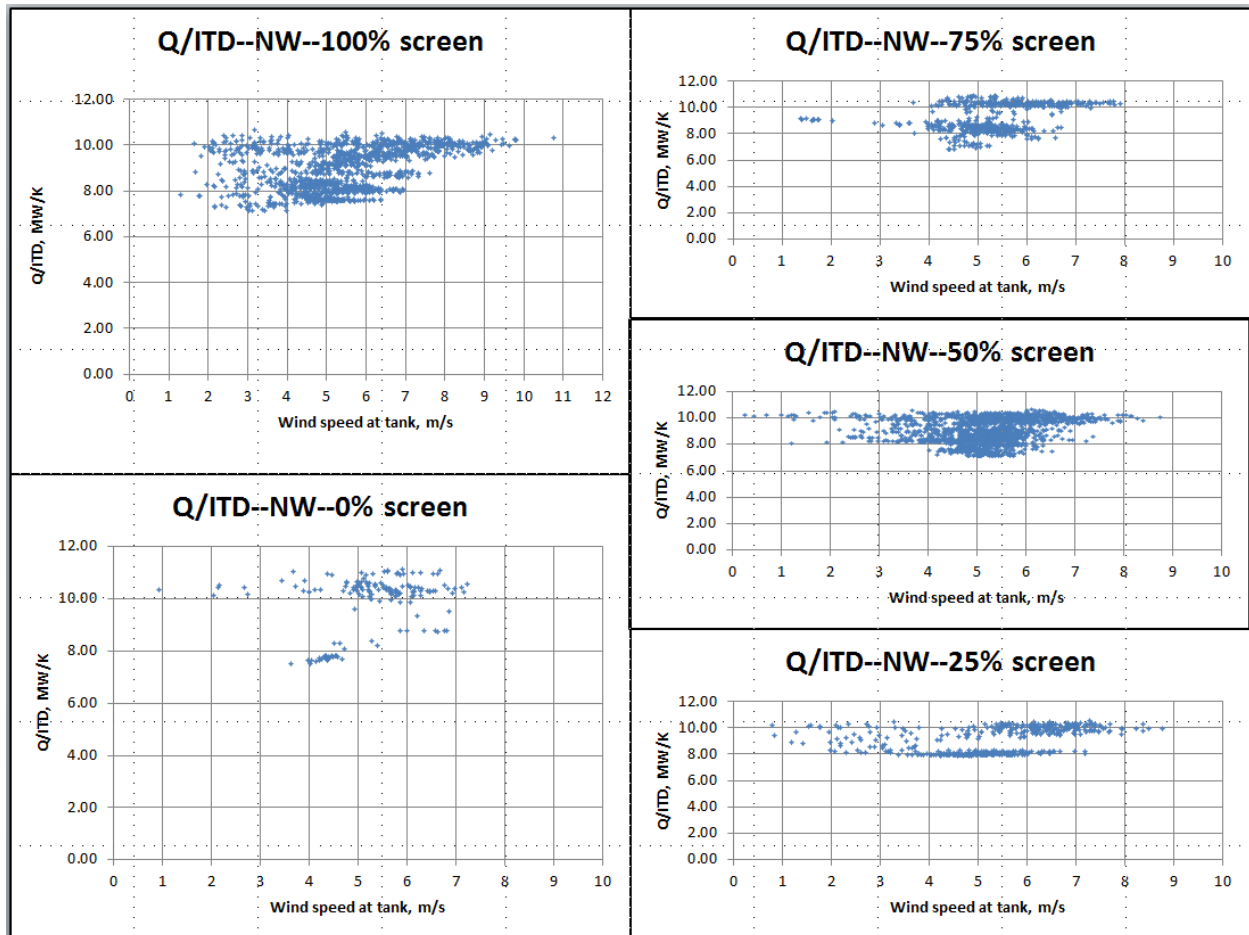


Figure 96: Effect of Screen Position on Maximum Recirculation—NW Wind Direction

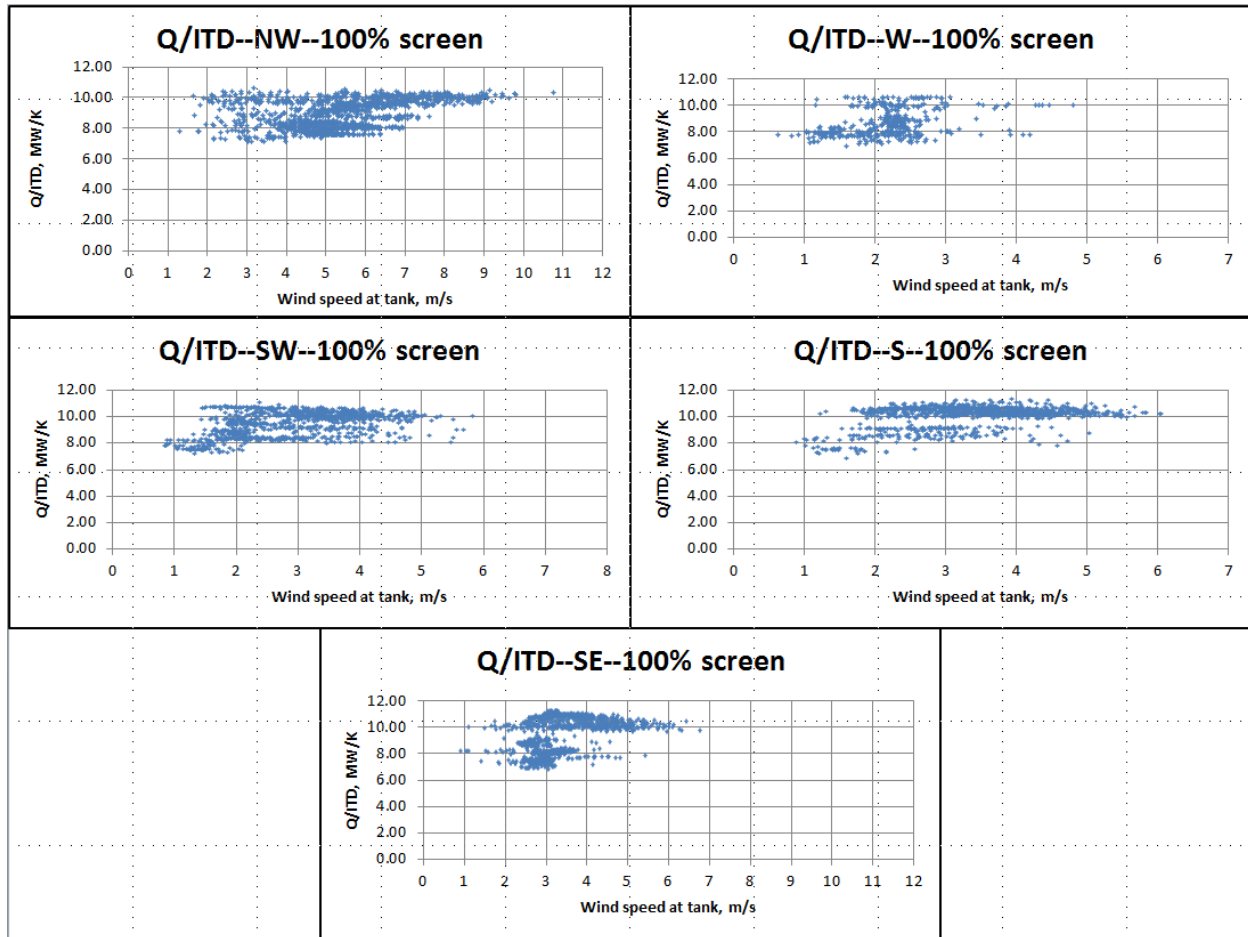


**Figure 97: Effect of Screen Position on ACC Thermal Performance—NW Wind Direction**



Figures 98 and 99 display the ACC thermal performance vs. wind speed for five wind directions with screens both fully deployed (Figure 98) and fully retracted (Figure 99). All cases with fully deployed screens range from about 7 MW/K to 11 MW/K with the lower values at generally lower wind speeds and in the range where recirculation is greatest. The results with fully retracted screens are essentially the same although the lower values are slightly higher at about 8 MW/K vs. 7 MW/K.

**Figure 98: Effect of Wind Direction on ACC Thermal Performance—Fully Deployed Screens**

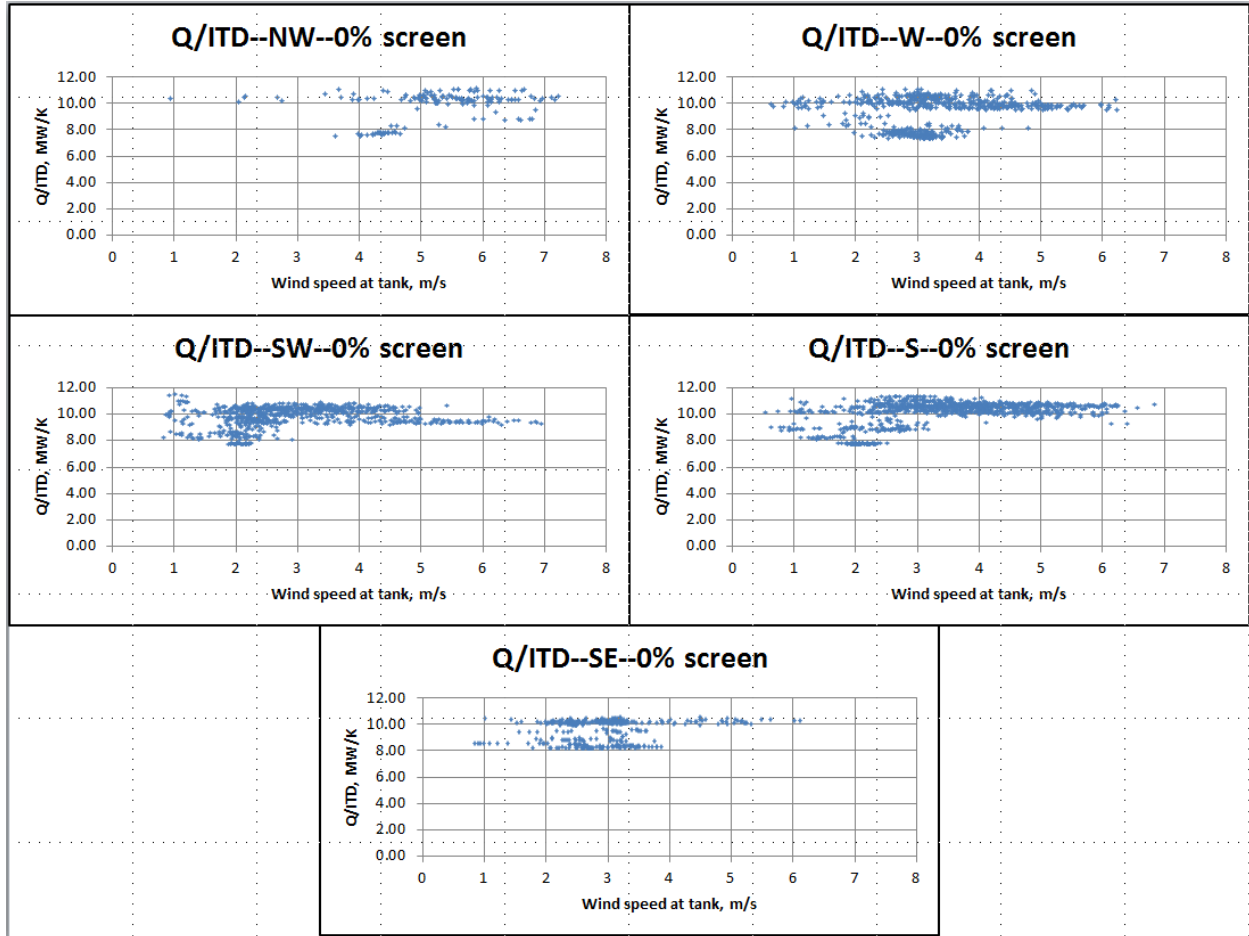


## 5.7 Wind-induced Dynamic Blade Loading

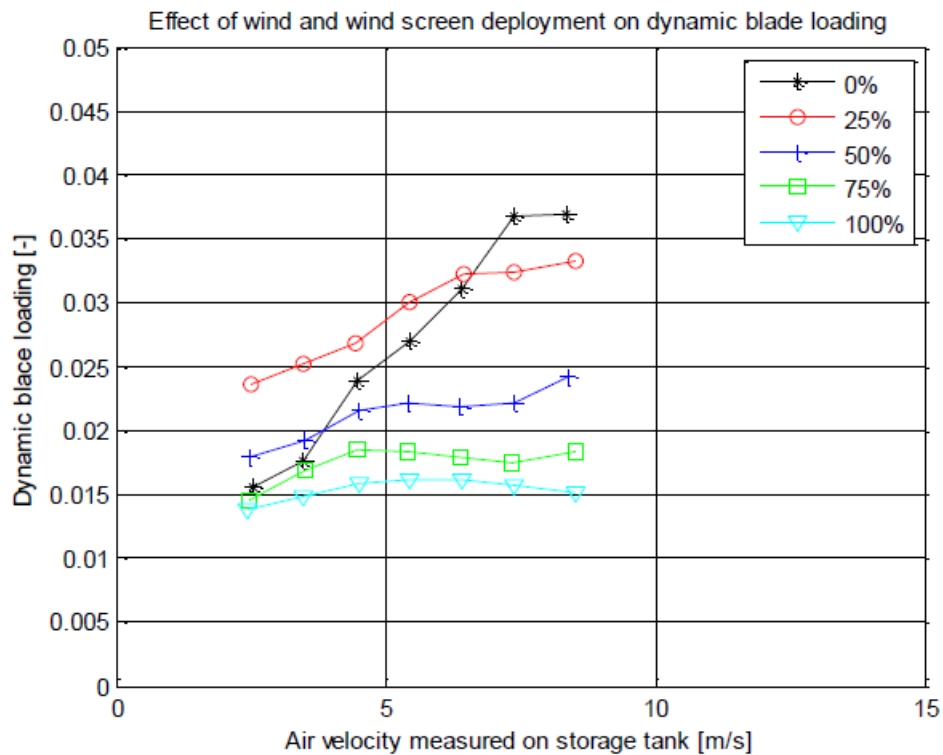
As noted in the introductory discussion in Section 1, an important effect of wind on ACCs is the imposition of wind-induced stress on the fan blades leading, in some instances, to blade damage or failure. To study this effect, dynamic loading measurements on 7 of the 9 blades on Fan 3.4 were recorded throughout the test period. Two representative examples of these measurements are shown in Figures 100 and 101. The following material is based on the Howden report (Holders 2015).

Figure 100 displays long-term, average values of the dynamic blade loading on Blade 3 of Fan 3.4 (Sensor 54L in Figure 49) vs. wind speed measured at the tank for the five screen positions.

Figure 99: Effect of Wind Direction on ACC Thermal Performance—Fully Retracted Screens



**Figure 100: Long-Term Average Blade Loading vs. Wind Speed for 5 Screen Positions**



Source: Holkers 2015

The dynamic blade loading is taken as 3 times the standard deviation of the output signal from load cell 54L. The high resolution (250 Hz) readings were averaged over 10 second (2,500 points) intervals and binned into 1 m/s ranges of wind speed as measured on the water tank (Sensor 21A in Figure 49).

The results show a significant increase in blade loading with increasing wind speed during periods when the screens are fully retracted or only 25 percent deployed. A 50 percent to 100 percent deployments, both the loading itself and the increase in loading with increasing wind speed are significantly reduced. During periods when the screens were fully deployed, the loading was reduced by a factor of between 2 and 3 at the highest (7.5 to >8 m/s) wind speeds and the effect of wind speed over the range from 2.5 to > 8 m/s was essentially eliminated. At the lowest wind speeds, the lower screen deployments (25 percent and 50 percent) appeared to increase the dynamic loading slightly. The reason for this is not fully understood but minimal screen deployment may introduce some flow disturbances at levels close to the fan inlet which are reduced or eliminated as the screen is further deployed.

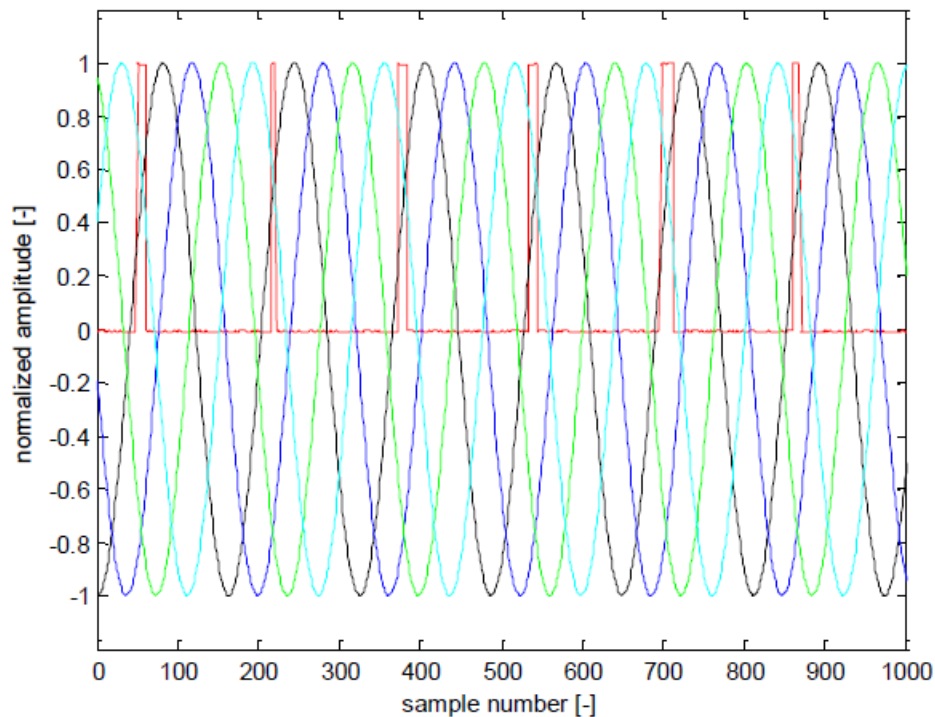
To understand the mechanism by which an increase in wind speed results in increased dynamic blade loading and the effect of screen deployment on the relationship between wind speed and blade loading, the high resolution data were examined in more detail. A few short (180 second)

periods during which significant changes in wind speed occurred were selected. The following plots and discussion are excerpted from the Howden topical report.

### 5.7.1 Blade Excitation Frequency

The 250 Hz load cell output from several of blades (Blades 1, 3, 5 and 7) were filtered to extract the signal that matched the fan operating frequency (93 rpm = 1.55 Hz). Figure 101 shows the normalized signals from the 4 blades and the tachometer pulse which occurs once per revolution. The pulses are separated by approximately 160 ( $\approx 250/1.55$ ) samples.

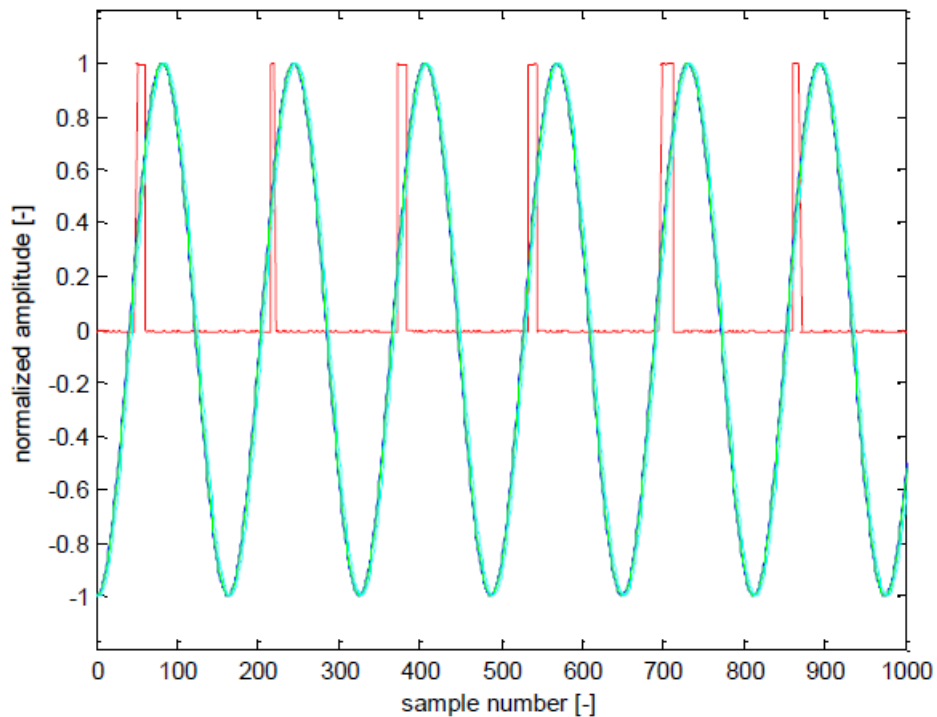
**Figure 101: Filtered Sample Load Cell Outputs and Tachometer Pulse**



Source: Holkers 2015

The filtered data sets were shifted to align them all with the Blade 1 signal. The aligned peaks were separated by the sample time corresponding to one revolution as determined by the “one per revolution” tachometer pulse (Sensor 25 on Figure 49). The phase shift required to bring the different blade data sets into alignment coincides with the angle between the sampled blades confirming that the blades were excited once per revolution as shown in Figure 102.

**Figure 102: Aligned Pulses and Tachometer Pulse**



Source: Holkers 2015

### 5.7.2 Source of Excitation

An excitation frequency of “one per revolution” suggests a difference in air inlet velocity across the fan inlet area which would result in a varying angle of attack on the blades which varied cyclically and produced a corresponding variation in the lift/drag forces on the blades. This is to be expected from both flow visualization observations and cell inlet velocity measurements.

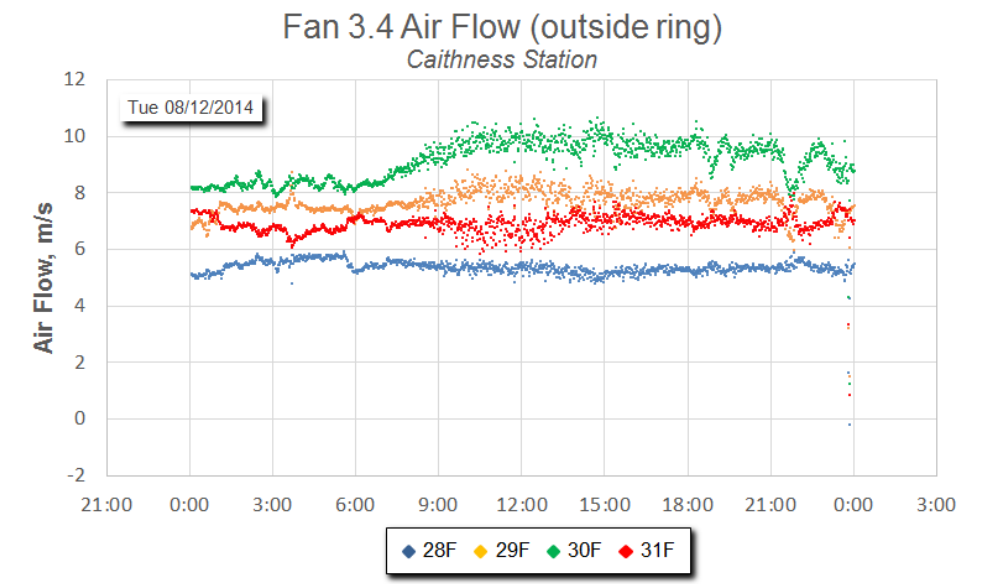
Figure 103 shows a smoke trace passing under a fan. While the angle of the photograph makes it difficult to see, the smoke passes under the upwind portion of the fan and turns upward into the downwind portion. Figure 104 presents anemometer readings of inlet velocity into Cell 3.4 during August 12, 2014 in four positions on the outer ring of anemometers at a radius approximately  $2/3$ 's of the way to the blade tips.

Anemometers #28F and #31F are in the upwind half of the inlet area and anemometers #29F and #30F are in the downwind half. The velocity at #30F is double that at #28F.

**Figure 103: Smoke Trace Under Fan**



**Figure 104: Inlet Air Velocity Variations**



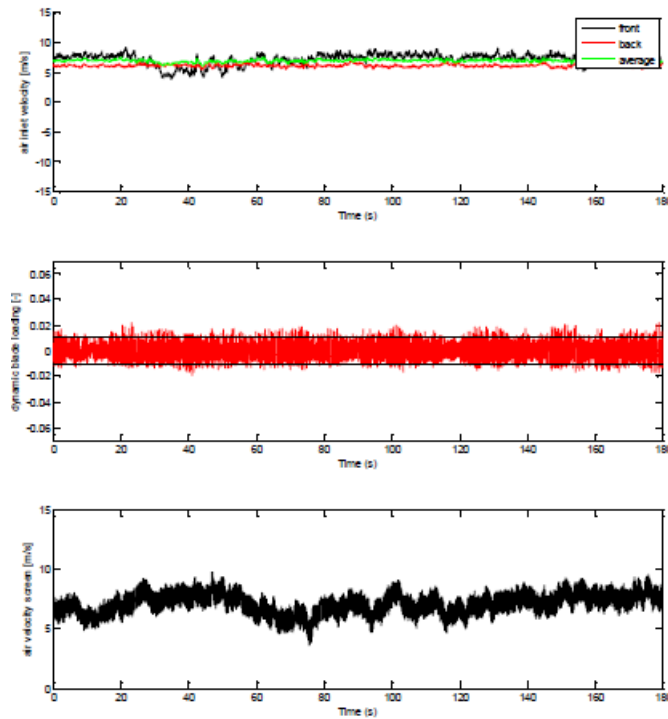
Detailed high resolution measurements of the variation in air inlet velocity over the Cell 3.4 fan inlet area are shown in the upper panel in Figure 105 for the following locations for a three minute period on July 30, 2014 (3:18 pm to 3:22 pm).

Front of the fan inlet area: Sensors (28F + 31F)/2

- Back of the fan inlet area: Sensors (29F + 30F)/2
- Average over the fan inlet area: Sensors (28F through 35F)/8

During this period, the inlet air velocity is reasonably uniform ( $V_{\text{front}} \approx V_{\text{back}} \approx V_{\text{average}}$ ) across the fan inlet area. The wind speed at the edge of Cell 3.4 is consistently below about 7.5 m/s corresponding to a wind speed at the tank of less than 4 m/s. The dynamic blade loading is low in the range of  $\pm 0.01$ .

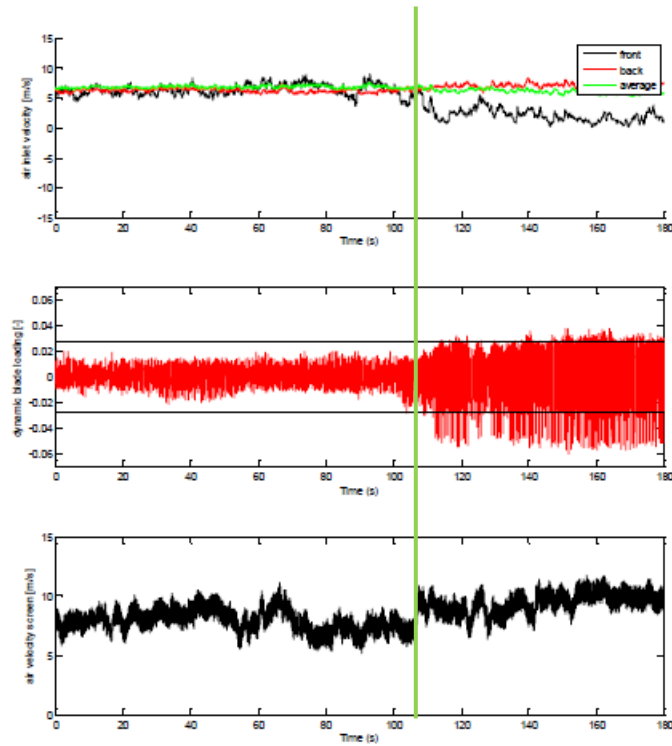
**Figure 105: Wind Speed, Inlet Velocity, and Blade Loading At Cell 3.4**



Source: Holkers 2015

Figure 106 illustrates, in the same format, a three minute period (also on July 30, 2014 from 3:45 pm to 3:48 pm) during which (at approximately 3:47 pm) the wind speed jumps to about 10 m/s at the edge of Cell 3.4 (corresponding to approximately 8.5 m/s at the tank). The increase in wind speed corresponds precisely to an increase in non-uniformity of the inlet air velocity and a significant (about threefold) increase in the dynamic blade loading.

**Figure 106: Effect of Wind Speed Increase**



Source: Holkers 2015

### 5.7.3 Effect of Screen Deployment

The results discussed above have been for periods during which the wind screen was fully retracted. The results in Figure 99 and 100 indicated that the increase in dynamic loading with wind speed was reduced or eliminated as the wind screen was deployed. This is attributed to the effect of the wind screen in reducing the non-uniformity in the air inlet velocity. This effect is seen in Figure 107 which plots inlet velocity variation from front to back of the fan inlet area for both fully retracted and fully deployed screens and also in Figures 108 and 109 which was taken from a separate analysis analyzing the same trend but plotting it against off-site wind speed. A reduction in non-uniformity is seen with screen deployment.

Figure 107: Effect of Screen Deployment on Inlet Velocity Variability

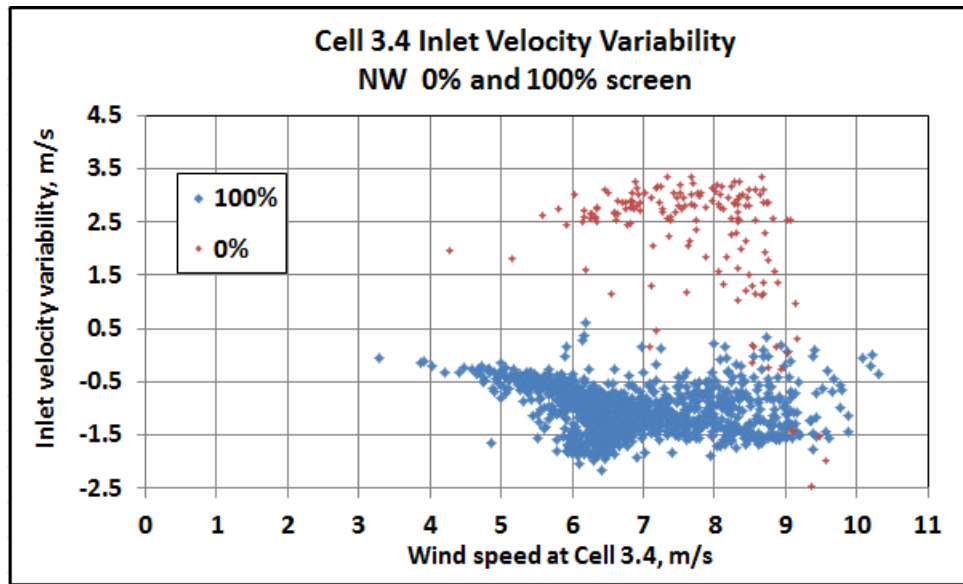
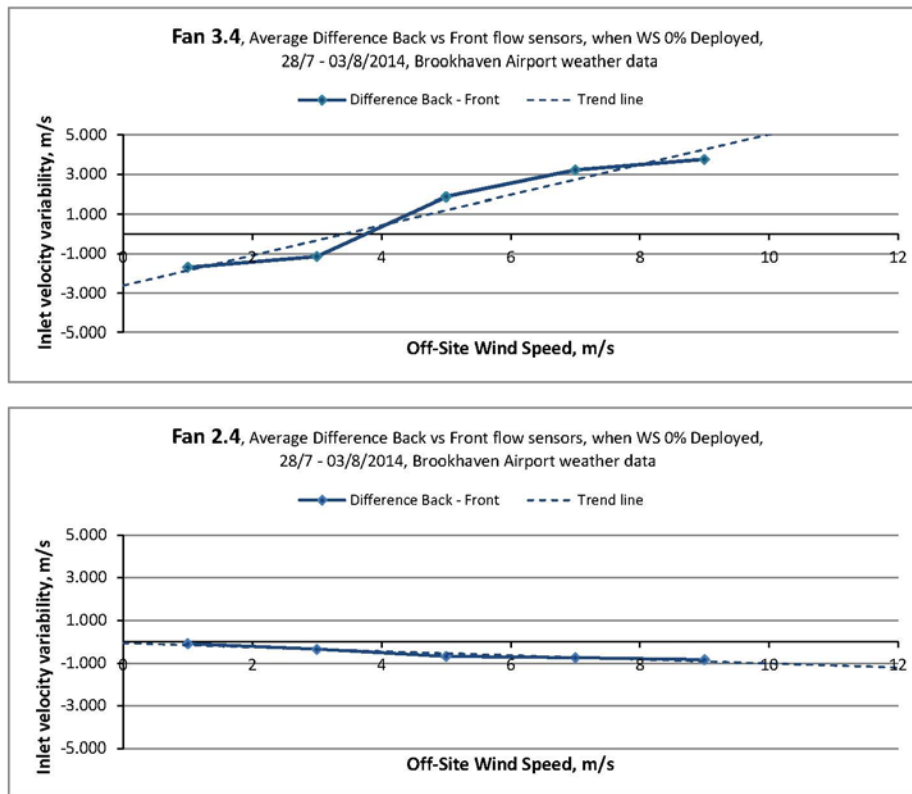
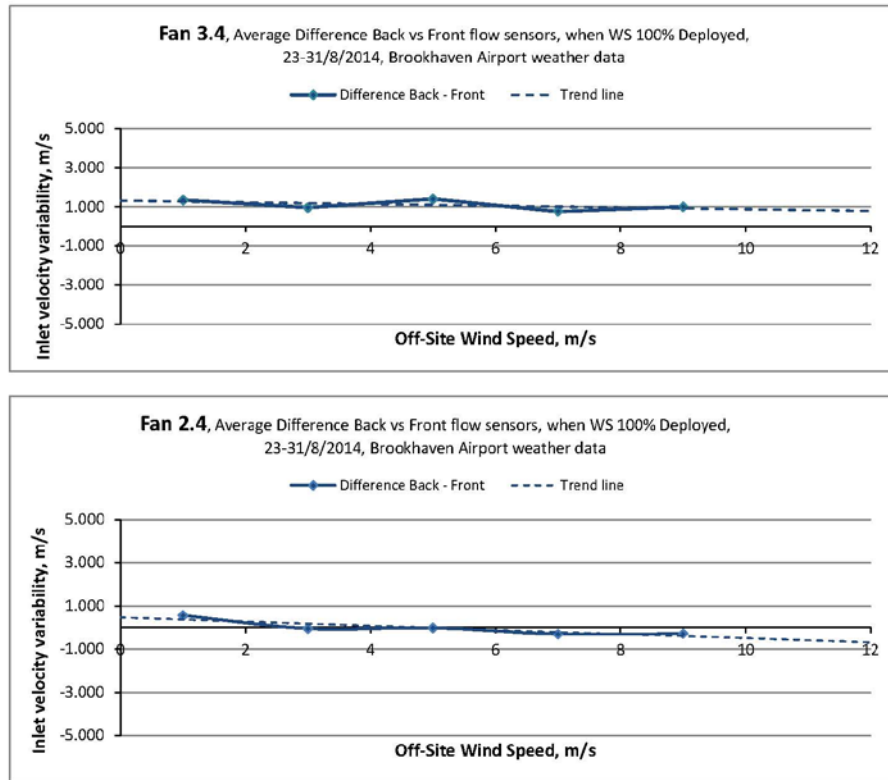


Figure 108: Fan 3.4 and 2.4 Inlet Velocity Variability, Screen Retracted



**Figure 109: Fan 3.4 and 2.4 Inlet Velocity Variability, Screen Deployed**



The test results, as illustrated by the selected examples discussed above, demonstrate conclusively that the wind screens essentially eliminated any increase in wind-induced blade loading when deployed at Caithness up to wind speeds at the edge of the monitored cell up to over 10 m/s.

## CHAPTER 6: Modeling Results

The field testing described in Section 5 was supplemented by two modeling efforts; a physical modeling in a wind tunnel and analytical (CFD) modeling.

### 6.1 Physical Modeling

The physical modeling element of this study was conducted at the Atmospheric Boundary Layer (ABL) wind tunnel at the University of California at Davis. The facility, the model and the instrumentation are described in Section 4.3 and Appendix B.

The focus of the physical modeling work was three-fold:

- To provide increased physical understanding of mechanisms affecting the airflow patterns observed in the field and governing the behavior and effectiveness of wind screens
- To provide guidance and corroboration to the analytical modeling effort and
- To simulate field conditions, both qualitatively and quantitatively airflow patterns around, under and through an air-cooled condenser operating in complex surroundings.

The activities in each of these areas are discussed separately in the following sections.

#### 6.1.1 Governing Flow Mechanisms

Three issues were investigated in detail; the flow resistance characteristics of the porous screen fabrics, the effect of ACC-induced wind on wind speed measurements and the effect of tank blockage on wind speed measurements.

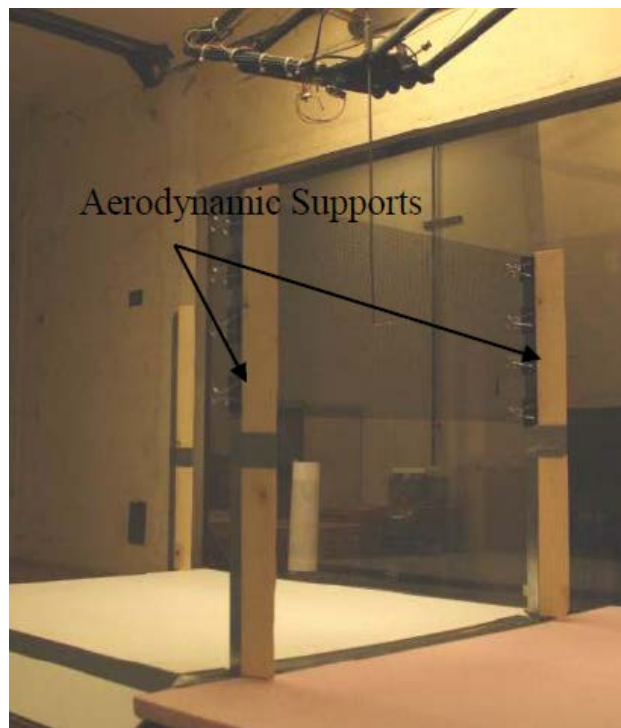
##### 6.1.1.1 Porous Fabric Characteristics

The effect of the presence of a porous screen on the flow of incoming air as a function of screen porosity, incoming wind speed and angle of incidence was investigated. The situation in which air encounters a porous barrier is different if the barrier is suspended in an otherwise open flow area from the case where the barrier fills the flow area in a closed tube or tunnel. In the latter case, all the air must pass through the porous screen and simply incurs a drop in static pressure. In the first case, which is the pertinent one in this study, some portion of the air is diverted around the screen; some portion passes through it and will have a velocity immediately downstream of the screen lower than the approach velocity. Far downstream the two portions of the incoming air will again combine. The reason for expecting that the presence of porous screens upwind of the fan inlets will benefit ACC performance is that the air passing through the screen will be slowed just under the fan inlet and will be more easily turned upward to by the fan to enter the cell. However, the air diverted around the bottom of the screen remains at a high velocity and passes beneath the fan at an even lower level than it would in the absence of a screen. This portion of the flow is, therefore, less likely to be entrained into the cell. The balance between these two flows determines the net effectiveness of the screen.

Tests in the wind tunnel were designed to characterize the effect of a porous screen barrier over a range of screen porosities, incoming wind speeds and angle of incidence of the wind to the plane of the barrier. The design, conduct and results of these tests are described in detail in Larson (2015) and summarized here.

Panels made of fabric of varying porosity (40, 60, 75 and 88 percent solidity) were mounted in the wind tunnel. Aerodynamic supports were constructed to hold the frame without introducing flow disturbances at the edges of the panel. A picture of the frame with 40 percent solidity fabric mounted in the wind tunnel normal to the incoming flow direction is shown in Figure 110.

**Figure 110: Set-Up for Measurement of Wind Screen Characteristics**



The frame holding the panel could be turned at differing angles to the incoming flow from  $90^\circ$  (flow normal to the plane of the screen) to angles of  $22.5^\circ$ ,  $45^\circ$  and  $67.5^\circ$  to the direction of incoming flow. Velocity measurements were taken from the center of the screen plane upstream and downstream of the fabric.

Two quantities characterize the fabric and determine its behavior as a wind screen and its effect on the airflow approaching and entering the ACC. These are the wind break effectiveness (WBE) and the pressure drop coefficient (PDC).

#### **6.1.1.2 Wind Break Effectiveness**

The effectiveness of the screen in reducing the airflow velocity was characterized by a “Wind Break Effectiveness” (WBE) defined as:

$$WBE = (1 - \bar{V}_{\text{downstream}} / V_{\infty}) \times 100 \text{ ( percent )}$$

Plots displaying the variation in WBE with distance downstream from the screen for three different incoming wind speeds are shown in Figures 111 through 114 for screens of 40 percent, 60 percent, 75 percent and 88 percent solidity.

**Figure 111: WBE for 40 Percent Solidity Fabric**

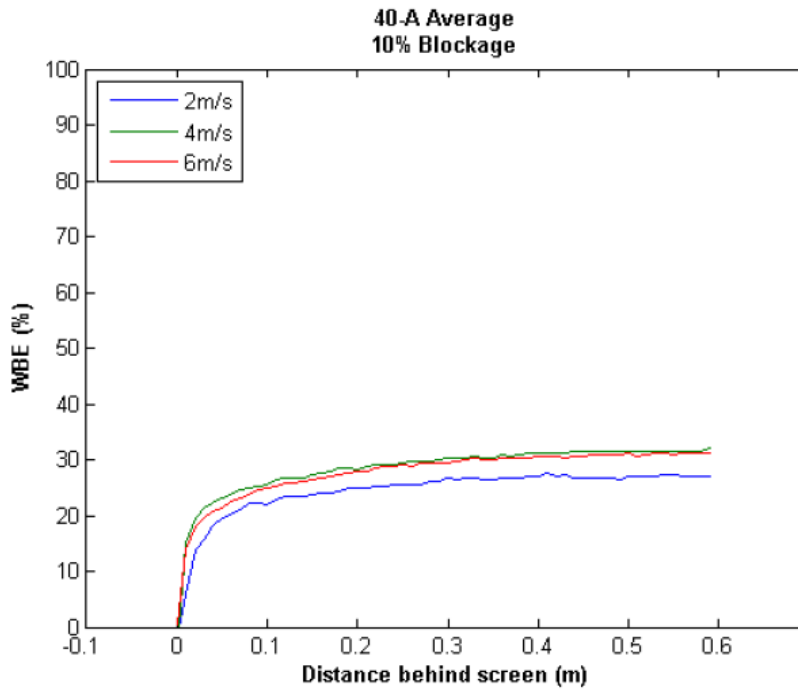


**Figure 112: WBE for 60 Percent Solidity Fabric**

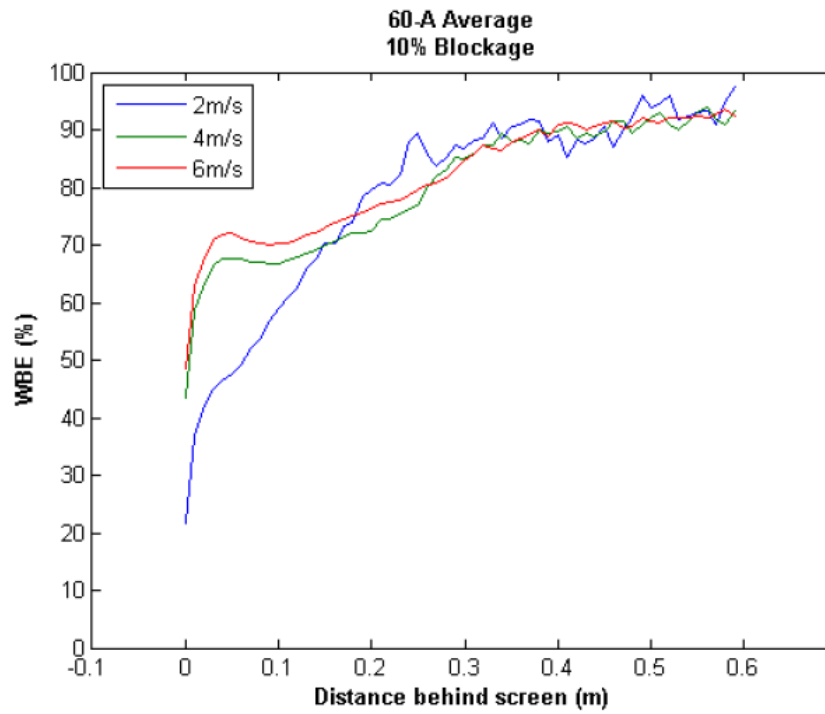


**Figure 113: WBE for 75 Percent Solidity Fabric**

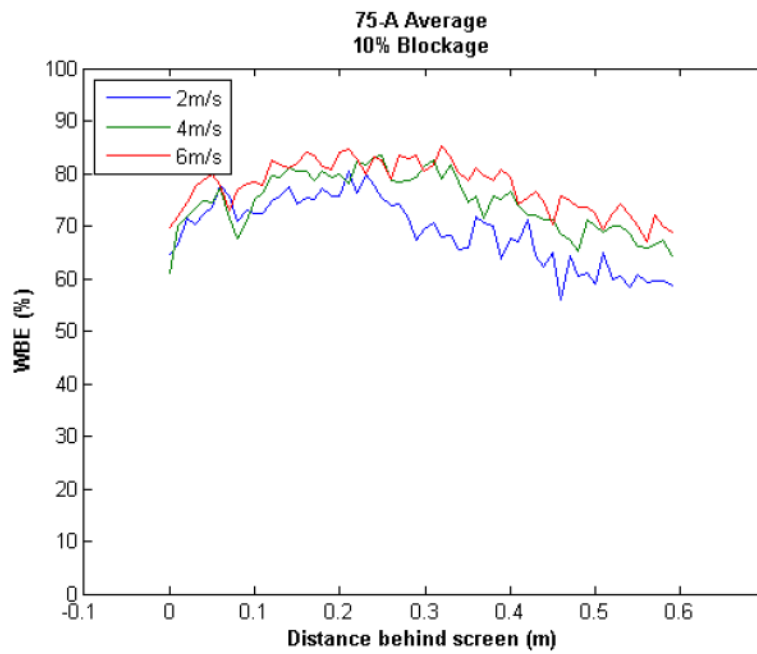
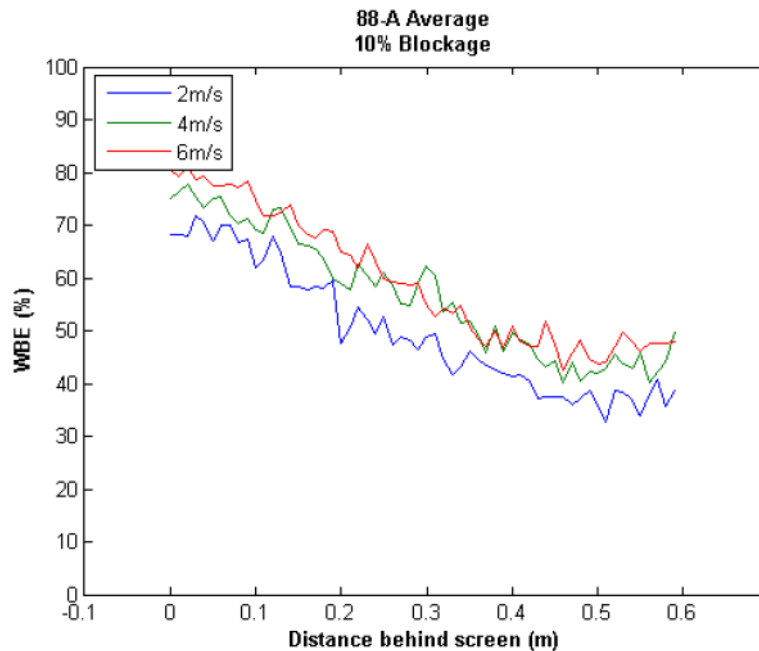


**Figure 114: WBE for 88 Percent Solidity Fabric**



The 60 percent solidity fabric shows the most desirable performance. The more porous fabric (40 percent solidity, Figure 111) shows little slowing of the air immediately behind the screen and a rapid re-convergence of much of the incoming air further downstream. The higher solidity fabrics (Figures 113 and 114) divert large amounts of the flow producing a very low speed region immediately behind the screen which persists downstream particularly in the case of the 75 percent solidity fabric (Figure 113). The higher solidity screens act much like bluff bodies by blocking the air and creating a wake region behind them.

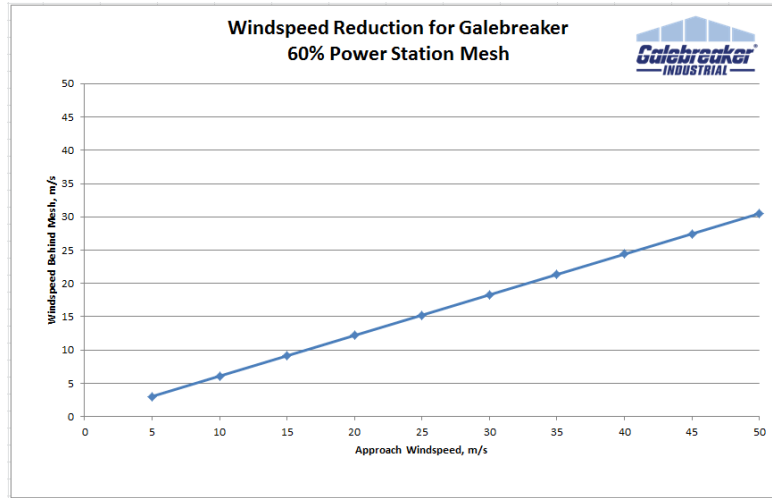
Limited measurements were made at varying angles of incidence. These results are discussed in more detail by Larson (2015), but it was determined that no definite conclusions can be drawn due to the limitations of a single-wire, hot wire anemometer and the inability to determine wind direction.

The fabric used for the screens installed at Caithness is the 60 percent solidity material and reasonable airflow behavior around and behind the screens is to be expected. The characteristics of the screen used in the analytical model will be selected to match the wind tunnel results as is discussed in a later section.

It should be noted that Galebreaker, the wind screen vendor, has run other tests on both the WBE and the pressure drop coefficient and have reported values which differ from those in this report. The discrepancies stem from differences in both the design and methodology of the tests and the definition of terms.

The WBE reported by Galebreaker for the 60A fabric (60 percent solidity) is displayed as a single value of approximately 40 percent for wind speeds ranging from 5 to 50 m/s (~ 11 to 110 mph) as shown in Figure 115.

**Figure 115: WBE From Galebreaker Tests**



The current wind tunnel measurements for the 60A fabric, shown in Figure 6-3, are displayed as varying values ranging from approximately 40 percent to over 90 percent depending on the distance behind the screen the downstream measurement is taken with the 40 percent level measured only immediately behind the screen. The results are reasonably consistent for approach wind speeds varying from 2 to 6 m/s (~4 to 13 mph) with the exception of the 2 m/s case, which diverges from the 4 and 6 m/s cases if measured very close to the screen (<0.15 m downstream). Tests described in (Larson *et al.* 2015) were all made with the downstream measurements made within 150 mm of the fabric making a direct comparison of the Galebreaker results with those obtained in the wind tunnel tests in this study difficult.

#### 6.1.1.3 Pressure Drop Coefficient (PDC)

The pressure drop coefficient,  $C_p$ , reported by Galebreaker, is based on measurements made in a duct in which the fabric filled the entire duct and all of the approaching air passed through the fabric and defined as:

$$C_p = \Delta p / (1/2) \rho U^2$$

Where  $\Delta p$  is the pressure drop across the fabric,  $\rho$  is the density of air and  $U$  is the velocity of the air passing through the fabric. For the 60A fabric, the PDC was reported to be 6.8. This is the conventional definition for a pressure drop coefficient used when the airflow through the fabric is known.

The pressure drop coefficient used in the current CFD work is defined differently and based on different measurements to account for the fact that, in the wind screen application of interest,

the amount of incoming air passing through the screen is not known since the screen deflects some fraction of the incoming flow around, rather than through, the screen.

The PDC used in the CFD model is defined as:

$$C_p = \Delta p / (1/2) \rho U_\infty^2$$

where  $U_\infty$  is the far-upstream approach velocity. The PDC was selected as the value which best matched the results of the wind tunnel measurement of the airflow upstream and downstream of the test fabric panel.

Figure 116 panel. There are free stream tunnel wind speeds of approximately 4 and 6 m/s (expressed as wind tunnel fan speeds of 1000 and 1500 revolutions per minute (RPM)). Each of the two speeds was run with two different size panels; a larger panel occupying approximately 10 percent of the tunnel cross-section and a smaller one occupying about 5 percent. The runs with different panel sizes were done to determine the effect of tunnel blockage on the flow diverted around the sides of the panel and how it rejoined with the flow passing through the panel. The measurements extended about 0.6 m downstream of the panels in a region where a continuing reduction in air velocity downstream of the center point of the panel was observed.

**Figure 116: Wind Tunnel Measurements of Air Velocity Up/Downstream of Fabric**

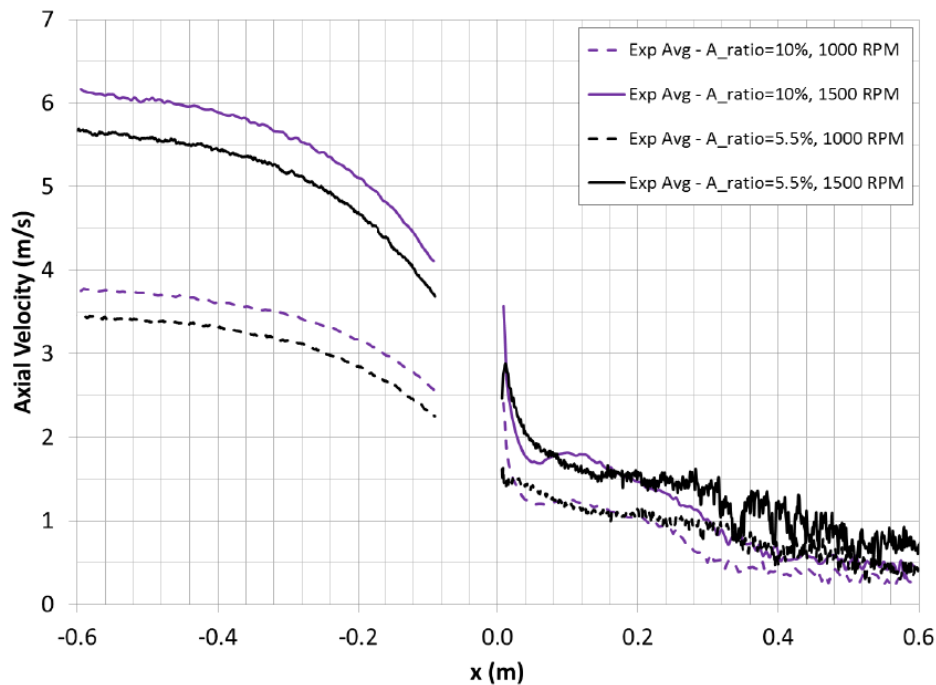


Figure 116 shows the results of CFD calculations of the effect of the screen on both upstream and downstream velocity for these four cases. The calculations used three different values of a pressure drop coefficient (PDC) defined as:

$$PDC = \Delta p / (1/2 \rho U_{\infty}^2)$$

to characterize the flow resistance of the screen. Values from 0.9 to 1.1 appeared to bracket the wind tunnel measurements with 0.9 giving better agreement with the smaller (5.5 percent blockage) panel and 1.2 better, agreement with the larger (10 percent) panel. A value of 1.0 was selected as a reasonable approximation as indicated by the red line in Figure 117.

**Figure 117: CFD Computational Variations vs. Tunnel Measurements**

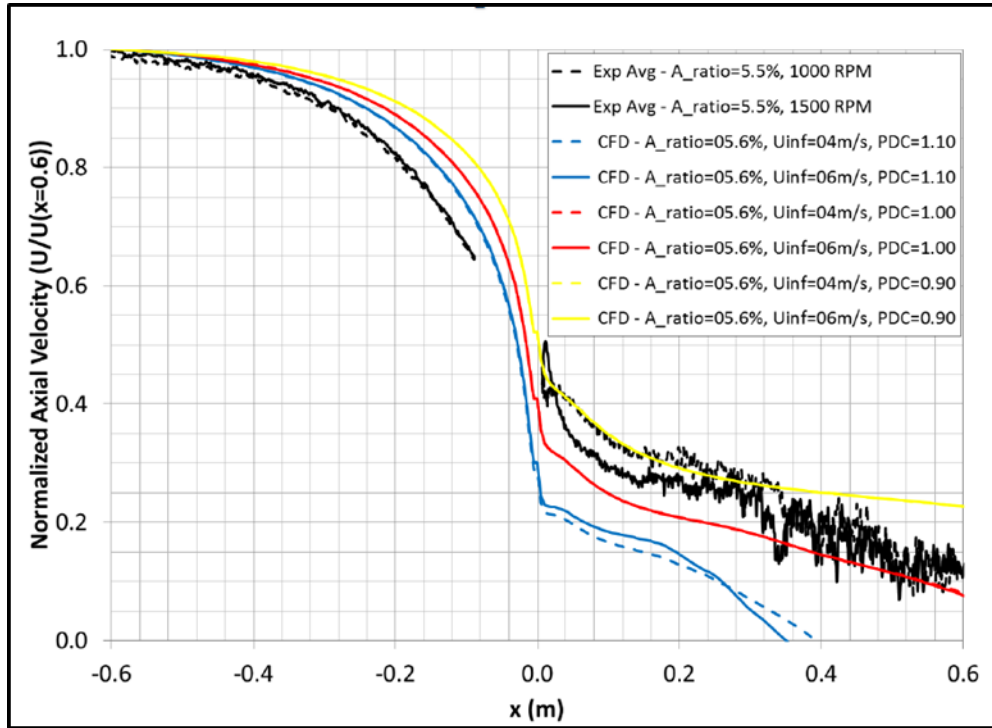
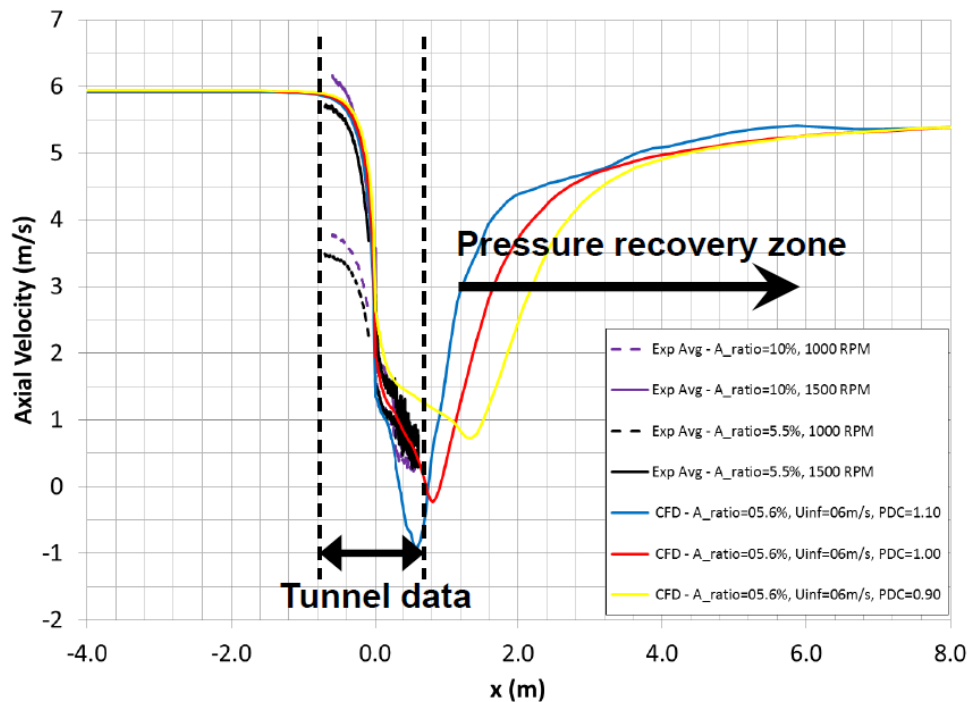


Figure 118 replots the comparisons with wind tunnel data and extends the computational results further downstream into the pressure recovery zone where the flow diverted around the panel rejoins the flow that went through the panel and accelerates it back to near the upstream value.

Figure 118: CFD Extension Into Pressure Recovery Zone



### 6.1.2 Effect of ACC and Tank on Field Measurements of Wind Speed

As initially discussed in Section 5 in the context of determining ambient wind speed and direction for the field tests, the measured wind speed and direction at the top of the water tank at the southwest corner of the ACC (See Sensors 21A and 23D in Figure 4.3) were intended to be the primary determinant of ambient wind conditions. It was noted, however, that the tank measurement could potentially be influenced by two factors: ACC-induced air flow and the blockage effect of the tank itself.

The ACC, when operating with all fans at full speed, draws in a large amount of air. This will induce airflow at some distance from the perimeter of the ACC at or near the fan deck height. This might create measureable air currents around the top of the tank and produce erroneously high wind speed readings particularly during periods of very low to no natural wind.

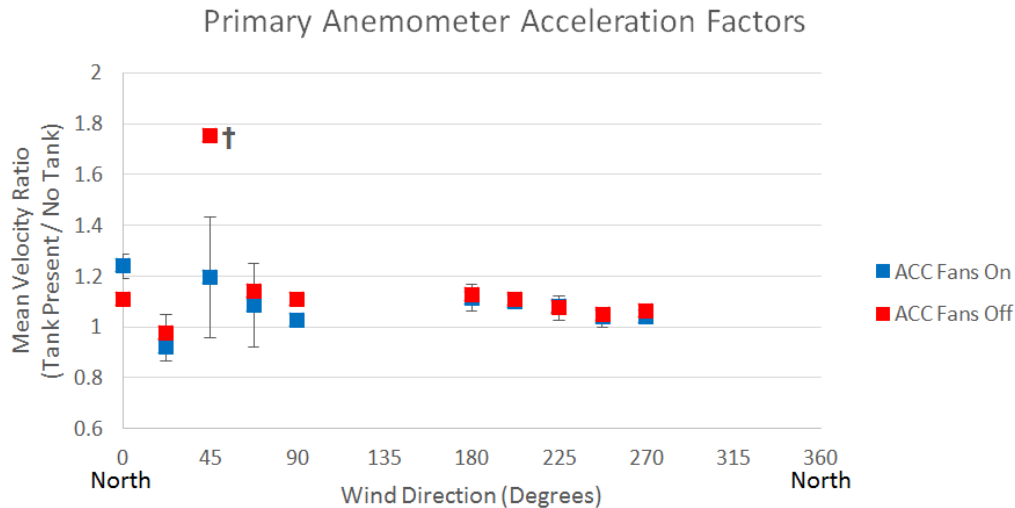
Second, the presence of the tank itself presents a blockage to approaching wind which may accelerate the air over the top of the tank where the wind speed measurements are being made. Both of these issues were examined in the wind tunnel through a series of wind speed measurements at the location of the site anemometer under all combinations of the four conditions of for winds from all achievable directions:

- Tank present
- Tank absent

- ACC fans on
- ACC fans off

One set of results is summarized in Figure 119.

**Figure 119: Effect of ACC-Induced Winds and Tank Blockage on Wind Speed Measurements**

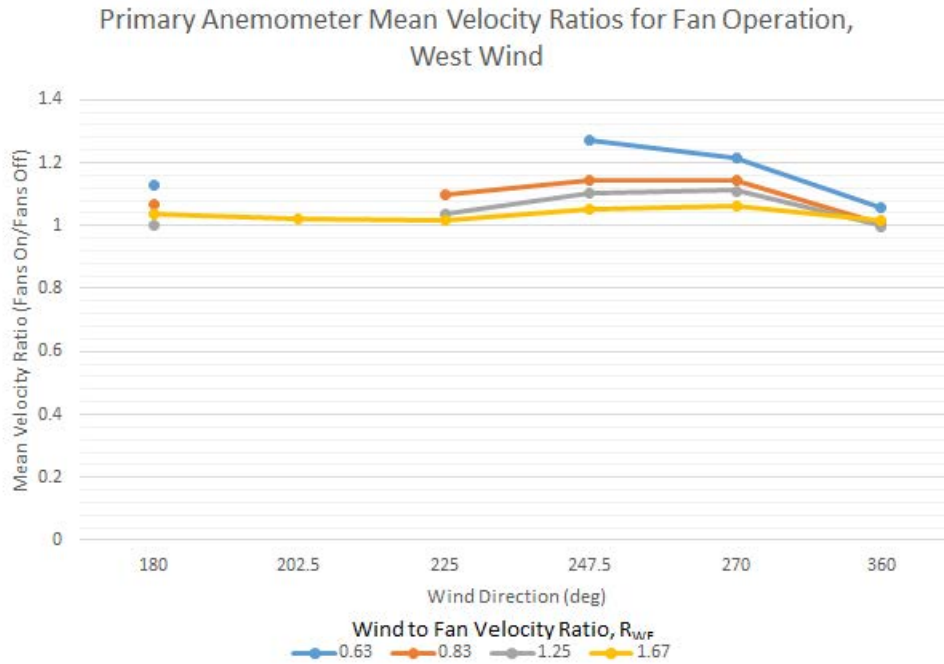


Several points are noteworthy. First, the presence of the tank and the resultant blockage of incoming air does appear to have a consistent effect of perhaps a 5 to 15 percent increase in the ratio of velocities measured when the tank is present compared those that would be measured with no tank present.

Second, for most conditions the effect of ACC-induced wind on the “tank present/no tank” velocity ratio is negligibly small, particularly for the wind directions of primary interest for the field tests of winds from the southwest quadrant. The results from the northeast quadrant show somewhat more variability and are more erratic. However, winds from this direction are rare at the site, and it is in the northeast quadrant where major structural interferences for wind approaching the ACC are present as seen in Figure 48. However, it is possible that the ACC-induced airflow could affect both “tank present” velocity and the “no tank” velocity equally with a negligible effect on the ratio. Therefore, the results in Figure 119 alone do not rule out a more significant effect of ACC-induced airflow.

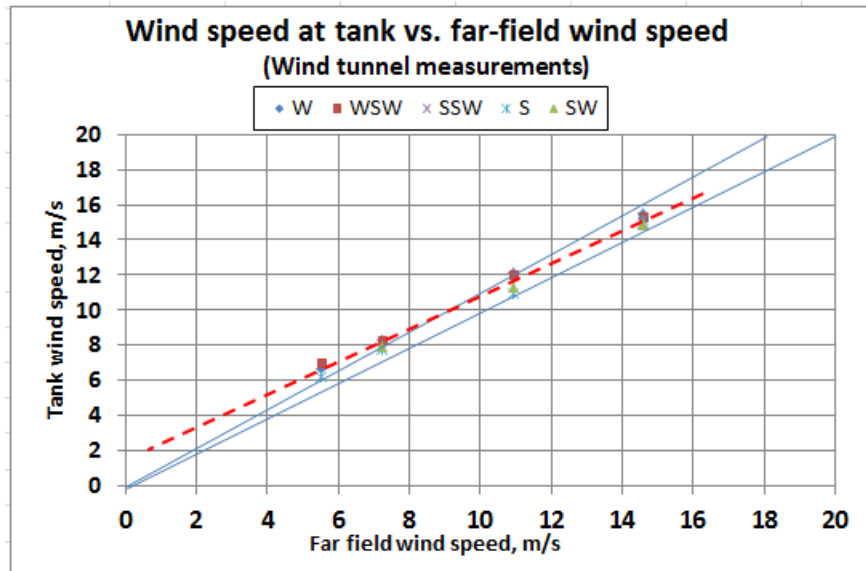
Figure 120 presents the (fans on/fans off) velocity ratio for four wind tunnel approach air speeds over the range of relevant wind directions. The four wind speeds are expressed as a “Wind to Fan Velocity Ratio” where the fan velocity is defined as the average air velocity over the fan area. For the Caithness ACC a typical fan velocity is about 8.7 m/s. Note that this is higher than the “fan inlet velocity” reported throughout this report since that velocity was measured at the bottom of the fan shroud which has a diameter of 11.66 meters compared to the fan diameter of 10.44 meters.

**Figure 120: “Fans on/Fans off” Velocity Ratio vs. Wind Direction**



Assuming that the measured wind speed for the “no tank/fans off” condition correctly represents the far-field wind speed, the ambient wind speed for both the “fans on” and “fans off” conditions can be extracted from the combined data in Figures 119 and 120. A plot of the measured wind speed taken at the top of tank with all fans at full speed vs. the far-field wind speed estimated from the wind tunnel modeling results is presented in Figure 121.

**Figure 121: Measured Wind Speed at Tank vs. Estimated Far-Field Wind Speed**



The lower line in Figure 121 would represent perfect agreement; the upper line represents far-field estimates 10 percent greater than the measurements at the tank. They indicate that the measured results over most of the wind speed range for directions between south and northwest are within 10 percent of the far field wind speed. At the lowest wind speeds of 2 to 3 m/s, extrapolated results suggest a maximum difference of measured wind speed at the tank in excess of the far field wind speed with all fans at full speed of about 1.0 to 1.5 m/s. This is reasonably consistent with the low wind speed differences between the Brookhaven measurements and the tank measurements at the lowest wind speeds shown previously in Figure 72

### 6.1.3 Selection of Base Case Model Runs

The choice of which plant/ACC/ambient conditions to model was based on the following considerations. Since both the physical and computational modeling were done at steady conditions of constant wind speed, wind direction and ACC fan status and heat load, a useful comparison with field data would be best achieved against field data obtained under “as steady as possible” conditions. Therefore, out of the 18 months of continuous field testing, periods were searched for with the following characteristics.

#### 6.1.3.1 Ambient Conditions

- Wind speed: +/- 0.5 m/s
  - Low speed—2 – 3 m/s
  - Mid-range-- ~ 6 m/s (equal to nominal design fan inlet velocity)
  - High speed—8 – 9 m/s
- Wind direction: +/- 20°

- Southwest to northwest direction
  - Relatively unobstructed approach
  - Approximately normal to windward screen on Cell 3.4
- Reasonable agreement with directional information from surrounding airports
  - Suggestive of no major weather variability in the area
- Duration of steady conditions:  $\geq 5$  minutes

#### 6.1.3.2 Plant/ACC operating conditions

- All fans at full speed
- Constant steam unit output/constant ACC heat load
- Screens fully deployed or fully retracted

Extensive data searching throughout the entire 18 month test period yielded a number of periods satisfying these criteria. Plots were constructed for these periods of inlet air velocity for Cells 3.4 and 2.4 and static pressure in Cells 3.4, 2.4 and 1.4. A few example plots are shown in Figures 122, 123, and 124. The plots are segregated into separate time periods, designated by the small numbers above the abscissa (1 through 8), which are of different duration and may be months apart but have similar characteristics.

**Figure 122: Inlet Air Velocities in Cell 3.4 During Selected “Steady” Periods**

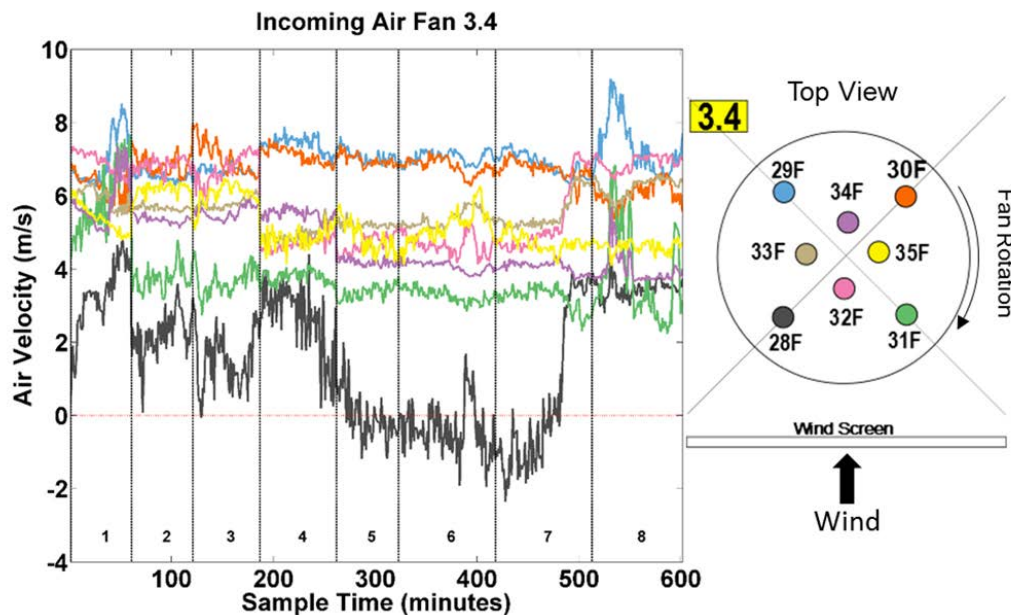


Figure 123: Inlet Air Velocities in Cell 2.4 During Selected “Steady” Periods

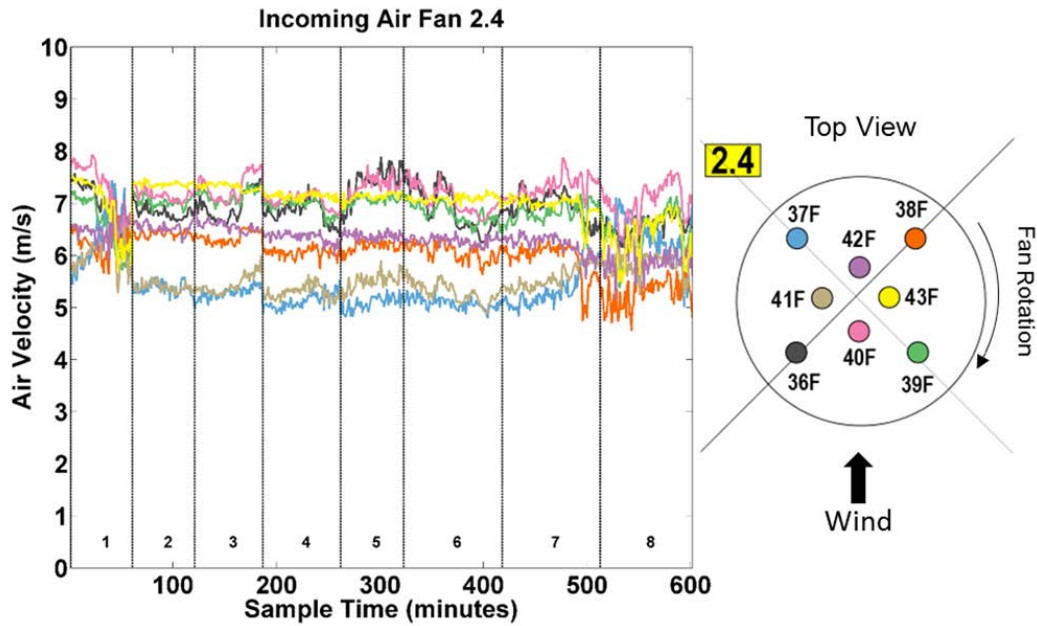
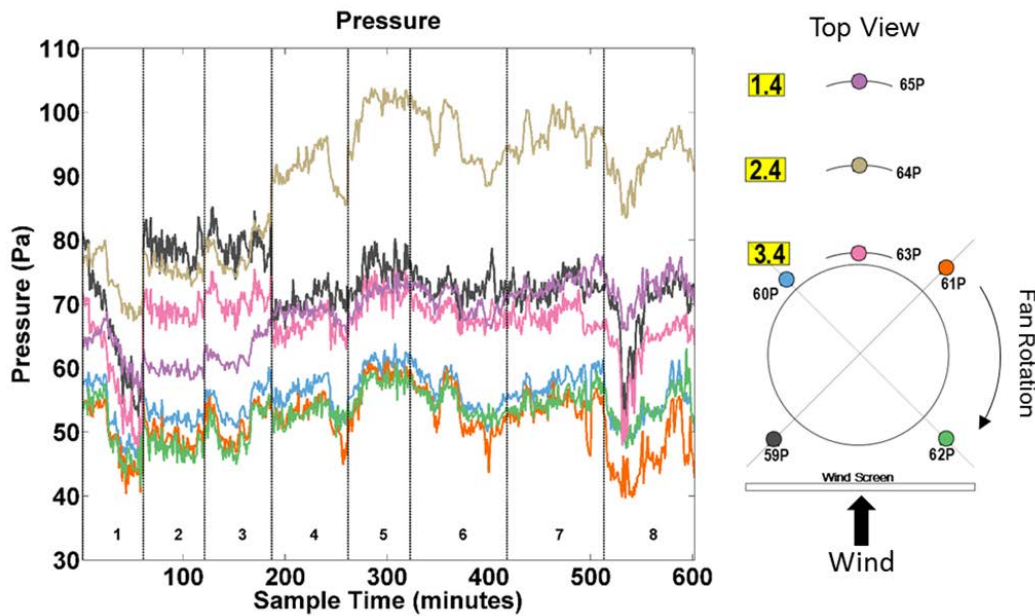


Figure 124: Static Pressure in Cells 3.4, 2.4, and 1.4 During Selected “Steady” Periods



An important feature of these plots is that measurements of inlet velocities and static pressures under comparable, steady conditions are very consistent in the different time periods even though the periods may be months apart. This essentially confirms that the site and wind characteristics which control ACC behavior have been correctly identified and that the

selection, placement and methodology of field data acquisition are apparently correct and reliable.

After extensive screening and evaluation of preferred test conditions for physical and computational modeling, four “steady” periods were selected and are listed in Table 4. Because most of the field test period was spent with the screens deployed and because winds at speeds above 6 to 7 m/s rarely occurred, the number of observations for retracted screens at a mid-range of wind speed and for any conditions at high winds speeds are much fewer in number than those at lower speed with deployed screens. Unfortunately this precluded comparisons of, for example, different screen positions at high wind speeds which might have provided greater understanding of the benefit of screens on thermal performance with high winds.

**Table 4: Steady Test Periods Selected For Modeling**

Screen Configuration	Condition	$\bar{\theta}$ (deg)	$\bar{V}$ (m/s)	Total Observations (minutes)	$\theta$ RMS (deg)	V RMS (m/s)
Retracted	1	275.4	3.10	192	4.34	0.22
Retracted	2	270.6	5.37	16	7.85	0.36
Deployed	3	262.3	6.21	602	9.71	0.14
Deployed	4	267.2	8.64	51	10.48	0.38

#### 6.1.4 Modeling of Field Test Conditions

Extensive wind tunnel testing was conducted on a model of the full-scale ACC at Caithness. The wind tunnel, model, instrumentation and testing protocol were described briefly in Section 4.3 and are presented in detail in Larson (2015) and Larson (*et.al.* 2015). The following section presents the results and conclusions of the tests.

Proper modeling of a full-scale facility in a wind tunnel requires that a number of scaling criteria be satisfied. Particular constraints in this instance place limits on the size of the model relative to the cross-sectional dimensions of the tunnel and to the thickness of the boundary layer in the test section. Additionally, the ratio of wind speed to fan exit velocity should be the same for the model and for the full-scale situation. This constraint, coupled with operating limits of the wind tunnel fan, sets the range of ambient wind speeds at the site that can be properly simulated. These criteria, along with analyses confirming that they are met, are described in detail in Larson *et al.* (2015).

In conformity with these limitations, the following test conditions were selected.

- Wind direction: Westerly--perpendicular to the upwind, screened edge of Cell 3.4
- Wind speeds:
  - m/s (6 m/s or 13.4 mph full scale)—gives velocity at fan deck height equal to fan exit velocity

- 4 m/s (9 m/s or 20 mph full scale)—expected to have significant adverse effect of fan performance
- Screen position: fully retracted and fully deployed

Figure 125 shows the wind direction, orientation of the model in the tunnel and the cells under which the airflow was measured.

**Figure 125: Schematic of Tested Cells**

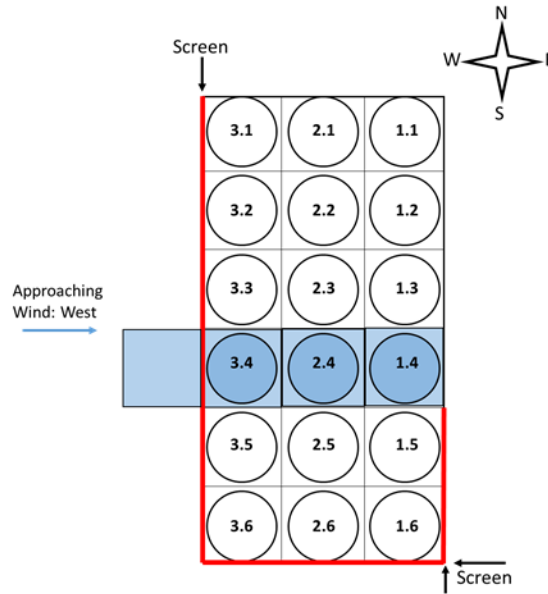


Figure 126 defines the coordinate system used in the plots of the wind tunnel measurements presented in the following section; specifically, for Figures 128 through 135.

- The horizontal location, plotted on the abscissa (x-direction), is the physical distance in the model from the windward edge of the upwind cell (Cell 3.4).
- The dimensionless vertical location, plotted on the ordinate (y-direction), is the height above grade, normalized by the cell height, shown in Figure 125 as 7.2 cm.
- The dimensionless velocity, expressed by the color coding, is the measured quantity, normalized by the wind tunnel free stream velocity. The measured quantity is measured with a single hot-wire anemometer where the wire is aligned with the z-axis. Therefore, the reported quantity is the air speed in the x-y plane, assumed to be horizontal.
- The z-dimension is measured from the outer radius of the fan in toward the hub and normalized by the cell height (7.2 cm). The model fans are 8 cm in diameter so the fan diameter corresponds to  $8/7.2$  or  $z = 1.1$  and the cell/fan centerline is at  $z = 0.55$ . The chosen values of 0.67, 0.89 and 1.1 are on the same side of the hub with 0.67 near the

hub; 0.89 in mid-span and 1.1 at the blade tip. The locations of these slices are shown in Figure 127.

The measurements taken in the wind tunnel consist entirely of wind speeds at specific points on a well-defined grid under and around the model of the ACC. The measured speed is assumed to be primarily horizontal and in the downwind direction at each point. Therefore, all information about the effect of wind speed, wind direction and screen position on mass flow into the various fans must be inferred from the point-to-point variation in these speed measurements. There is no direct measurement of airflow into the cells. These quantitative measurements are supplemented by flow visualization in the form of videos of traces of smoke injected into the flow at various points at the open inlet plane between the fan deck and the ground in front of the windward cell.

**Figure 126: Definition of Coordinates in Plots of Results**

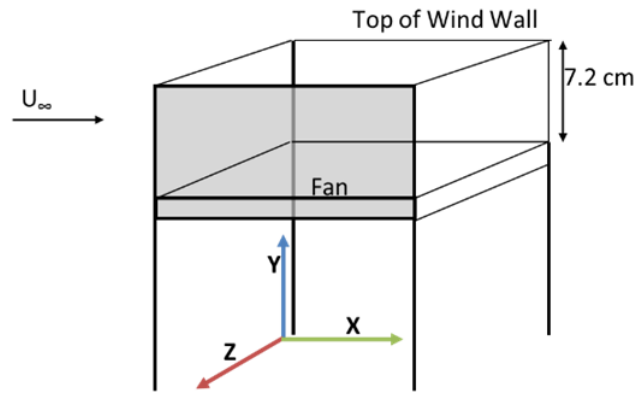
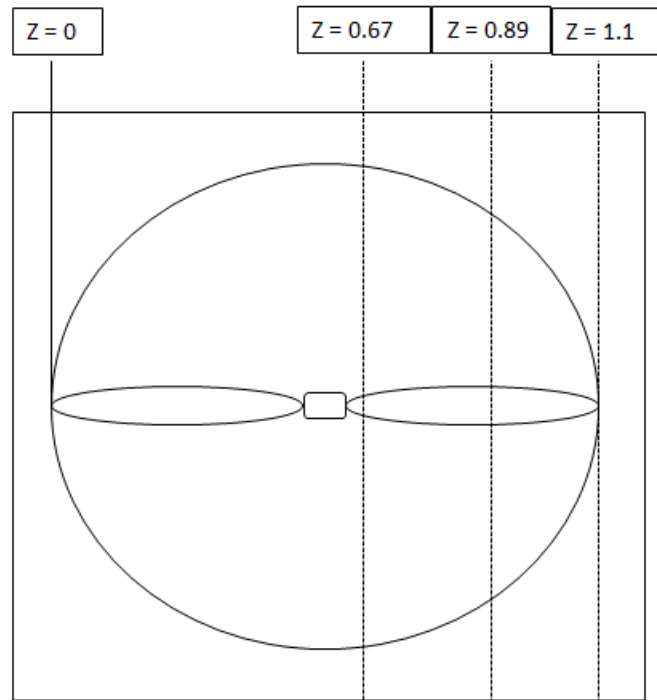


**Figure 127: Normalized “Z-Locations” of Measurements**



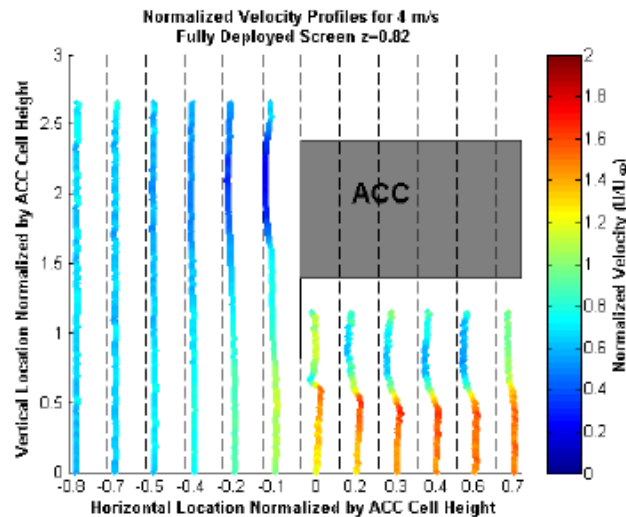
The speed measurements are presented in two formats. The first, used in Figures 129 through 134, provides a visual display of wind speeds at different heights above the ground up to just below the fan deck/fan inlets in at six equally spaced locations in the windward direction (y-axis) under each cell and in three slices at given points on the z-axis. Figures 129 through 131, all at model wind speeds of 2.4 m/s (corresponding to 6 m/s at full scale), are at  $z = .67$  (near fan hub),  $z = .89$  (mid-span of blades) and  $z = 1.1$  (under blade tips). Figures 132 through 134 are at the same locations for a model wind speed of 4 m/s (10 m/s full scale). In all figures, the left-hand panel is for screens fully retracted and the right-hand panel for screens fully deployed.

The second format, used in Figures 135 through 137, displays the averaged velocities over each of the vertical measurement columns described in the first format. This average is assumed to represent the horizontal mass flow in the windward direction at each location in the windward direction and at each slice on the z-axis. The plotted values are normalized to display the relative mass flow rates. A description of how the variations in these relative mass flow rates are interpreted in an attempt to infer the flow into the various cells is given in a later paragraph.

Figure 128 shows an example set of measurements, presented in the first format, in the region upstream of, and under, Cell 3.4 at the locations shown in Figure 54 with a free stream tunnel velocity of 4 m/s with fully deployed screens at a z-value of 0.82. Note the deceleration of the incoming flow as it approaches the windwall and the acceleration of the air around the bottom of the windscreen. Under Cell 3.4 there is a high velocity stream near the ground and lower

velocity air behind the screen consistent with the intuitive physical expectation of the effect of porous barriers on flow into the ACC.

**Figure 128: Example Measurements**



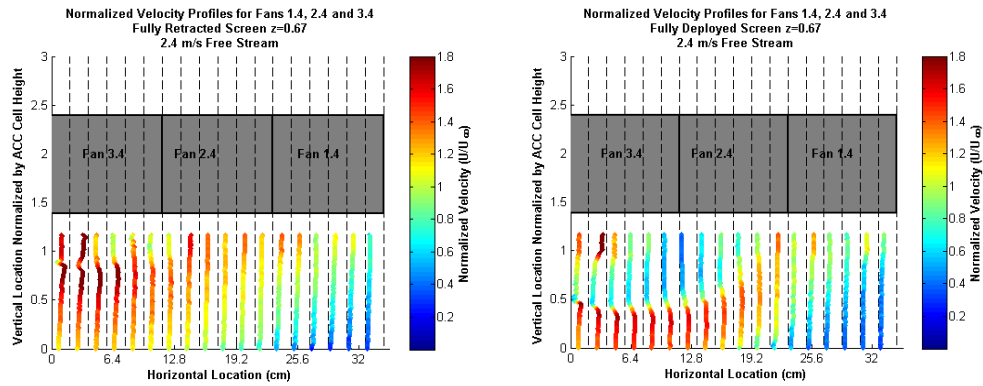
Source: Holkers 2015

The remaining plots are for the regions under the three cells in Row 4 (3.4, 2.4 and 1.4) without the upstream region to the windward of Cell 3.4. There is little difference among the three lateral locations. The slice under the hub ( $z = 0.67$ ) shows a slight reduction in the airspeed under the midpoint of each cell at the heights closest to the fan inlets for both retracted and deployed screens. The slice at the outer edge of the fan inlet ( $z = 1.1$ ) shows slightly lower speeds at all locations presumably because the measuring points are outside the projected fan inlet area.

All lateral locations with retracted screens show a high speed region in the upper left hand corner (close to the fan inlet in the windward half of Cell 3.4). The speed diminishes at lower heights near the windward inlet plane ( $x = 0$ ) and with increasing distance in the windward direction (increasing  $x$  at all levels).

Deployment of the screen alters this pattern. With the screen deployed, the speed in the area behind the screen ( $y > 0.75$ ) are substantially reduced from the midpoint of Cell 3.4 forward to the mid-point or downwind edge of Cell 2.4. The speed at the inlet plane ( $x = 0$ ) below the screen ( $y < 0.75$ ) is significantly higher than it was for the screen retracted. This diverted portion of the incoming air continues at high speed until it is about under the mid-point of Cell 2.4. In all cases, the speeds under Cell 1.4 are little affected by the deployment of the screen. In all cases with the screen deployed, there is a small region just inside the screen and just below the fan deck where the speed is still high and seemingly unaffected by the deployment of the screen. This is not understood but may be the result of the difficulty of locating the hot wire probe in this position with the screen in place.

**Figure 129: Velocity Measurement Under Row 4 Cells at 2.4 m/s;  $z = .67$  (Retracted vs. Deployed)**



The mid-span plots ( $z = 0.89$ ) in Figure 130 are essentially the same as the near-hub case.

**Figure 130: Velocity Measurement Under Row 4 Cells at 2.4 m/s;  $z = .89$  (Retracted vs. Deployed)**

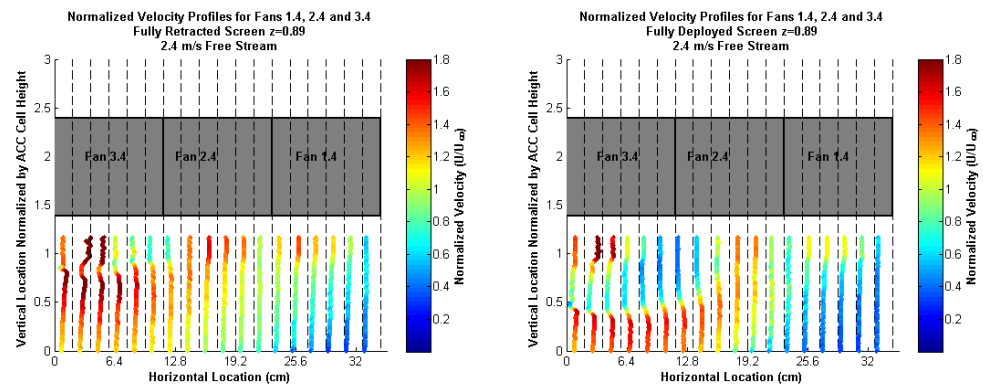
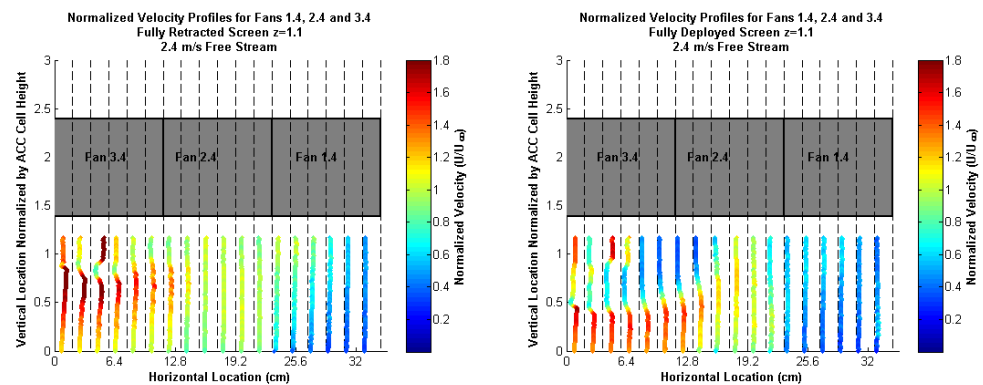


**Figure 131: Velocity Measurement Under Row 4 Cells at 2.4 m/s;  $z = 1.1$  (Retracted vs. Deployed)**



The succeeding three figures (Figure 132, 133 and 134) are for identical conditions as for the preceding three except that the free stream velocity is 4 m/s (10 m/s full scale). The general

patterns, the differences among the three lateral positions and the effect of the screen are essentially the same. In all cases, with the screens retracted, the low velocity region extending downwind from below the mid-point of Cell 3.4 persists further. Also, the speed of the diverted portion of the incoming air which enters below the screen ( $y < 0.75$ ) is at a lower speed than it was in the case of the lower free-stream velocity. The reason for this is not entirely clear, but may be due to the higher stagnation pressure on the outer surface of the screen forces a larger fraction of the air through the screen and diverts correspondingly less.

The overall conclusion from this set of 12 observations is that the screens reduce the air speed flowing across the fan inlets which would be expected to improve fan performance and result in higher airflow into the cells. At the wind speeds modeled this is consistent with the averaged field results shown in Figures 75 through 77. Measurements at the lowest wind speeds at which field tests indicated a reduction in flow to Cell 3.4 with screen deployment could not be modeled in the wind tunnel. Therefore, there is no physical model confirmation of that field observation. The primary effects are the expansion of the region of reduced velocity behind the screen in the upper region near the fan inlets and an extension of the accelerated high speed region near ground level further downwind under Cell 2.4. The downwind region under Cell 1.4 is affected very little as a function of increasing wind speed.

**Figure 132: Velocity Measurement Under Row 4 Cells at 4. m/s;  $z = .67$  (Retracted vs. Deployed)**

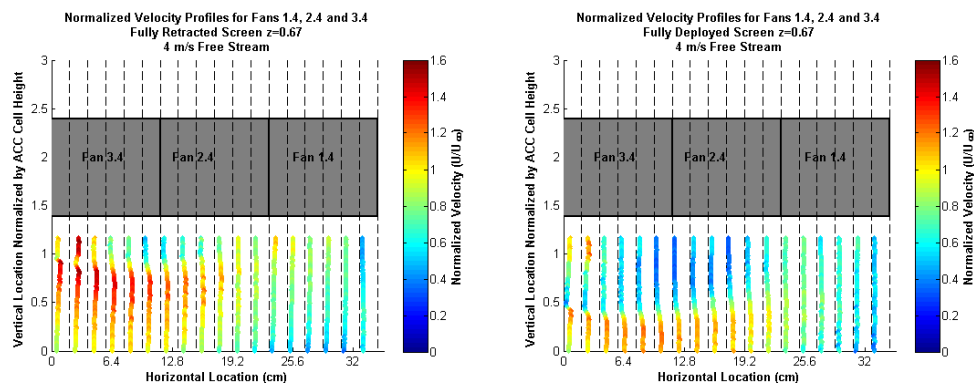


**Figure 133: Velocity Measurement Under Row 4 Cells at 4. m/s;  $z = .89$  (Retracted vs. Deployed)**

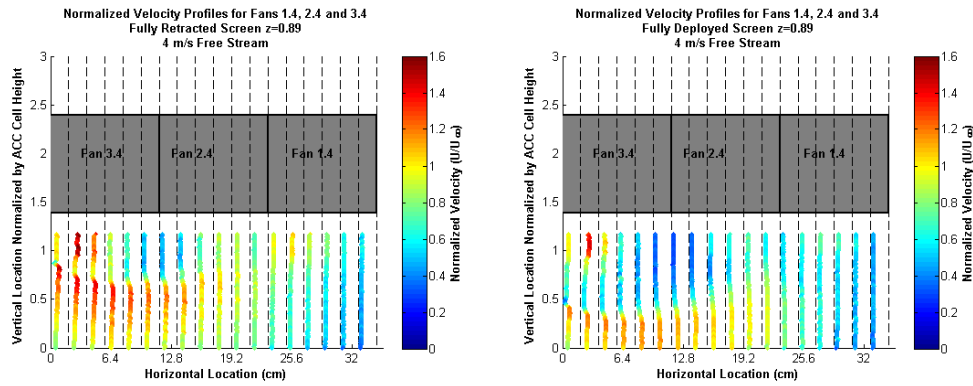
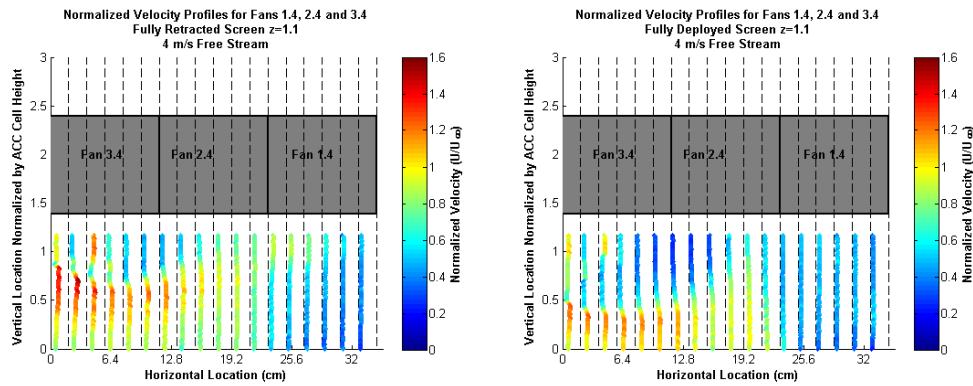
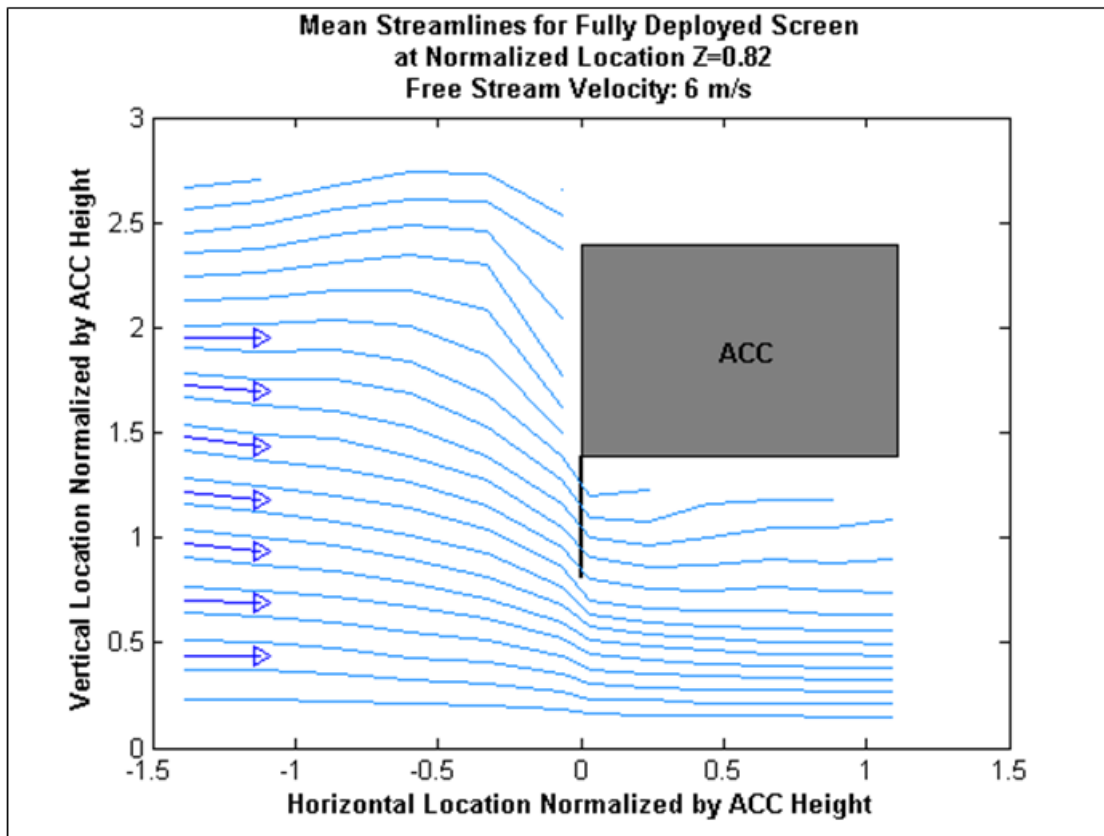


**Figure 134: Velocity Measurement Under Row 4 Cells at 4. m/s;  $z = 1.1$  (Retracted vs. Deployed)**



The measurements displayed in these preceding plots can be processed to generate streamline diagrams give which a better visual impression of the air flow patterns beneath the cells. Figure 135 provides an example of such a plot at the mid-span location ( $z = 0.89$ ) with a free steam velocity of 6 m/s (15 m/s full scale). The wind screens are fully deployed. Note that in this plot the horizontal location, shown on the abscissa, is normalized by the cell height. The decelerated region behind the screen and up near the fan inlets is clearly visible with wide streamline separation in contrast to the more closely spaced streamlines in the accelerated region near ground level.

Figure 135: Streamline Patterns



Additional processing of the data, referred to above as the second presentation format, was conducted in an attempt to obtain a quantitative determination of the air flow into each of the cells and of the effect of screen deployment on such flows. This was done by integrating the velocity measurements as a function of height at each of the measurement locations shown in Figure 54. Assuming the measured velocities to be primarily horizontal, successively decreasing values in the downwind direction should represent a reduction in the horizontal mass flow in that direction as a result of flow being withdrawn from the region and into the cells by the fans.

Figures 136 through 138 display the results of this analysis as plots of the horizontal mass flow, normalized by the flow at the upwind edge of Cell 3.4 with the screen retracted, vs. horizontal distance from the upwind edge of Cell 3.4. While the overall trend of decreasing horizontal airflow in the downwind direction is consistent with the above assumptions, features of the plots are implausible and make it impossible to draw any definitive conclusions regarding the effect of screen deployment on the airflow into the cells from this analysis.

There are a number of instances, particularly under Cell 2.4 where the calculated horizontal airflow increases with downwind direction. There is no plausible explanation for this. It is presumably the result of an inaccuracy or an artifact in the measurements and is unexplained. In addition, it is difficult to measure precisely the velocity in the upper area just below the

windwall of the ACC inlet at the upwind edge of Cell 3.4 (the  $x = 0$  plane) particularly with the screen deployed. Therefore it is assumed that it is the same for all cases for purposes of normalization. This assumption may lead to larger uncertainties in direct comparisons of the retracted/deployed runs.

**Figure 136: Horizontal Mass Flow Underneath Fans 2 & 4 m/s;  $z = 0.67$ ; Retracted and Deployed**

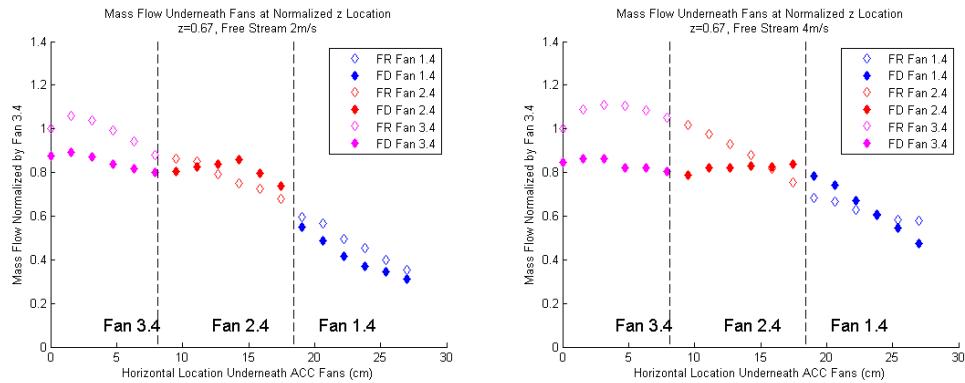


**Figure 137: Horizontal Mass Flow Underneath Fans 2 & 4 m/s;  $z = 0.89$ ; Retracted and Deployed**

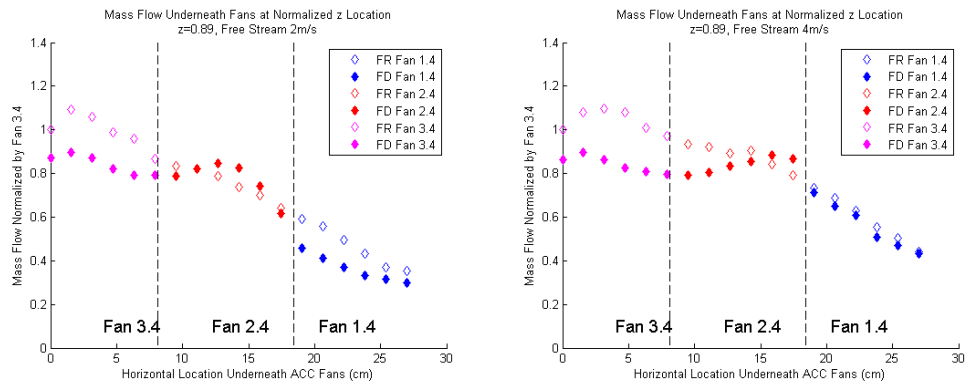
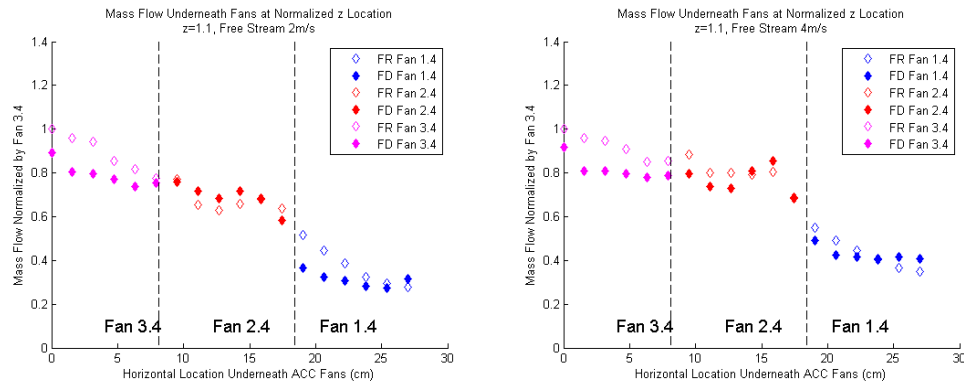


**Figure 138: Horizontal Mass Flow Underneath Fans 2 & 4 m/s;  $z = 1.1$ ; Retracted and Deployed**



Finally, in addition to the quantitative data presented and discussed above, video recordings of smoke visualization runs were made. A single frame, clipped from one of the runs, shows a side-by-side comparison of the flow pattern underneath Row 3 with and without the screens deployed is shown in Figure 138. The free stream velocity was 2.4 m/s. The images are reasonably consistent with the data plots in Figure 130 and show the high velocity accelerated region extending far down Row 4 in the absence of the screen and the turning up of the flow toward the fans occurring earlier with the screens deployed.

**Figure 139: Comparative Images From Video Recording**



## 6.2 Numerical Modeling

The analytical modeling element of this study was intended to provide a tool which could be calibrated and validated with the field test data and the wind tunnel results. The model would then have the capability to make reasonable predictions of the effect of wind screens of different types and different arrangements at different locations. A description of the approach, methodology and computational grid details was reviewed briefly in Section 4. While a validated model was not achieved, sufficient progress was made to give some quantitative insight into the governing physics of the fluid flow problem around an ACC and to provide a starting point and guidance toward the eventual completion of a usable model.

Essential elements of the model development are the specification of appropriate boundary conditions for the incoming wind profile and adequate representation of fan performance and of the flow resistance of the heat exchanger bundles and the screens themselves. The basis on which the suitability of the chosen values for all of these elements was the agreement of the calculated airflows into Cells 3.4 and 2.4 with the flows measured in the field. An inherent difficulty was that the effect of the internal component performance characteristics and the effect of dynamics of the flow of the incoming air could not be separated, and the several elements could not be determined and optimized simultaneously.

### 6.2.1 Fan/Bundle Characteristics

A sequential approach was taken by selecting cases at “near zero” wind speed where the incoming flow dynamics were not significant and with no screens present to correspond to conditions on which the original fan specifications were based. For cases with an ambient wind speed of 0.3 m/s, values for the pressure jump across the fans and the pressure drop across the condenser tube bundles could be iterated around values close to those inferred from the original fan specifications and standard correlations for finned tube bundles of the appropriate geometry until acceptable inlet velocities to the fans in Row 4 were obtained. Values of 110 Pa for the fan pressure jump and 78 Pa for the heat exchanger bundle pressure drop were arrived at. The corresponding results for the fan inlet volume flows and velocities are given in Table 5 and correspond well to the specified design value ( $V_{\text{des}} = 576 \text{ m}^3/\text{s}$ ) particularly for Cells 1.4 and 3.4. The value for Cell 2.4 is slightly higher than the specified value, but the average of the three is acceptably accurate. Cell 3.6 was not measured in the field but is a corner cell for which the inlet air path is, on the average shorter than the other three. Cell 1.4 was also not measured but, in still air conditions, should be essentially the same as Cell 3.4.

This agreement, in the absence of high momentum, disruptive airflow beneath the fan inlets, was taken as confirmation that the values used for the fan and bundle characteristics were adequate. However, at ambient wind speeds as low as 3 m/s (6 to 7 mph), the agreement was poor. This was attributed to the fact that the incoming flow dynamics were not properly characterized.

**Table 5: Fan Inlet Velocities in Near-Zero Wind Conditions**

$U_{\infty}$ (m/s)	Screen PDC	Tot Fan Press (Pa)	Fan	$\dot{m}^*$ -	$\dot{m}$ (kg/sec)	$\dot{V}$ (m <sup>3</sup> /sec)	$V_{fan}$ (m/s)
0.3	0	110.0	1,4	20.3	788	643	7.62
			2,4	23.6	914	746	8.85
			3,4	19.3	748	610	<b>7.24</b>
			3,6	21.9	848	692	8.20

### 6.2.2 Incoming wind profile

The representation of the incoming wind evolved in several steps. It was first determined that a model of Caithness site conditions would assume that the wind measured on the tank at the southwest corner of the ACC (See Figure 48) would be used as the value of the incoming wind at fan deck height. The initial, and simplest, assumption was that of uniform incoming wind speed with no provision for a ground level boundary layer. Due to high acceleration of the flow blocked by the ACC windwall, this resulted in excessively high inlet air velocities under the ACC and very low flow into the upwind cell at wind speeds within the normal range occurring at the site.

The uniform inflow condition did not take into account the significant shear layer that exists over the ground in atmospheric boundary layer flows. Even at relatively modest wind speeds (3 to 9 m/s) the ACC is still low to the ground in comparison to the thickness of the boundary layer. Therefore, a developed boundary layer profile, illustrated in Figure 140, was imposed on the incoming flow based on an appropriate power law and set to give the desired velocity at fan deck height. Recognizing that obstructions in the form of off-site buildings and a row of trees existed upwind of the ACC for the case of westerly winds (See Figure 141), upwind, ground level blockage was added to the model.

Table 6 shows the effect of adding a boundary layer and upstream obstructions on the calculated inlet velocities to the fans in Row 4 and the agreement with measured values in the field. The “PDC = 0” indicates no screen present. As indicated in Table 6, these modifications did not significantly improve the agreement between the calculated value of the fan inlet velocity in Cell 3.4 and the measured value. Again, as seen in Table 6, the agreement, while slightly improved, was still unsatisfactory.

Additional cases were run to explore the effect of both increased wind speed and the presence of screens. The results for wind speeds of 3 m/s and 6 m/s for fully retracted and fully deployed screens at each wind speed are shown in Table 7 for the calculated inlet air velocity in Cells 3.4, 2.4 and 1.4. These cases were run assuming uniform incoming air velocity.

Figure 140: Incoming Airflow Boundary Layer

- $z_{ref}$  = Deck Height  $\approx$  Water Tank Anemometer
- $z_{ref} = 38.5 \text{ ft} = 11.7 \text{ m}$
- $u_{ref} = U_{\infty} = 3 \text{ m/s}$
- Roughness Coefficient
  - $\alpha = 0.25$
  - Forest and woodlands

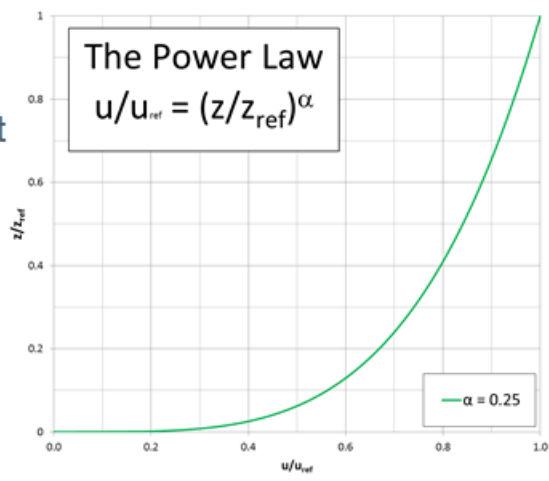


Figure 141: Upwind Buildings and Trees



Table 6: Effect of Modifying Incoming Flow Characteristics

Case	$U_{\infty}$	Screen	Fan	$V_{fan}$	$V_{exp-avg}$
	(m/s)	PDC		(m/s)	(m/s)
Uniform Inlet Flow	3	0	1-4	7.56	
			2-4	6.43	
			3-4	1.19	
No Trees with BL	3	0	1-4	7.56	-
			2-4	6.43	6.78
			3-4	1.19	6.83
Trees with BL	3	0	1-4	6.4	-
			2-4	6.9	6.78
			3-4	1.94	6.83

Table 7: Effect of Wind Speed and Screen Position

$U_{\infty}$	Screen	Tot Fan Press	$DP_{AFrame}$	Fan	$\dot{m}_{dot}^*$	$\dot{m}_{dot}$	$Vol_{dot}$	$V_{fan}$	$V_{exp-avg}$
(m/s)	PDC	(Pa)	(Pa)		-	(kg/sec)	(m <sup>3</sup> /sec)	(m/s)	(m/s)
3	0	110.0	78.0	1,4	20.2	782	638	7.56	-
				2,4	17.2	665	543	6.43	6.78
				3,4	3.2	123	100	1.19	6.83
3	1.1	110.0	78.0	1,4	15.6	604	493	5.85	-
				2,4	18.8	730	596	7.07	-
				3,4	5.3	206	169	2.00	-
6	0	110.0	78.0	1,4	16.6	644	526	6.23	-
				2,4	16.4	637	520	6.16	6.34
				3,4	4.8	187	152	1.81	5.87
6	1.1	110.0	78.0	1,4	14.1	545	445	5.28	-
				2,4	17.5	679	554	6.57	6.41
				3,4	5.2	203	166	1.96	5.04

The effect of the fully deployed screen at the low (3 m/s) wind speed was a slight increase in the inlet velocity to Cells 3.4 and 2.4, but, in the case of Cell 3.4, not enough to match the value measured in the field. The substantial decrease in the inlet velocity in Cell 1.4 is not understood and seems inconsistent with the modest increase for Cell 2.4.

At the higher (6 m/s) wind speed, the reduction in flow compared to the low speed case with no wind screen is consistent with field experience. For Cell 3.4, the trend with wind speed is as expected but at unrealistically low values. The trend and agreement for Cell 2.4 appears satisfactory, but this may be fortuitous. The presence of the screen for the higher speed cases shows some improvement for Cell 3.4 which is consistent with the field measurements, but the absolute values are unrealistically low.

The results for Cell 2.4 appear generally consistent with field results. No field data were obtained for Cell 1.4, and the model results cannot be validated.

### 6.2.3 Detailed Representation of Flow

In addition to the simple single point calculation of cell average inlet velocity, however, the CFD analysis yields large amounts of information of the velocity patterns and pressure distributions across the entire flow fields. These results, similar to the flow visualization results from the physical modeling effort, can provide insight into and understanding of important features of the flow and how they are affected by ambient conditions and wind screen presence. While these results do not contribute to the qualitative comparisons with field measurements, they are presented here to give some qualitative understanding of the importance of air flow dynamics in front of and underneath the ACC and how they influence performance. The following figures (Figures 142 through 146) provide some illustrative examples.

Figures 142 and 143 show the distribution of air velocity under, within and above the ACC under very light (0.3 m/s) wind conditions. Figure 142 shows the total vector magnitude of the velocity; Figure 143, only the vertical velocity. Several observations are noteworthy.

- Even in light winds, the inlet airflow is pushed downwind under the upwind cell.
- The downwind cell shows an inlet air distribution established by the fan-induced inlet flow with rapid turning of the air flow from the ACC inlet area under the windwall into the fan inlet shroud.
- The vertical velocities (Figure 6.33) are relatively symmetric under Cell 2.4 and 1.4 and show some displacement to the downwind side of the inlet under Cell 3.4.
- Even the light winds move the exit plume in the downwind direction and have a significant influence on the airflow patterns inside the A-frames in all three cells.
- The blockage of air above the fan hubs is clearly evident in all cases.

Figure 142: Total Velocity Vectors For “Near-Zero” Wind Speed Conditions; No Screen Present

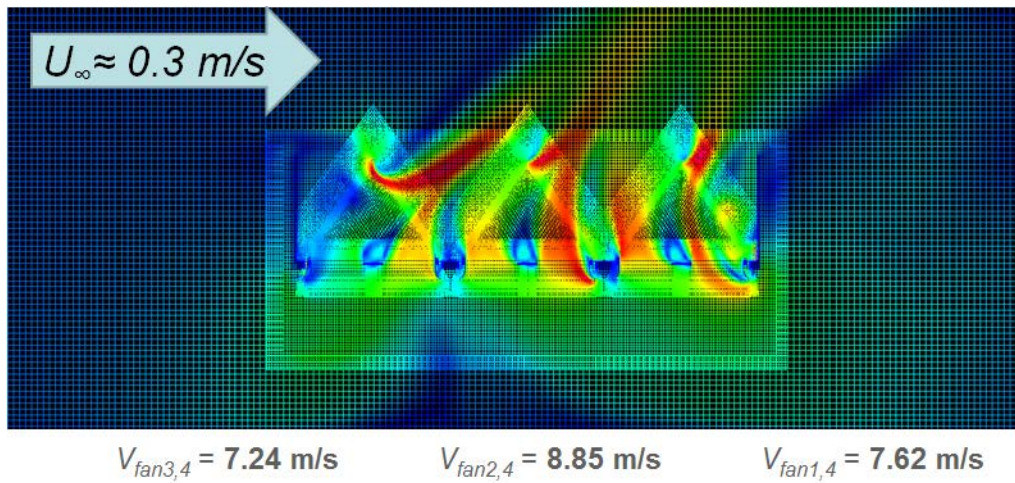


Figure 143: Vertical Velocity Vectors For “Near-Zero” Wind Speed Conditions; No Screen Present

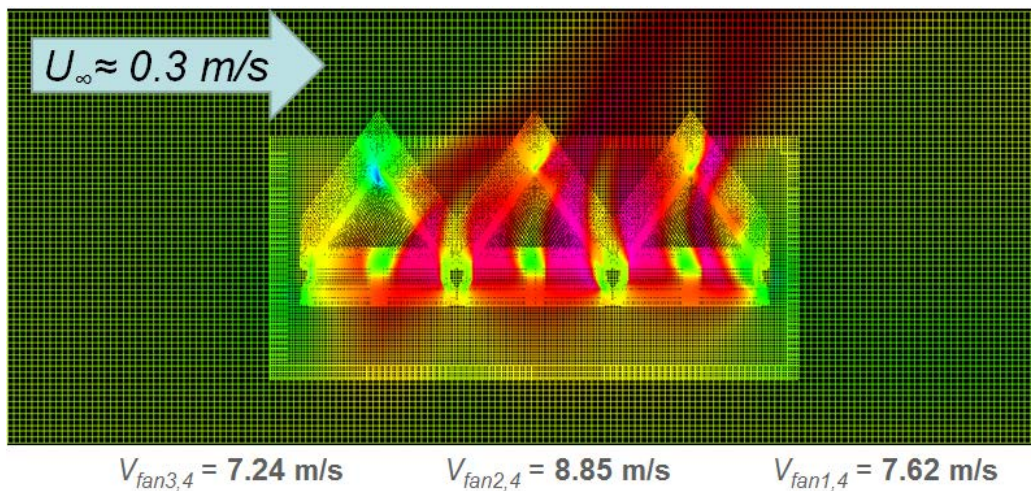
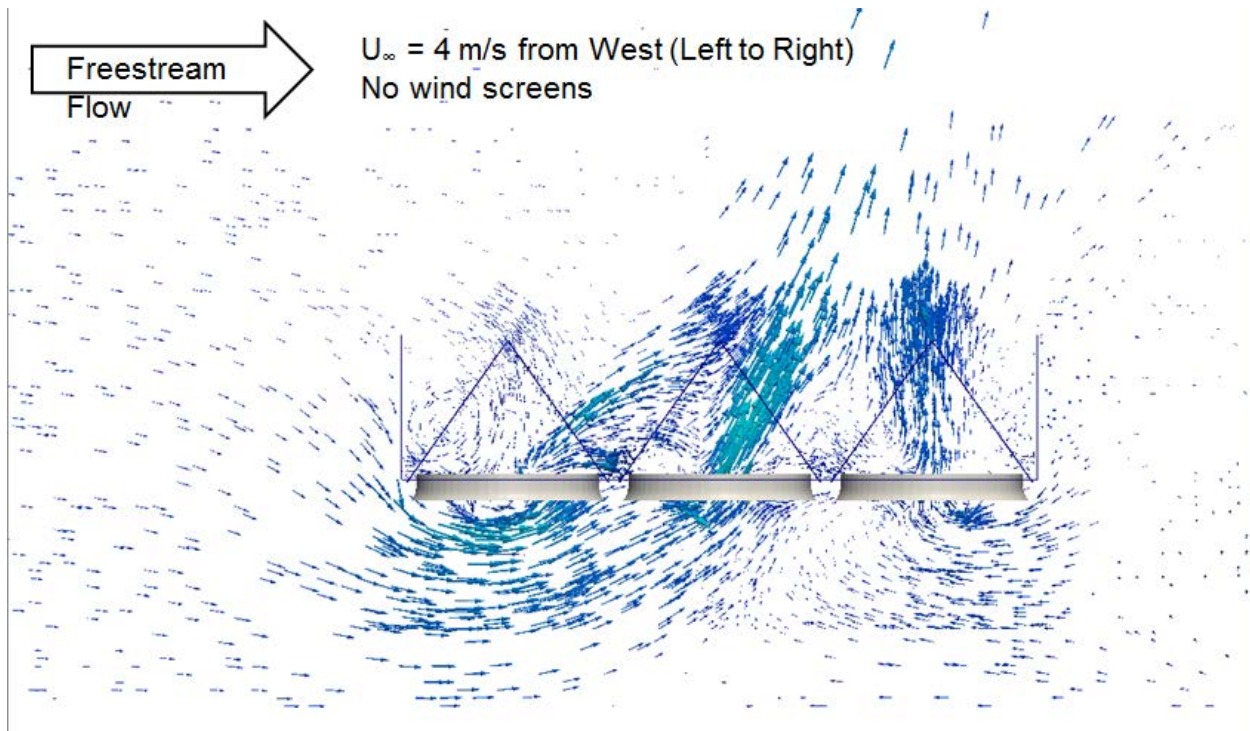


Figure 144 shows the velocity vectors for the case of uniform incoming wind, no screen and a moderate wind speed of 4 m/s. The vector length is indicative of the local air speed. At this wind speed, a clear bypassing of the upwind half of the upwind fan (Cell 3.4) is seen accompanied by some diversion of flow into the central cell (Cell 2.4). The inlet to the downwind cell (Cell 1.4) remains reasonably symmetrical and similar to the low wind case. Important observations include:

- The downwind diversion of the incoming wind by the windwall creates an accelerated flow under the upwind portion of the ACC inlet area.
- Some flow exiting the downwind side of Cell 3.4 appears to enter Cell 2.4 through the upwind heat exchanger bundles. This occurrence is unexpected and has not been

validated in the field. It has not been observed to our knowledge, although no specific attempts to observe or monitor it have been made.

**Figure 144: Total Velocity Vectors for 4 M/S Wind; Uniform Profile; No Screen Present**



An alternative representation shows the streamline patterns for selected cases. Displays of streamline patterns in Figures 145 and 146 provide additional insight in a different format. Figure 145 shows a relatively smooth approach flow for a 3 m/s wind with a boundary layer but with no upstream blockage and no screen. Figure 146 adds upstream blockage to simulate the presence of buildings and trees to the west of the ACC with a dramatic effect on the flow patterns in front of and under the ACC. However, as was seen in Table 6, the introduction of this blockage resulted in some, but insufficient, improvement. The diversion of the wind off the windwall and the accelerated flow under the upwind cell continues to be present and is the apparent cause of the low calculated inlet flow to the upwind cell.

**Figure 145: Streamline Patterns for 3 M/S Wind; No Upstream Blockage; No Screen Present**

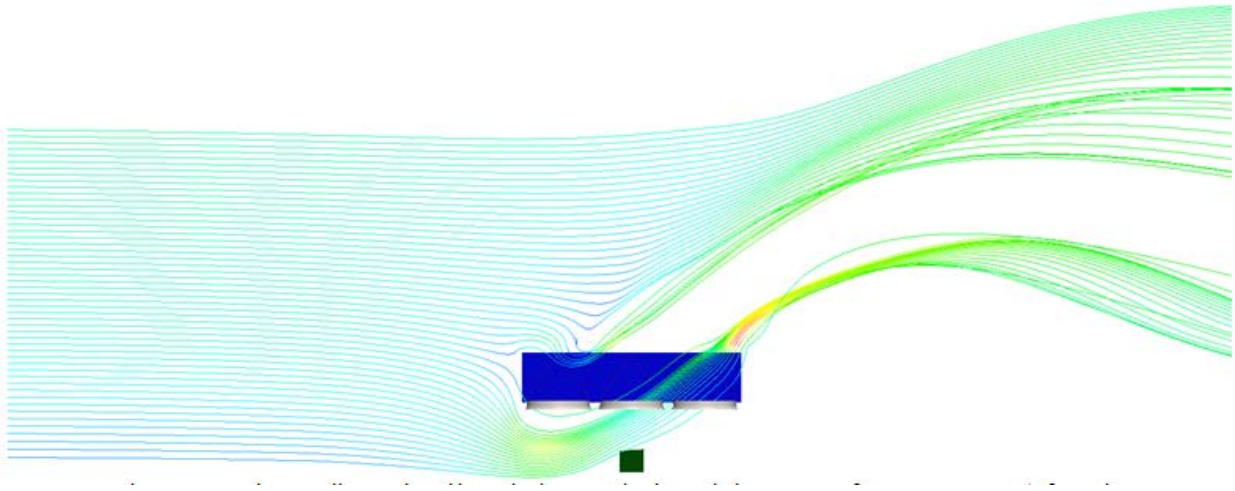
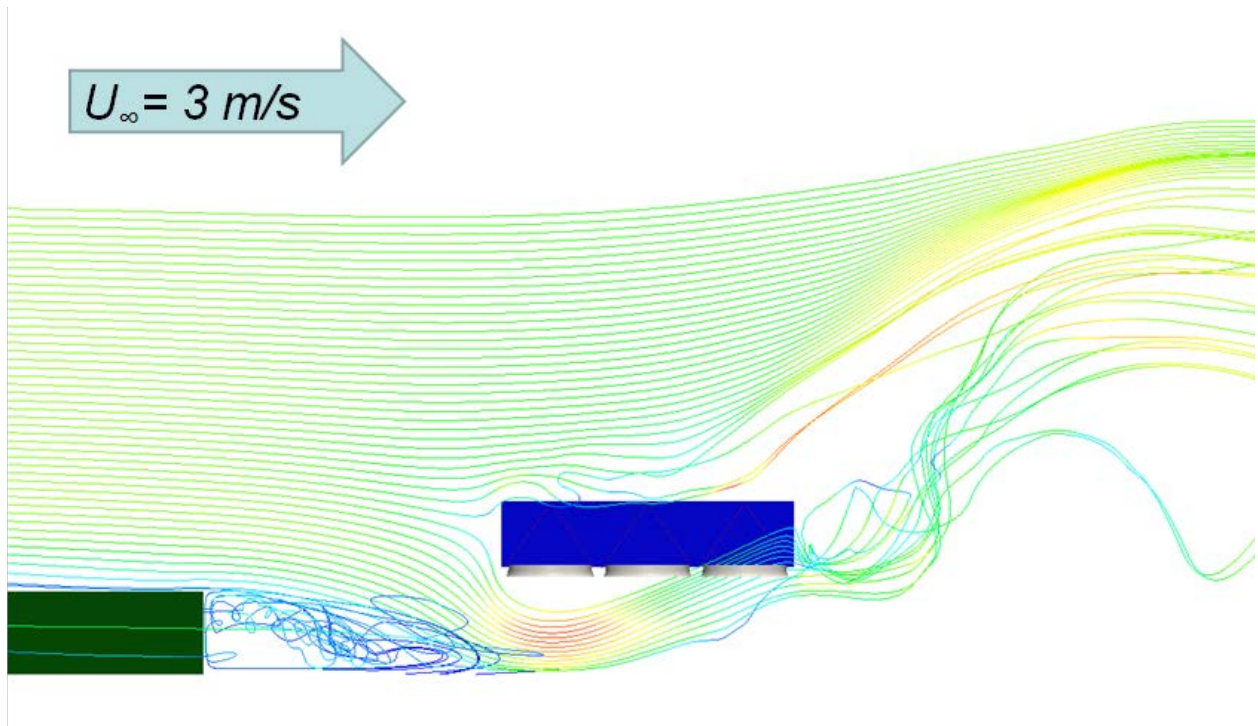


**Figure 146: Streamline Patterns for 3 M/S Wind; Upstream Blockage; No Screen Present**



#### 6.2.4 Deflection of Diverted Flow

The detrimental effect of a downdraft off the upwind windwalls acting as an air curtain has been recognized and discussed in the literature for some time (Kroger and M. Owen 2011; (. It was decided to use the existing CFD model in its current state of development to explore what

the effect of a horizontal lip or ledge might be even though no such ledge exists on the Caithness ACC.

Figure 147 shows a schematic version of how such a ledge might be installed at the bottom of an ACC windwall. Figure 148 shows the comparison of the velocity profiles for the same condition of wind speed (3 m/s), screen position (retracted) and upstream blockage with and without the ledge. It is clear that the presence of the ledge could cause a dramatic difference in the flow upstream of and under the ACC.

**Figure 147: Simulation of Horizontal “Lip” Concept**

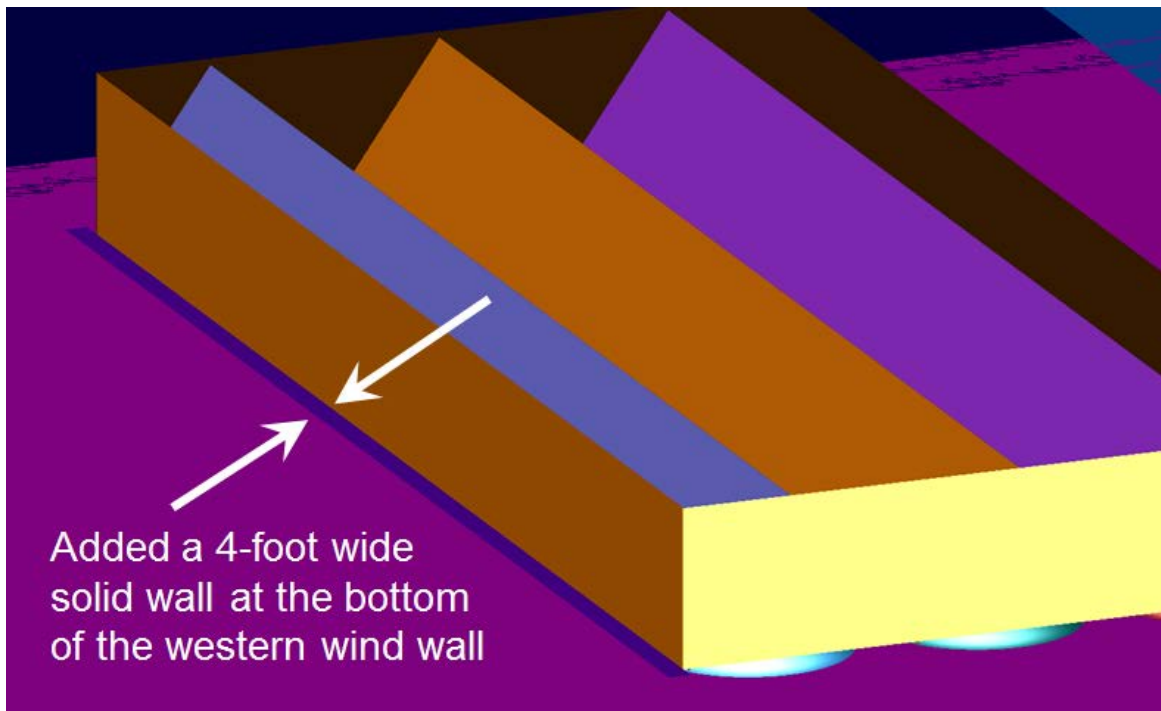
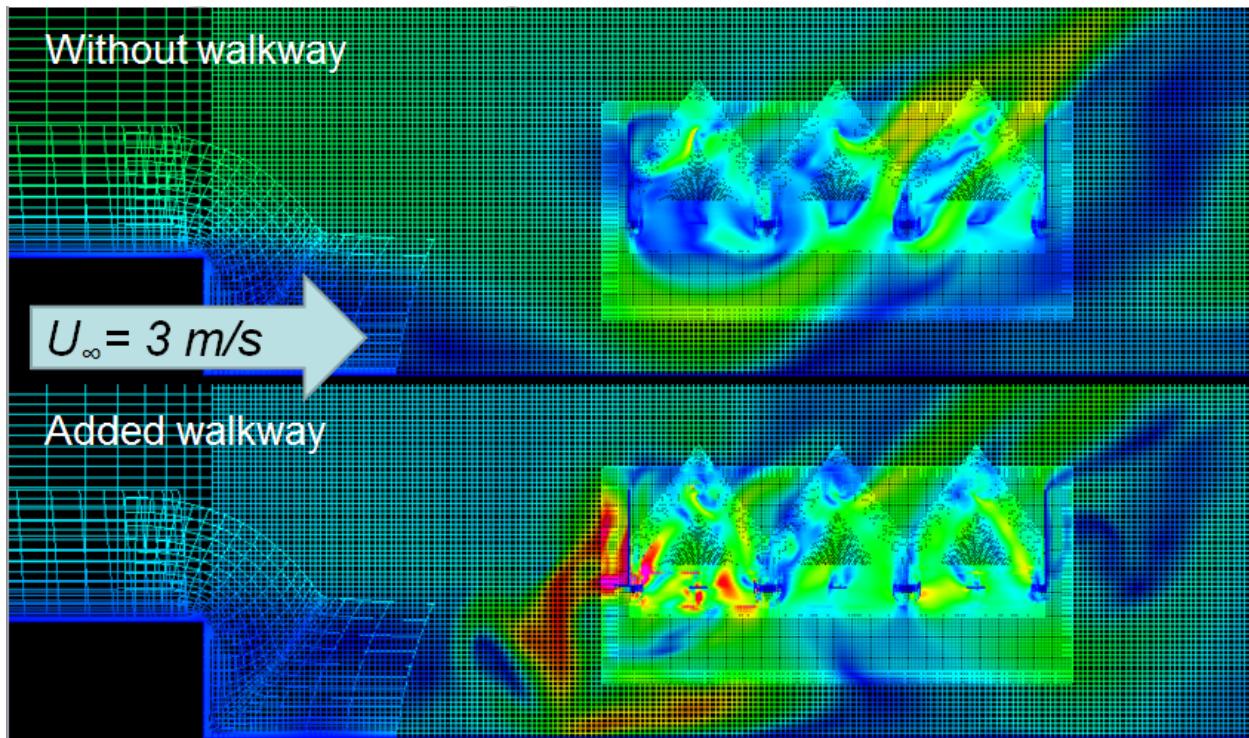


Figure 148: Comparative Effect of Hypothetical “Lip” On Incoming Flow Dynamics

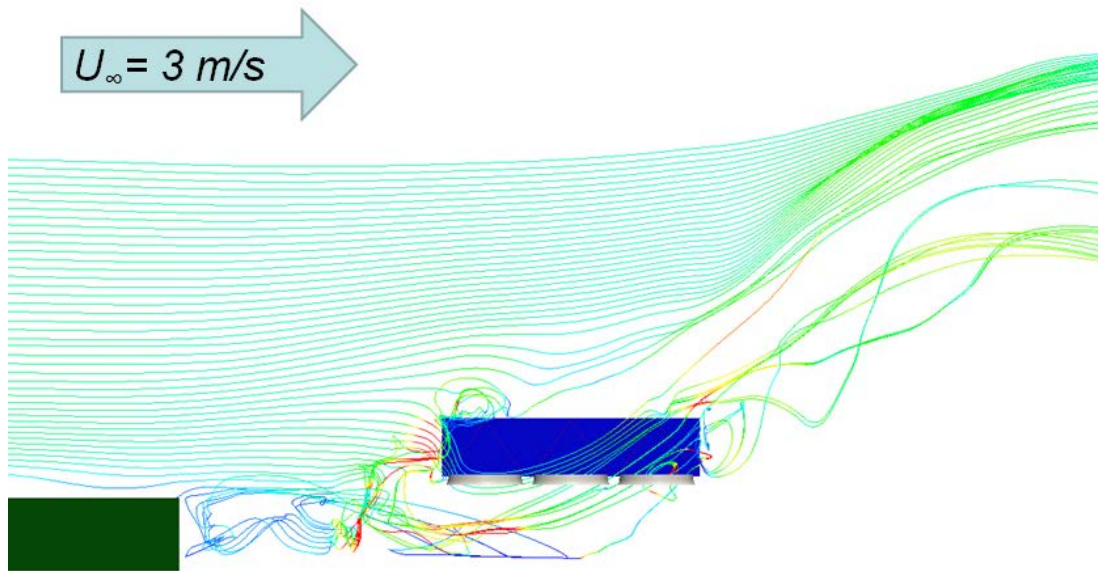


Figures 149 and 150 illustrate a comparison of the streamline patterns, both with the ledge in place but with (Figure 149) and without (Figure 150) blockage and also indicate a dramatic effect.

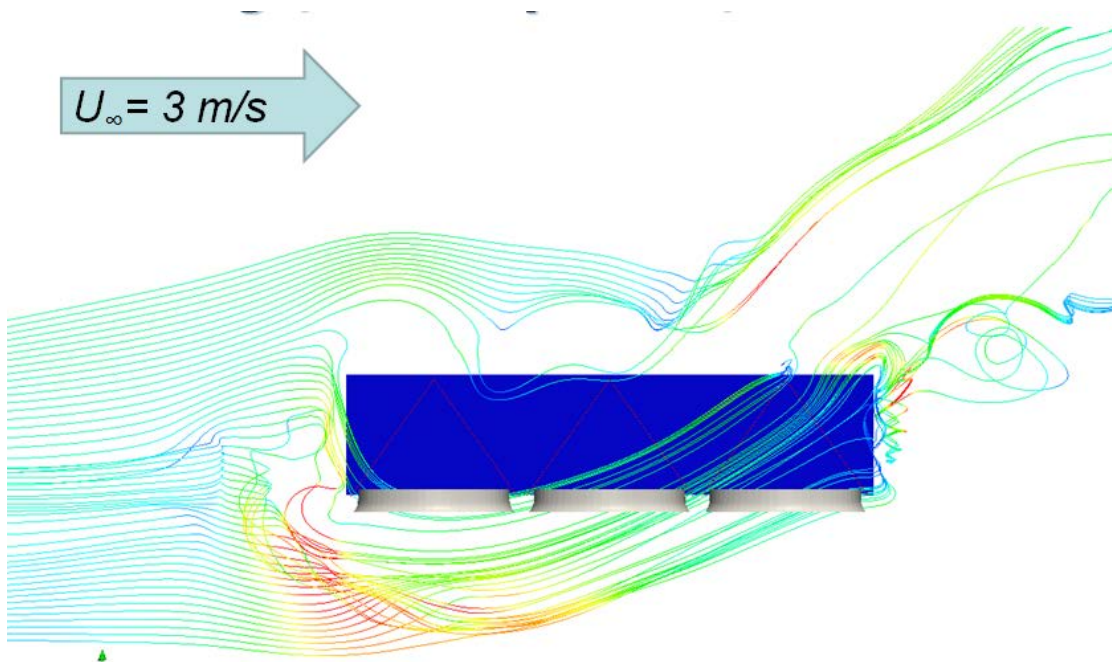
Figure 151 illustrates a comparison to the conditions of Figure 150 but with the screen fully deployed.

Figure 152, by comparison to Figure 150, illustrates the same condition at a higher wind speed of 6 m/s.

**Figure 149: Total Velocity Vectors for 3 M/S Wind; Upwind Blockage and “Lip” In Place; No Screen Present**



**Figure 150: Total Velocity Vectors for 3 M/S Wind; No Upwind Blockage; “Lip” In Place; No Screen Present**



**Figure 151: Total Velocity Vectors for 3 M/S Wind; No Upwind Blockage; “Lip” In Place; With Screen Present**

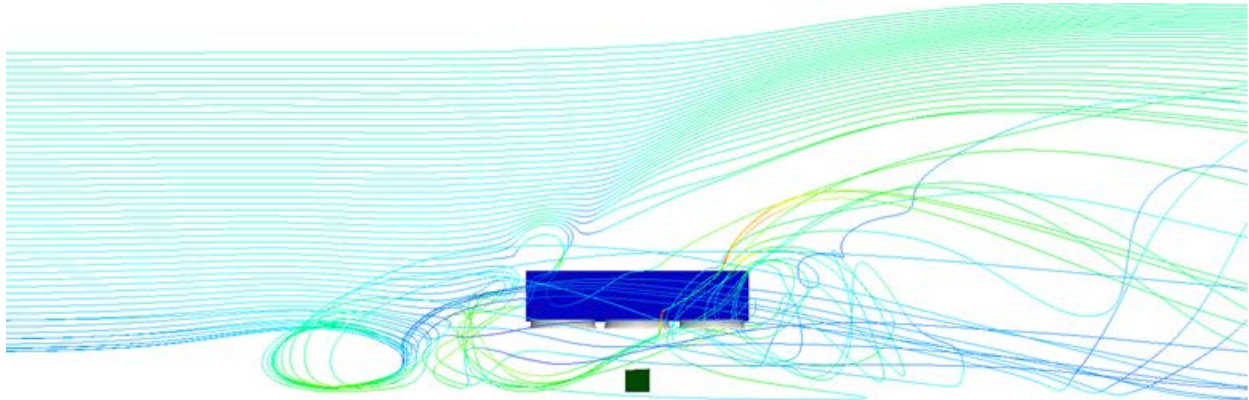
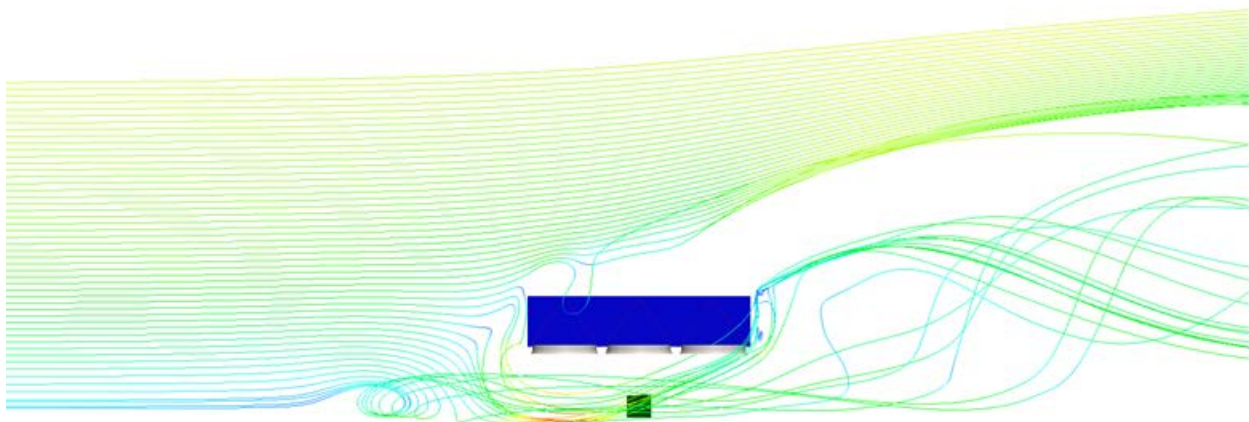


**Figure 152: Total Velocity Vectors for 6 M/S Wind; No Upwind Blockage; “Lip” In Place; No Screen Present**



Finally, Tables 8 and 9 present a summary table of the comparative results for the several conditions investigated.

Table 8: Summary of Inlet Velocity Comparisons for Cell 3.4

Ledge	$U_{\infty}$	Screen	Tot Fan Press	$\overline{DP_{AFrame}}$	Fan	$\overline{m_{dot}}$	$\overline{Vol_{dot}}$	$\overline{V_{fan}}$	$\overline{V_{exp\_avg}}$	Error
	m/s	PDC	$\overline{dP}$ (Pa)	$\overline{dP}$ (Pa)		kg/sec	m <sup>3</sup> /sec	m/s	m/s	%
None	3	0	110	78.0	3,4	380.4	310.5	3.68	6.83	46.09%
Present	3	0	110	78.0	3,4	658.1	537.2	6.37	6.83	6.75%
Present	6	0	110	78.0	3,4	385.4	314.6	3.73	5.87	36.46%
Present	3	1.1	110	78.0	3,4	712.6	581.7	6.90	6.83	-0.97%

Table 9: Summary of Inlet Velocity Comparisons for Cell 2.4

Ledge	$U_{\infty}$	Screen	Tot Fan Press	$\overline{DP_{AFrame}}$	Fan	$\overline{m_{dot}}$	$\overline{Vol_{dot}}$	$\overline{V_{fan}}$	$\overline{V_{exp\_avg}}$	Error
	m/s	PDC	$\overline{dP}$ (Pa)	$\overline{dP}$ (Pa)		kg/sec	m <sup>3</sup> /sec	m/s	m/s	%
None	3	0	110	78.0	2,4	841.6	687.0	8.15	6.78	-20.14%
Present	3	0	110	78.0	2,4	823.6	672.3	7.97	6.78	-17.56%
Present	6	0	110	78.0	2,4	662.5	540.8	6.41	6.34	-1.12%
Present	3	1.1	110	78.0	2,4	810.8	661.9	7.85	6.78	-15.73%

## CHAPTER 7: Summary and Conclusions

Wind is known to adversely affect thermal performance of ACCs through reduced airflow and increased hot air recirculation and to increase the mechanical stresses on ACC fan blades. Wind screens and barriers of various types have been shown to mitigate these adverse effects in many cases. This study was undertaken with the goal of increasing the understanding the mechanisms by which wind screens helped, to quantify the beneficial effects and to develop guidelines for the selection and design of wind screens.

Increased understanding of the physical mechanisms which determine the effect of windscreens was obtained through more than one year of continuous field testing and extensive wind tunnel modeling. However, the complete development of an analytical (CFD) model, which was to have been used to generalize the test results, was not achieved. As a result, the goal of producing guidelines for windscreen selection and design could not be met.

The study had three elements: field tests, physical modeling and computational modeling. The results and conclusions from the work follow.

### 7.1 Field tests

Measurements of fan inlet velocity, fan static pressure, fan motor current, cell inlet temperature and blade loading were made on an 18-cell ACC equipped with retractable wind screens. The screens could be fully retracted, fully deployed or set at any intermediate position. Ambient wind speed and direction were monitored along with plant operating conditions including unit output, steam flow, turbine exhaust pressure and fan status (off, half speed, full speed for all 18 fans). Test measurements were made at one minute intervals over the course of 18 months and presented as a function of wind speed and direction.

The results, which are presented in detail in Section 5, can be summarized as follows:

#### 7.1.1 Effect on Air Flow

The following discussion is based on a nominal “base case” of fully retracted screens and very low (essentially still air) wind speeds.

For the windward cell (Cell 3.4):

- With the screens fully retracted, wind speeds above 3 to 4 m/s caused a drop-off in the average inlet velocity from just less than 7 m/s to approximately 5.8 m/s at a wind speed of over 8 m/s.
- With the windscreens fully deployed at the highest wind speed of over 8 m/s, the inlet velocity was approximately 6.3 m/s, significantly increased above the fully retracted case.
- At the lowest wind speeds, deployment of the screens reduced the inlet velocity from just less than 7 m/s to less than 6 m/s.

- At wind speeds greater than approximately 7 to 7.5 m/s, inlet air velocity with the fully deployed screens was greater than it was with the screens fully retracted.

#### *7.1.1.1 For the Downwind Cell (Cell 2.4):*

- For the base case of low wind speed and fully retracted screens, the inlet velocity to the downwind cell was slightly lower than for the windward cell.
- For all screen deployments and at all wind speeds, the inlet velocity to the downwind cell was increased over the base case.

#### *7.1.1.2 For Cells 3.4 and 2.4 combined:*

- The inlet velocities averaged for the two cells, showed a slight decrease below the base case conditions at the lowest wind speeds and an increase at the highest speeds.

On the basis of measurements taken over two months of summer testing in 2014 and averaged over all wind directions from northwest to southwest, the results suggest that a 50 percent deployment of the screens was the most favorable in that:

- There was less reduction in airflow at the lowest wind speeds compared to full deployment.
- The increase in airflow at the highest wind speeds experienced during the test period was essentially the same as for the fully deployed screens and an improvement over the fully retracted screen conditions.

Additional tests are being conducted at the site following the conclusion of this study.

Measurements at higher wind speeds than were ever experienced at Caithness should be investigated to determine site characteristics for which a reduced screen size selection might be recommended.

### **7.1.2 Effect on Recirculation**

- No significant effect on either the average or maximum recirculation could be discerned as a function of screen position over all speeds and directions.

### **7.1.3 Effect on ACC Thermal Performance**

- The ACC thermal performance was quantified using a commonly accepted figure of merit,  $Q/ITD$ , where  $Q$  is the thermal load and  $ITD$  is the temperature difference between the steam condensing temperature and the temperature of the incoming ambient air.
- Again no consistent or significant effect of screen position was discernible at all wind speeds and directions.

### **7.1.4 Blade loading**

- Deployment of the screens resulted in a significant decrease in dynamic blade loading under higher wind speeds.

- The reduction is related to the presence of the screens creating a much more uniform inlet velocity profile for the air entering the fans.
- It is expected that the reduction in dynamic loading will have the effect of protecting the fan blades against wind-induced damage and of prolonging their life.
- Although no quantitative measurement of damage or blade lifetime could be made as part of this study, it is noted that no fan blade problems or failures have occurred since the installation of the screens, which was the purpose for which they were installed.

## 7.2 Physical Modeling

Detailed measurements of wind speed were made around and under a scale model of the ACC and site at which the field tests were conducted. The wind conditions that were modeled were westerly winds at speeds corresponding to the high range encountered at the site. Tests with fully retracted and fully deployed screen simulations were made.

- The model results were reasonably consistent with field measurements and observations; specifically:
  - The overall conclusion from the model tests is that the screens reduce the air speed flowing across the fan inlets which would be expected to improve fan performance and result in higher airflow into the cells.
  - At the wind speeds modeled this is consistent with the averaged field results described above.
  - Measurements at the lowest wind speeds at which field tests indicated a reduction in flow to Cell 3.4 with screen deployment could not be modeled in the wind tunnel. Therefore, there is no physical model confirmation of that field observation.
  - The primary effects are the expansion of the region of reduced velocity behind the screen in the upper region near the fan inlets and an extension of the accelerated high speed region near ground level further downwind under Cell 2.4. The downwind region under Cell 1.4 is affected very little as a function of increasing wind speed.
- An improvement in inlet velocity uniformity with the presence of screens was observed as it was in the field tests.
- Flow visualization recorded on video was consistent with specific velocity measurements in both the model and the field and with smoke tests run at other times (not as part of this study) in the field.

The correspondence of the wind tunnel results with field observations suggests that a model of a new (as yet unbuilt) ACC at a selected site could be useful in predicting the general effects of different wind screens and increase the likelihood of a successful wind screen/barrier design in a new application.

## 7.3 Numerical Modeling

A computational fluid dynamics (CFD) model was constructed to represent the ACC and the surrounding structures at the site where the field tests were conducted. The intent was to demonstrate the ability to calculate air velocities and pressures around, under and inside the ACC as a function of wind speed and direction which agreed reasonably with those values measured in the field and in the wind tunnel. Credible results at all but at very low wind speeds were not achieved. However:

- Good representation of field conditions was achieved at near-zero ( $< 0.3$  m/s) wind speed, suggesting that:
  - The representation of the fan performance and the flow losses across the heat exchanger bundles was sufficiently accurate.
  - The failure to reproduce realistic air flows into the windward cell at other than near-zero wind speeds suggests that the flow dynamics of the incoming wind is the aspect of the model that was not adequately represented.
  - Some qualitative understanding of the important effects on the dynamics of flow approaching and entering an ACC was obtained; specifically,
    - The details of the upwind boundary layer or the presence of those upstream obstructions near ground level which exist at Caithness did not appear to have important effects.
    - Details of windwall features, such as a ledge or lip at the bottom of the upwind windwall, were shown to have a large effect of the incoming flow patterns and appeared to improve the correspondence with measured results
    - Since no such lip or ledge exists on the Caithness unit, no conclusions can be drawn about the influence of this effect on full-scale performance.

Although quantitative results were not obtained and the goal of producing a computational tool capable of generalizing test results from the field or the wind tunnel was not achieved, some increased understanding of the important physics was obtained to serve as a starting point for additional modeling efforts.

## 7.4 Additional observations

### 7.4.1 Agreement with Observations Elsewhere

While the measurements made in the current study demonstrated no discernible improvement in ACC thermal performance from the deployment of the screens, such improvements have been reported elsewhere.

- Figure 11 and 14 of this report displays data showing clear performance enhancements after the installation of solid wind barriers at WyGen (Figure 11) and a porous, cruciform screen at El Dorado (Figure 14)

- Figures 23 and 25 show reported reductions in turbine exhaust pressure at Coryton (Figure 23) and Kings Lynn (Figure 25), both plants in the UK.
- Results from the Mystic Plant in Massachusetts (Avyazain 2015) presented at the recent Air Cooled Condenser Users Group meeting indicated a significant increase in plant output as a result of the installation of wind screens.

Prior to the start of testing, plant staff stated that they had never observed wind effects on plant performance of any consequence. It is believed that the absence of an observed thermal performance improvement at Caithness may be the result of several factors.

1. Neither the wind speeds nor the ambient temperatures at Caithness are at levels which would result in high turbine backpressures for the design plant heat load and the size of the ACC.
2. At the highest turbine backpressures encountered during the test period, predictions based on the properties of condensing steam and the turbine characteristics suggest that a modest improvement in ACC thermal performance would not result in a significant improvement in plant performance.
3. These conditions differ from those at other plants where high winds and high summertime temperatures results in operating at much higher turbine backpressures where effects of small changes on plant performance are to be expected. This was certainly the case at WyGen, El Dorado and Mystic and perhaps so at Coryton and Kings Lynn.

#### 7.4.2 Fully Retracted Screens Vs. No Screens Installed

It should be recognized that the configuration with the screens “fully retracted” is not the same as the configuration that would exist if no screens were installed at all. The housing into which the fabric screens retract and the length of screen still exposed when “fully” retracted extends 28 inches (0.7 m) below the bottom of the windwall and support beam and blocks an area that would be open if no screens existed. The computational modeling results suggest that the dynamics of the flow approaching and flowing around the bottom of the windwall can have an important effect on the calculated results. However, the importance of this difference could not be explored in the field tests.

#### 7.4.3 Cleanliness of Screens

It was noted that airborne dirt and debris led to some degree of blockage on the screens during the test period. This may have had some effect on the results, but this effect could not be quantified.

## GLOSSARY

Term	Definition
ACC	Air-cooled condenser
CFD	Computational fluid dynamics
WBE	Wind break effectiveness
ABL	Atmospheric boundary layer
ITD	Initial temperature difference
HRSG	Heat recovery steam generator
OEM	Original equipment manufacturer
CAD	Computer aided design
CAM	Computer aided modeling
PDC	Pressure drop coefficient

## REFERENCES

- Ayvazian, J. 2015. Galebreaker Wind Screen Installation on Unit 8 ACC Mystic Station Exelon Generation, Boston, MA. Presented at 7th Annual ACC Users Group Conference, Gettysburg, PA, September 21-24. <http://acc-usersgroup.org/wp-content/uploads/2015/10/01.J.Ayvazian-Mystic-8-Station-Wind-Shields.pdf>.
- Basham, Scott. 2014. Air-Cooled Condenser Maintenance and Vibration Issues and Solutions. Presented at ACCUG Meeting, San Diego, CA, September 22. <http://acc-usersgroup.org/wp-content/uploads/2014/10/North-Battleford-Energy-Centre.Scott-Basham-Northland-Power.pdf>
- California Energy Commission, Program Opportunity Notice (PON-11-502), Issued 2014, Available at <http://www.energy.ca.gov/>
- Duvenhage, K., and Kröger, D.G. 1996. The Influence of Wind on the Performance of Forced Draft Air-Cooled Heat Exchangers. *Journal of Wind Engineering and Industrial Aerodynamics*, Vol. 62, 259-277.
- Kim, D. and White, B. A Wind-Tunnel Study of Wind Effects on Air-Cooled Condensers. Electric Power Research Institute. Publication 1024752. December.
- Kröger, D.G. 1998. *Advanced Heat Exchangers and Cooling Towers*. Bergel House Inc., New York. 875 pages.
- Kroger, D.G. and M. Owen. 2011. Numerical Investigation of Air-Cooled Condenser Performance Under Windy Conditions. California Energy Commission publication, CEC-500-2011-021.May. <http://www.energy.ca.gov/2011publications/CEC-500-2011-021/CEC-500-2011-021.pdf>.
- Larson, R. C. 2015. Experimental Investigation of Adverse Wind Effects on Air Cooled Condensers: Wind Tunnel Testing on a Model Power Plant., Master of Science Thesis, Department of Mechanical and Aerospace Engineering, University of California at Davis. .
- Larson, R. C., R. Parker and B. White, 2015. Wind Effects on Air-Cooled Condensers (Part 2): Wind-Tunnel Testing on a Model Power Plant.. Presented at the 14th International Conference on Wind Engineering, Porto Alegre, Brazil, June 21-26.
- Maulbetsch, J. and M. DiFilippo, Effect of Wind Speed and Direction on the Performance of Air-Cooled Condensers. California Energy Commission publication CEC-500-2013-065, July. <http://www.energy.ca.gov/2013publications/CEC-500-2013-065/CEC-500-2013-065.pdf>.
- Maulbetsch, J. and M. DiFilippo. 2006. Effects of Wind on ACC Performance", Presented at, EPRI Cooling Tower Conference. Des Moines, Iowa. August.1.
- Maulbetsch, J., M. DiFilippo and J. O'Hagan. 2011.Effect of Wind on Air-Cooled Condenser Performance. ASME Paper No. IMECE2011-63137.

Mortensen, Ken. 2011. Improved Performance of an Air Cooled Condenser (ACC) Using SPX Wind Guide Technology at Coal-Based Thermoelectric Power Plants. SPX Final Report, March. [http://www.netl.doe.gov/File percent20Library/Research/Coal/ewr/water/6549-Final.pdf](http://www.netl.doe.gov/File%20Library/Research/Coal/ewr/water/6549-Final.pdf).

Parker, R., R. Larson and B. White. 2015 Wind Effects on Air-Cooled Condensers (Part 1): Determination of Comparable Wind Cases for Modeling. Presented at the 14th International Conference on Wind Engineering, Porto Alegre, Brazil, June 21-26,

Villafuerte, R. 2012. ACC Issues and Concerns., Presented at Air Cold Condenser User Group Meeting., Gillette, WY, September 24. <http://acc-usersgroup.org/presentations/2012-conference/16-acc-issues-and-concerns>.

Wilber, Karl and John Maulbetsch. 2005. Air-Cooled Condenser Design, Specification, and Operation Guidelines. Electric Power Research Institute, Palo Alto, CA. Publication 1007688. <http://www.epri.com/abstracts/Pages/ProductAbstract.aspx?ProductId=000000000001007688>.

## **APPENDIX A: Instrumentation and Data Acquisition System — Howden Report No. ECD 1307**

This appendix is available as a separate volume,  
publication number CEC-500-2016-047-AP.